GUSTAVO DE SOUZA CARVALHO

PERFORMANCE ANALYSIS OF DIFFERENTIAL AND RELATIVE GLOBAL NAVIGATION SATELLITE SYSTEM POSITION ESTIMATION

LAVRAS – MG

2022

GUSTAVO DE SOUZA CARVALHO

PERFORMANCE ANALYSIS OF DIFFERENTIAL AND RELATIVE GLOBAL NAVIGATION SATELLITE SYSTEM POSITION ESTIMATION

Dissertação apresentada à Universidade Federal de Lavras, como parte das exigências do Programa de Pós-Graduação em Engenharia de Sistemas e Automação para a obtenção do título de Mestre.

Prof. DSc. Felipe Oliveira e Silva

Advisor

LAVRAS – MG

2022

Ficha catalográfica elaborada pelo Sistema de Geração de Ficha Catalográfica da Biblioteca Universitária da UFLA, com dados informados pelo (a) próprio (a) autor(a).

Carvalho, Gustavo de Souza

Performance Analysis of Differential and Relative Global Navigation Satellite System Position Estimation / Gustavo de Souza Carvalho. lº ed. rev., atual. e ampl. — Lavras : UFLA, 2022.

107 p. : il.

Dissertação (mestrado)—Universidade Federal de Lavras, 2022.
Orientador: Prof. DSc. Felipe Oliveira e Silva.
Bibliografia.

1. TCC. 2. Monografia. 3. Dissertação. 4. Tese. 5. Trabalho Científico — Normas. I. Universidade Federal de Lavras. II. Título.

GUSTAVO DE SOUZA CARVALHO

PERFORMANCE ANALYSIS OF DIFFERENTIAL AND RELATIVE GLOBAL NAVIGATION SATELLITE SYSTEMS POSITION ESTIMATION - ANÁLISE DE DESEMPENHO DA ESTIMATIVA DE POSICIONAMENTO RELATIVO E DIFERENCIAL PARA SISTEMAS GLOBAIS DE NAVEGAÇÃO VIA SATÉLITE

Dissertação apresentada à Universidade Federal de Lavras, como parte das exigências do Programa de Pós-Graduação em Engenharia de Sistemas e Automação para a obtenção do título de Mestre.

APROVADA em 29 de Abril de 2022

.

Prof. DSc. Felipe Oliveira e Silva	UFLA
Prof. DSc. Gabriel Araújo e Silva Ferraz	UFLA
Prof. DSc. Danilo Alves de Lima	UFLA
Prof. Dsc. Helio Koiti Kuga	INPE

FELIPE OLIVEIRA E SILVA:09960645673

Digitally signed by FELIPE OLIVEIRA E SILVA:09960645673
DN: CN=FELIPE OLIVEIRA E SILVA:09960645673, OU=UFLA - Universidade Federal de Lavras, O=ICPEdu, C=BR
Reason: I am approving this document
Location:
Date: 2022.07.06 11:08:27-03'00'
Foxit PDF Reader Version: 12.0.0

Prof. DSc. Felipe Oliveira e Silva
Orientador

LAVRAS – MG
2022

ACKNOWLEDGEMENTS

To God who, through grace, allowed this realization in my life, guiding every step, giving me strength and taking care of every detail.

To my parents Francisval and Ismênica, for all the support, encouragement, attention and love that have always been essential.

To my siblings Talita and Henrique, for their complicity, companionship and support in difficult times.

To my friend Frederico Mota, who was with me during this journey, sharing the difficult moments but also the joyful ones.

To Professor Felipe, for the great friendship, guidance, encouragement, patience and teachings that were important during the making of this work, which contributed positively to my academic growth.

To the LabNav Study Group and TROIA Robotics Team, especially my colleagues Marcus Vinícius Pacheco and Marcos Ferreira, who were always available to help me during the experimental tests.

I thank the Federal University of Lavras (UFLA), especially the Master's Program in Systems Engineering and Automation, for the infrastructure necessary to carry out this work.

To the Brazilian Agricultural Research Corporation (EMBRAPA) for the financial support and to all those who directly or indirectly contributed to the completion of this work.

This work was supported by the Research Development Foundation (FUNDEP - ROTA 2030), under grant 27192.02.02/2021.01.00, the Brazilian National Council for Scientific and Technological Development (CNPq), under grant 313160/2019-8, the Brazilian Agricultural Research Corporation (EMBRAPA), under grant 212-20/2018, and the Minas Gerais Research Foundation (FAPEMIG), under grant CAG-APQ-01449-17.

My sincere thanks to everyone.

RESUMO

Desde os primórdios da civilização, a necessidade de se determinar a posição de pontos na superfície terrestre tem sido uma preocupação do ser humano, seja para mapear o ambiente, delimitar fronteiras ou auxiliar na navegação. Com o início da era espacial e o surgimento de novas tecnologias, foi possível desenvolver sistemas de posicionamento e navegação com cobertura global e larga faixa de precisão e custo. A agricultura é uma área que se beneficiou dos serviços de navegação fornecidos por Sistemas de Navegação Global via Satélite (GNSS), principalmente no que diz respeito à Agricultura de Precisão (AP), que tem por objetivo identificar a variabilidade espacial e temporal no campo para reduzir custos e aumentar a produção. A agricultura de precisão já é uma realidade para agricultores de grande porte que podem recorrer a serviços de posicionamento de alta precisão, tais como as técnicas Diferencial (DGNSS) e Relativa (RGNSS), o posicionamento Cinemático em Tempo Real (RTK) ou Sistema de Aumento Baseado em Satélite (SBAS). Pequenos e médios produtores, por outro lado, possuem acesso restrito a tais tecnologias devido ao alto custo dos equipamentos ou das assinaturas envolvidas. Uma alternativa para o problema apresentado é utilizar a Rede Brasileira de Monitoramento Contínuo (RBMC) como bases de referência para se computar correções de posicionamento diferencial e/ou relativo, e assim, obter, de forma gratuita, maior exatidão nas estimativas de posição, uma vez que os dados da RBMC são de livre acesso ao público. A principal contribuição deste trabalho é uma análise de desempenho das técnicas de posicionamento DGNSS e RGNSS, com o objetivo de se obter uma exatidão de posicionamento a nível submétrico. Uma análise da degradação espacial e temporal da técnica RGNSS é apresentada com base em dados experimentais coletados de estações pertencentes à RBMC. Resultados experimentais mostram que é possível atingir posicionamento horizontal a nível submétrico com 68% de probabilidade (1σ) utilizando estações de referência distanciadas em até 2100 km e com latência de comunicação de até 1500 s. Resultados adicionais, considerando um *rover* em movimento, e equipado com receptor GNSS de baixo custo, demonstram que é possível obter precisão de posicionamento horizontal de 1,5 m, com 68% de probabilidade, para distâncias entre receptores de aproximadamente 1500 km e latência de 3000 s.

Palavras-chave: GNSS. DGNSS. RGNSS. Análise de Desempenho.

ABSTRACT

The human being has been concerned with the knowledge of his position on Earth's surface since the dawn of civilization, whether to map the environment, delimit borders, or assist in the navigation. With the beginning of the space age and, consequently, the advent of new technologies, it was possible to develop positioning and navigation systems with global coverage in a broad range of accuracy and cost. Agriculture is one of the application fields that benefited from navigation services provided by Global Navigation Satellite Systems (GNSSs), especially the Precision Agriculture (PA), which aims at identifying and treat spatial and temporal diversity in the field to reduce costs and increase production. Precision agriculture is already a reality for large landowners who can use several systems that provide high accuracy positioning services, such as Differential (DGNSS) and Relative (RGNSS) techniques, Real-Time Kinematics (RTK) positioning techniques or Satellite-Based Augmentation Systems (SBAS). Small and medium-size farmers, in turn, have restricted access to such technologies due to the high cost of the required equipment and subscriptions. An alternative to the presented problem is to use GNSS receivers of the Brazilian Network for Continuous Monitoring of GNSS (RBMC) as reference stations to compute differential and/or relative position corrections, and then, obtain, at no costs, more accurate position estimates, since RBMC data is freely accessible to the public. The main contribution of this work is a performance analyses of DGNSS and RGNSS approaches, with the objective of achieving position accuracy at a submetric level. An analysis of the spatial and temporal degradation on RGNSS positioning estimates is presented based on real GNSS data collected from stationary high-cost GNSS receivers belonging to RBMC. Experimental results show that submetric horizontal positioning is attainable at 68% of probability (1σ) with reference stations distanced up to 2100 km and communication latency up to 1500 s. Additional results, considering a moving rover equipped with low-cost GNSS receiver, demonstrate position accuracy below 1.5 m for baseline distances between receivers of about 1500 km and latency up to 3000 s.

Keywords: GNSS. DGNSS. RGNSS. Performance Analysis.

LIST OF FIGURES

LIST OF TABLES

LIST OF SYMBOLS

c	speed of light
T	orbital period or ionosphere propagation error
$\vec{a}$	acceleration magnitude
a	denotes antenna/receiver body coordinate frame
r	geometric range
Φ	Argument of latitude
Δ	denotes an increment or difference
δ	small increment or error
e_o	elipse eccentricity
ε	denotes measurement residual
$\widehat{\ }$	denotes estimated value
η	white noise source
$\nabla\rho_{dc}$	differential correction
I	ionosphere propagation error
M	multipath error
m	mass or number of transmitters
$-$	denotes prediction
ρ	denotes pseudorange
s	denotes satellite body coordinate frame
$\tilde{\ }$	measured (corrupted) variable
t^s_{sa}	time of signal arrival from satellite s
t^s_{st}	time of signal transmission from satellite s
$+$	denotes after measurement update
W	weighting factor
E^s	Ephemires error of satellite s
ω_{ie}	Earth's rotation rate
ξ	residual

LIST OF ABBREVIATIONS AND ACRONYMS

AFS	Atomic Frequency Standards
AS	Anti-Spoofing
BDS	BeiDou Navigation Satellite System
BPSK	Binary Phase Shift Keying
C/A	Coarse/Acquisition
CDMA	Code Division Multiple Access
CME	Common-Mode Errors
COSPAS-SARSA	*Cosmicheskaya Sistyema Poiska Avariynich Sudov*-Search and Rescue Satellite-Aided Tracking
CS	Comercial Service
DCM	Direction Cosine Matrix
DGNSS	Differential GNSS
DoD	Department of Defense
DOP	Dilution of Precision
ECEF	Earth-Centered Earth-Fixed
ECI	Earth-Centered Inertial
EKF	Extended Kalman Filter
EU	Europe Union
FDMA	Frequency Division Multiple Access
FOC	Full Operational Capability
GEO	Geosynchronous Equatorial Orbit
GLONASS	*Globalnaya Navigatsionnaya Sputnikovaya Sistema*
GNSS	Global Navigation Satellite System
GPS	Global Positioning System
HOW	Hand-Over Word
ICAO	International Civil Aviation Organization
IGSO	Inclined Geosynchronous Orbits
ILS	Iterated Least Squares
ILS	Iterated Least Squares
IMU	Inertial Measurement Unit

INS	Inertial Navigation System
IWLS	Iterated Weighted Least-Squares
LADGNSS	Local-Area DGNSS
MCS	Master Control Station
MEO	Medium Earth Orbit
MSF	Military Space Force
NAVSTAR	Navigation System with Time And Ranging
NCME	Non-Common Mode Errors
OS	Open Service
P	Precise
PA	Precision Agriculture
PPS	Precise Positioning Service
PRC	People's Republic of China
PRN	Pseudo Random Noise
PRS	Public Regulated Service
PVT	Position, Velocity and Time
RADGNSS	Regional-Area DGNSS
RBMC	Brazilian Network for Continuous Monitoring of GNSS
RF	Radio-Frequency
RF	Russian Federation
RGNSS	Relative GNSS
RLS	Recursive Least Squares
RTK	Real Time Kinematics
SA	Selective Availability
SAR	Search and Rescue Service
SATNAV	Satellite Navigation System
SBAS	Satellite-Based Augmentation System
SPS	Standard Positioning Service
SV	Space Vehicles
TLM	Telemetry Word
TOA	Time Of Arrival
UAV	Unmanned Aerial Vehicles

UERE	User-Equivalent Range Error
UF	Unscented Filter
USA	United States of America
UTC	Coordinated Universal Time
WADGNSS	Wide-Area Differential GNSS

CONTENTS

Parte I

First Part: Introduction and Literature Review

1 INTRODUCTION

1.1 Motivation

The human being has been concerned with the knowledge of his position on Earth's surface since the dawn of civilization, whether to map the environment, delimit borders, performing farming activities or assist in the navigation. The observation of celestial bodies (e.g., stars and planets) and the deployment of triangulation techniques have been used to determine a specific location on Earth for centuries. However, since these techniques were associated with many errors in celestial object position estimation (reaching hundreds of meters), they did not allow obtaining precise information for the final desired location. With the start of the space age and, consequently, the advent of new technologies, it was possible to develop high-precision positioning and navigation systems with global coverage via both optical techniques (which use the visible part of the electromagnetic spectrum) and radio techniques (e.g., Navy Navigation Satellite System and Global Navigation Satellite System) (HOFMANN-WELLENHOF; LICHTENEGGER; COLLINS, 2012).

Figuring as the main Brazilian economic activity, agriculture has undergone significant transformations over the last decades. With the growing trend towards the urbanization of cities, increased labor costs, and automation of production processes, new agricultural cultivation models have become imperative. Under this circumstances arose the concept of Precision Agriculture (PA), which can be defined as a set of techniques that treat agricultural crops according to the spatial and temporal variability intrinsic to them, aiming at reducing agricultural inputs, and increasing productivity, and individualized production (MOLIN; AMARAL; COLAÇO, 2015). Regardless of the agricultural activity performed within the scope of the PA, an essential requirement is the availability of precise positioning of the machines and implements, whether for surveying georeferenced field data (soil sensor readings, soil attribute maps, etc.) or for their autonomous guidance. The problem of precise positioning at a low-cost, therefore, is essential to the progress of PA.

In Full Operational Capability (FOC) since 1995, the Global Positioning System (GPS) is the most reliable Global Navigation Satellite System (GNSS) currently available, providing three fundamental observables that allow Position, Velocity and Time (PVT) estimation, namely: pseudorange (coarse distance between the satellite and the receiver during the transmission and reception of the GPS signal), Doppler shifts (related to the relative velocity of the

pair satellite-receiver), and carrier phase (fine distance between satellite and receiver expressed in cycles of the carrier wave) (TEUNISSEN, 1991). However, even though GNSS Standard Position Service (SPS) can provide satisfactory estimation for user position, its accuracy does not meet the requirements for PA activities. A solution is to use Differential GNSS (DGNSS) or Relative GNSS (RGNSS) to improve the position estimation of a rover in the vicinity of a reference station by mitigating some errors that corrupt GNSS measurements and are common to both receivers.

Different approaches based on DGNSS/RGNSS techniques are available on the market that allow even better accuracy and reliability in user positioning, such as Real-Time Kinematics (RTK) (a variant of relative positioning) and Satellite-Based Augmentation System (SBAS), a type of Wide-Area Differential GNSS (WADGNSS). Among the two aforementioned options, RTK is more widespread in PA, consisting of a reference station equipped with a high-quality GNSS receiver that transmits instantaneous raw observables (carrier phase measurements) to a moving receiver via radio links. This, however, limits the separation distance between them to be up to 15 km (MOLIN; AMARAL; COLAÇO, 2015). SBAS, in turn, consists of scattered continental reference stations, which compute differential corrections and make them available to subscribed users via geostationary communication satellites. A limiting factor for the use of RTK and SBAS are the high costs of the required equipment and subscriptions, making it difficult for small and medium producers to invest in PA on their rural properties. In addition, since the corrections provided by SBAS are mainly from reference stations located in the USA or Europe, the accuracy of these corrections is degraded in Brazilian territory (due to the long distances to Brazil).

There are two main degradation factors DGNSS and RGNSS systems are prone to (MONTEIRO; MOORE; HILL, 2005): the baseline separation, which is the physical distance between reference station and rover, and the communication latency between the computed correction and actual time of use (for DGNSS) or the time it took to the rover to access the reference station raw observables (for RGNSS). Recent works have investigated the effects of communication latency on GPS position estimation accuracy (RAHMAN; FARRELL, 2019; RAHMAN; AGHAPOUR; FARRELL, 2020). This work aims at expanding the aforementioned analysis for the Brazilian scenario, a topic not sufficiently addressed in the literature yet.

1.2 Objectives

In light of the high-precision and high-cost positioning solutions previously presented and their limitations with respect to the Brazilian scenario, this work has the general objective of providing a performance analyses of DGNSS and RGNSS approaches, using stationary and moving, high- and low-cost GNSS receivers or position estimation, as well as receivers belonging to the Brazilian Network for Continuous Monitoring of GNSS (RBMC) as reference stations to compute DGNSS/RGNSS corrections.

The specific objectives are:

- Implement the GNSS, RGNSS, and DGNSS algorithms to compute navigation solutions;
- Compare positioning accuracy obtained via standalone GNSS, DGNSS, and RGNSS techniques with simulated GNSS observables data;
- Evaluate the performance of position solutions computed based on real data (GPS observables) from high-cost georeferenced receivers belonging to RBMC, and also from low-cost receivers mounted on a moving rover;
- Investigate the sensitivity of position estimation accuracy as function of baseline separation and communication latency between rover and reference station for a static and moving scenario.

1.3 Contributions

The main contribution of this work consists in the demonstration of use of open data from the Brazilian Network for Continuous Monitoring of GNSS (RBMC) in order to provide high accuracy (submetric) RGNSS horizontal position for a low-cost GNSS-equipped moving rover, as well as the presentation of a comprehensive analysis concerning the maximum latency and distance between rover and reference station that allows the latter.

Partial results of the aforementioned contribution were published in (CARVALHO et al., 2020; CARVALHO; SILVA, 2021), at the 17^{th}*and* 18^{th} IEEE Latin American Robotics Symposium - LARS 2020 and 2021. The final results of this work were submitted for consideration of publication in a Special Issue of the Journal of Intelligent & Robotic Systems (JINT), after the work published at LARS 2021 was selected as one of the best papers therein presented.

1.4 Work Structure

This work is organized in two parts. The first part presents an overview of GNSSs and it is subdivided as follows: Chapter 2 presents fundamental concepts involved in GNSS positioning along with basic information on the core GNSS constellations currently available. Additionally, it is discussed, in particular, how GPS is structured and the types of signals this system transmits. Chapter 2 also presents satellite orbit computation based on ephemeries data transmitted from satellites to receivers, and discusses the main sources of errors that corrupt pseudorange measurements, followed by three common algorithms used to compute user position, namely Iterated Least Squares, Iterated Weighted Least Squares and Extended Kalman Filter. Chapter 2 finishes with the description of Differential and Relative GNSS, two advanced techniques used to mitigate the effect of common-mode errors in GNSS observables. Chapter 2, in sequence, concludes the first part of this work, by presenting the main considerations and additional thoughts. The second part of this work presents simulated and experimental results in the form of scientific papers, submitted and/or approved for publication in different symposiums/indexed journals. Paper I, in particular, compares DGNSS and RGNSS approaches using simulated data. Paper II presents an analysis over the degradation effects of baseline distances in RGNSS position accuracy for a static scenario. Paper III analyses the communication latency degradation on RGNSS position accuracy again for static GNSS receivers. Finally, Paper IV presents analyses the baseline distance and latency communication degradation on RGNSS position accuracy now for a moving rover equipped with low-cost GNSS receiver.

2 GLOBAL NAVIGATION SATELLITE SYSTEMS: LITERATURE REVIEW

2.1 Basic Principles of Operation

Satellite navigation, or SATNAV, is the autonomous process of computing geospatial position by using the transit time of radio signals transmitted along a line-of-sight from artificial orbiting satellites to the receiver (herein also referred to as user) at a point whose position is to be determined. This concept is known as the one-way Time of Arrival (TOA) ranging, in which the satellite broadcasts radio signals referenced to on-board highly accurate atomic clocks to users with an embedded clock as well (KAPLAN; HEGARTY, 2005). These signals contain both a Pseudo Random Noise PRN code and a navigation message, which are used to determine the satellite-to-user range (pseudorange), and estimate the satellite‘s position (ephemeris), respectively (NOURELDIN; KARAMAT; GEORGY, 2012).

A SATNAV system with global coverage is referred to as GNSS, term conceived at the Tenth Air Navigation Conference, in 1991, when ICAO recognized that the future of the stand-alone navigation systems would rely on GNSS (HEIN, 2000). According to Kaplan and Hegarty (2005), a GNSS can be used to provide accurate, worldwide and three-dimensional position (latitude, longitude, and altitude/elevation), velocity, and navigation information to users with proper receiving equipment. Furthermore, it broadcasts time within the Universal Time Coordinated (UTC) timescale, which allows receivers to act worldwide as a synchronized time source with high precision. These features are collectively known as PVT solution.

According to Groves (2013), satellite navigation system's architecture consists in three components: the space segment, the control or ground segment, and the user segment. The space segment of the current GNSSs nominally consist of 24 or more satellites, also called SV, placed on Medium Earth Orbits (MEO), arranged in 3 to 6 orbital planes, with four or more satellites per plane. Such disposals ensure that in any circumstance, at least four SVs will be available in a good geometric position at any time and anywhere on Earth's surface. The control segment, in turn, is responsible for monitoring and maintaining the health and status of the satellites, besides sending to them navigation data, used to determine satellites' ephemeris, through uplinks. The user segment, finally, comprises multiple equipment receivers spread around the globe (DORSEY et al., 2006; SPILKER; PARKINSON, 1996).

The electromagnetic signals broadcast by the satellites travel at the speed of light. Since the receivers are also equipped with internal clocks, it is possible to measure the signal propaga-

tion time, and then convert it to a distance (geometric range r) by multiplying it by the speed of light c. Momentarily neglecting the existence of errors, a range measurement may be obtained as (GROVES, 2013):

$$r_{as} = (t^{s}_{sa,a} - t^{s}_{st,a})\, c, \tag{2.1}$$

where $t^{s}_{sa,a}$ is the time of signal arrival at receiver antenna a, $t^{s}_{st,a}$ is the time of signal transmission from a satellite s.

When a single ranging measurement from a satellite is used, the receiver position would lie somewhere on the surface of a sphere of radius r_{as} centered on that satellite. If a second measurement is simultaneously made using a signal from another satellite, then the user would be located on the circle formed by the intersection of both spheres centered in each satellite. Adding a third satellite range, the user is located at the intersection of the circle and the surface of the third sphere, which lies at two possible points. For most applications, however, one of those point solutions can be disregarded since it is not viable in practice. Figure 2.1 depicts this concept.

Figure 2.1 – Position *loci* from uncorrupted range measurements.

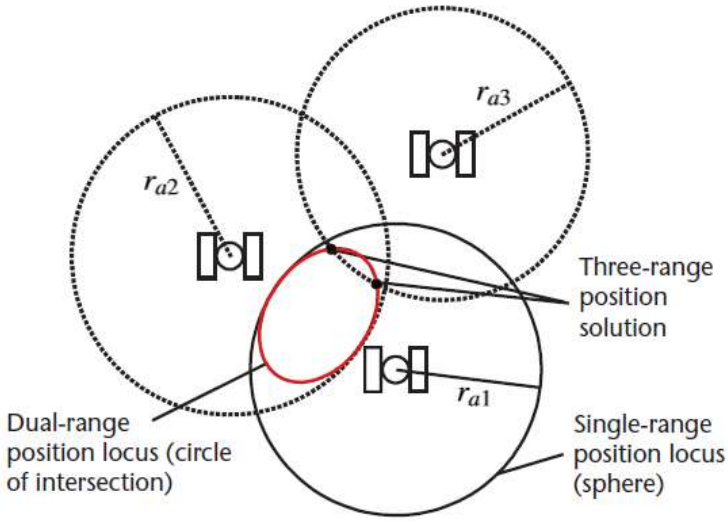

Source: (GROVES, 2013)

In practice, however, the clocks of either satellite and receiver are not synchronized with respect to GNSS time. The measured ranges are contaminated by both the satellite and receiver clock biases, which will result in a range measurement error. If the receiver clock is ahead by

δt_c^a and the transmitter clock ahead by δt_c^s from the GNSS time, a "pseudorange" measurement may now be defined as (GROVES, 2013):

$$\begin{aligned}\rho_a^s &= (\tilde{t}_{sa,a}^s - \tilde{t}_{st,a}^s)\,c \\ &= (t_{sa,a}^s + \delta t_c^a - t_{st,a}^s - \delta t_c^s)\,c, \\ &= r_{as} + (\delta t_c^a - \delta t_c^s)\,c\end{aligned} \tag{2.2}$$

where ρ_a^s is the pseudorange, $\tilde{t}_{sa,a}^s$ is the measured time of arrival, and $\tilde{t}_{st,a}^s$ is the transmission time deduced by the user equipment from the signal modulation.

The navigation message contains satellite clock corrections and, since the receiver's clock offset is common to all simultaneous measurements made using a given receiver, it is treated as an additional unknown parameter, which requires a fourth satellite to compute a position solution. Therefore, at least four satellites are necessary for the user to calculate its PVT solution: three of them for three-dimensional receiver's antenna position and a fourth to cancel its clock bias.

According to Groves (2013), the pseudorange measurement, $\tilde{\rho}_{a,C}^s$, after being corrected for some predictable errors, including the satellite clock error, may be expressed in terms of the ECEF satellite position, $\mathbf{r}_{es}^e$, user antenna position, $\mathbf{r}_{ea}^e$, and the range error due to the receiver clock offset, $\delta\rho_c^a$, as:

$$\tilde{\rho}_{a,C}^s = \sqrt{[\mathbf{C}_e^I \mathbf{r}_{es}^e(t_{st,a}^s) - \mathbf{r}_{ea}^e(t_{sa,a}^s)]^T [\mathbf{C}_e^I \mathbf{r}_{es}^e(t_{st,a}^s) - \mathbf{r}_{ea}^e(t_{sa,a}^s)]} + \delta\rho_c^a(t_{sa,a}^s), \tag{2.3}$$

where $\mathbf{C}_e^I$ is the DCM compensating for ECEF rotation during signal propagation, $\delta\rho_c^a = \delta t_c^a\,c$ and the measurement noise has been neglected. It shall be noticed that for a common time of arrival for a given user, all measurements have four unknowns in common, which implies that it is necessary to solve simultaneous equations for at least four pseudorange measurements to obtain the user position and the receiver clock offset.

2.2 Core Constellations of GNSS

Until the early 2000s, the term GNSS was commonly used to refer to the U.S. NAVSTAR GPS, since it was the first and most well-known navigation system using radio signals transmitted by orbiting satellites (AKOS et al., 2006). At that point, however, the Russian GLONASS

was also fully operational; moreover, other constellations have been developed over the years. Currently, there are four constellations in FOC: GPS (USA), GLONASS (RF), BDS (PRC) and Galileo (EU) (DORIDES, 2018). More details about the core GNSS constellations will be presented in the following subsections.

2.2.1 GPS

Standing as the most ancient and robust GNSS, the NAVSTAR-GPS, or merely GPS, is a satellite navigation system developed by the U.S. DoD. The GPS program began in the early 1970s when some governmental navigation programs were merged, but its FOC was attained only at the end of 1994 (MCDONALD, 2008; PARKINSON, 1997). It was originally conceived for military purposes, aiming at instantaneous determination of position and velocity (i.e. navigation), and precise coordination of time (i.e. time transfer), but was later made available to civilians as well. For this reason, the GPS offers two navigation services, the SPS and PPS, informally known as civil and military services, respectively (GROVES, 2013).

The SPS is a standard positioning and timing service that is available free of charge to all users worldwide, authorized and unauthorized. During the 1990s, the SPS delivered horizontal and vertical accuracy of 100 m and 140 m, respectively, and 340 ns in the time measures. For national security reasons, this service was intentionally degraded by the DoD using a technique called SA to limit the positioning accuracy for civilian users (GRAAS; BRAASCH, 1996). However, SA can be bypassed using differential techniques, and due to the increasing number of civilian and commercial applications of GPS, SA was deactivated on May 1, 2000. Until that date, PPS delivered better results (22 m horizontal, 27.7 m vertical, and 200 ns), but it was restricted for military force and authorized users, which remains nowadays. With the removal of SA, SPS accuracy improved about 10 times, and it still can be improved considerably with advanced methods of positioning.

Since its inception in the 1970s, GPS has continually evolved, and 72 satellites have been successfully launched into orbit so far. The need for improvement was driven not only by both the military and civil interests and requests, but also by competition since systems of other countries, like the European Galileo and the Chinese BeiDou, were on their initial stage developmental schedule in the early 2000s. On January 25, 1999, the GPS modernization program was officially announced, aiming at the improvement in terms of accuracy, availability, and integrity. As of April 18, 2022, there were a total of 31 operational satellites in the GPS cons-

tellation, not including the decommissioned on-orbit spares, from 4 generations of satellites, namely blocks IIR, IIR-M, IIF and III (AMERICA, 2022).

2.2.2 GLONASS

GLONASS, an acronym for *Globalnaya Navigazionnaya Sputnikovaya Sistema* (Global Navigation Satellite System, in English), is a military navigation system developed by the former Union of Soviet Socialist Republics (URSS) from the mid-1970s, in parallel to GPS. Like the U.S system, it was designed to provide an "unlimited number of air, marine, and any other type of users with all-weather three-dimensional positioning, velocity measuring, and timing anywhere in the world or near-Earth space", as stated by the Coordination Scientific Information Center (MOSCOW, 2008). The first GLONASS satellite was launched in 1982, and its FOC was declared in early 1996 with 24 satellites in orbit. However, after the dissolution of the Soviet Union, followed by Russia's economic difficulties, the full constellation was short-lived. The number of available satellites declined gradually due to lack of funding, reaching its minimum in 2001 with only 8 working spacecrafts (FEAIRHELLER; CLARK, 2006). In August 2001, a modernization program was announced, aiming at rebuilding the constellation, introducing new signals, and updating the control segment (REVNIVYKH et al., 2005). On 8 December 2011, GLONASS FOC was again achieved and since then it has been maintained.

Despite its military purpose, GLONASS signals were opened to the civil community in 1995, when the government of the Russian Federation released the Decree No. 237 entitled "On executing works in the use of the GLONASS global navigation satellite system for the sake of civil users", and guaranteed they would be available free of charge (HOFMANN-WELLENHOF; LICHTENEGGER; COLLINS, 2012). Thus, GLONASS looked very attractive to civil users in that time, since its signals were not affected by either SA or AS, delivering a positioning accuracy of 60 and 75 m in the horizontal and vertical components, respectively, with a 99.7% probability (MONICO, 2000).

GLONASS has similar operational requirements as GPS with some key differences in its configuration and signal structure. Its constellation nominally consists of 24 active satellites plus 6 spares, located in 3 orbital planes, each one containing 8 satellites equally spaced, with 64.8 degrees nominal inclination, an orbital altitude of 19.100 km and period of 11 h 15 min (POLISCHUK et al., 2002). The satellites are categorized into three generations (TEUNISSEN; MONTENBRUCK, 2017): first generation Glonass I/II (started in 1982); second generation

Glonass-M (started in 2003); and third generation Glonass-K (started in 2011). GLONASS uses FDMA, where two individual carrier frequencies are assigned to each SV, in contrast to GPS that uses CDMA, where every SV transmits the same two carriers modulated by PRN-codes specifically assigned to each satellite. The new generation of GLONASS SVs includes the CDMA signals in a new frequency in addition to the legacy FDMA signals.

2.2.3 Galileo

Galileo is a joint initiative of the European Commission, the European GNSS Agency (GSA) and the European Space Agency (ESA) to develop the European Union's Global Satellite Navigation System, a state-of-the-art SATNAV system designed to provide a highly accurate, guaranteed global positioning service. Unlike other global satellite navigation systems that were initially designed for military purposes, Galileo is a program under civilian control, i.e., it was conceived with service provision to end users at its core. Despite the difference in their conceptions, Galileo is interoperable with GPS and GLONASS, allowing the user equipped with proper receiver to successfully combine pseudorange measurements from more than one GNSS into PVT solutions.

Galileo program started in 2002 with the goal of making Europe to achieve technological independence with respect to other global navigation satellite systems. In 2016, the initial services became available, marking the beginning of Galileo's operational phase. In 2020, Galileo's FOC was declared with 26 operational satellites in orbit. The baseline constellation comprises 24 satellites plus 6 in-orbit spares, evenly spread in three MEO planes at $23,222$ km of altitude above Earth, which leads to a repeat cycle of the satellite-Earth geometry of 17 orbits in 10 sidereal days. The orbital planes have inclination of 56 degrees to the Equator.

Galileo satellites transmit permanently three independent CDMA signals, named E1 (1575.420 Hz), E5 (1191.795 Hz) and E6 (1278.750 Hz), providing four services (TEUNISSEN, 1991):

- Open Service (OS): a free mass-market service for positioning, navigation, and timing;
- Precise Positioning Service (PRS): service restricted to government-authorized users, for sensitive applications that require a high level of service continuity;
- Comercial Service (CS): a charged service complementing the OS, providing high accuracy, controlled access and authentication function to users.

- Search and Rescue Service (SAR): Europe's contribution to Cosmicheskaya Sistyema Poiska Avariynich Sudov-Search and Rescue Satellite-Aided Tracking COSPAS-SARSA, an international satellite-based search and rescue distress alert detection system.

For more information on Galileo system, see (COMMISSION,).

2.2.4 BeiDou

BeiDou Navigation Satellite System (BDS) is a global navigation satellite system independently developed and operated by China. The name BeiDou comes from the most important set of stars giving directions to people in the Northern Hemisphere, also known as Big Dipper. BeiDou was also designed to be compatible and interoperable with GPS and GLONASS constellations.

BeiDou project comprised a three-step development strategy, following a unique path from a regional and active to a global and passive system. The first step started in 1994 with the development of the first generation of satellites, BDS-1, and finished in 2000 with two in-orbit GEO satellites providing a regional active service capability of positioning and timing. The second step was from 2004 to 2012, where the second generation (BSD-2) was developed, comprising 5 GEO satellites, 5 IGSO satellites and 4 MEO satellites. In addition, BDS-2 included a passive positioning scheme, and provided users in the Asia-Pacific region with positioning, velocity, and timing measurements. The third step started in 2009 with the development of BDS-3. In 2020, Beidou-03 achieved global coverage, providing positioning, navigation and timing, global short message communication, and international search and rescue services, among other services.

The nominal space constellation of BDS-3 consists of 3 GEO satellites at an altitude of $35,786$ km, 3 IGSO satellites at an altitude of $35,786$ km and inclination angle of 55 degrees to the equatorial plane, and 24 MEO satellites at an altitude of $21,528$ km and inclination angle of 55 degrees to equator plane, plus 6 satellites in-orbit spares. The satellite ground tracks repeat after 13 rotations within 7 days. Besides other services previously mentioned, BDS-3 also provides radio determination satellite service, which includes rapid positioning, short-messaging, and precision timing via GEO satellites, a unique service among other GNSS constellations. For more information on BeiDou system, see (CHINA, 2019).

Table 2.1 summarizes some differences between all GNSS constellations herein presented.

Table 2.1 – Summary of the main differences between current GNSSs available in Full Operational Capability.

	GPS	GLONASS	GALILEO	BEIDOU
SVs	27 (+4)	24 (+3)	27 (+3)	27 (+3)
Orbital Planes	6	3	3	3
Orbit Inclination [°]	55	64.8	56	55
Mean Altitude [km]	22200	19100	23222	21528
Ground Track Repetition [Sideral Days]	1	8	10	7
SV Spacing	Uneven	Even	Even	Even
Signal Separation	CDMA	FDMA/CDMA	CDMA	CDMA
Navigation Message	Orbital Parameters	Positions, velocities, and accelerations	Orbital Parameters	Orbital Parameters
FOC	1995	1996	2020	2020

Source: (AMERICA, 2022; CHINA, 2019; MOSCOW, 2008; COMMISSION,)

2.3 GPS Architecture

GPS architecture, like other GNSSs, consists of three main components (FARRELL, 2008): the space segment, the control or ground segment, and the user segment, as illustrated in Figure 2.2.

The space segment consists of a baseline constellation of 24 GPS satellites, with a maximum of 36, orbiting Earth in 6 orbital planes equally spaced around the equator. The planes are identified by letter designators from A to F, each with four primary satellite slots distributed unevenly and indicated by its plane position number. The orbits are nearly circular with an orbital radius of 26,559 km (22, 200 km above Earth's surface), inclination angle of 55 degrees, and orbital period of roughly 12-hour (11 hr 58 minutes). Each SV emits coded radio signals which a GPS receiver will decode to determine important system parameters.

The control segment consists of a worldwide network of ground facilities that provide capabilities for monitoring, commanding, and controlling the GPS satellite constellation. It consists of a MCS, an alternate MCS, 11 ground antennas (uplink stations), and 16 monitoring sites (AMERICA, 2021). The monitoring stations are at precisely surveyed locations, equipped with synchronized clocks and high-precision receivers to obtain ranging measurements from each visible satellite and send these to the MCS. The MCS, in turn, uses these measurements to generate orbital models and clock estimates/predictions for each SV and determine whether any

Figure 2.2 – GPS segments architecture.

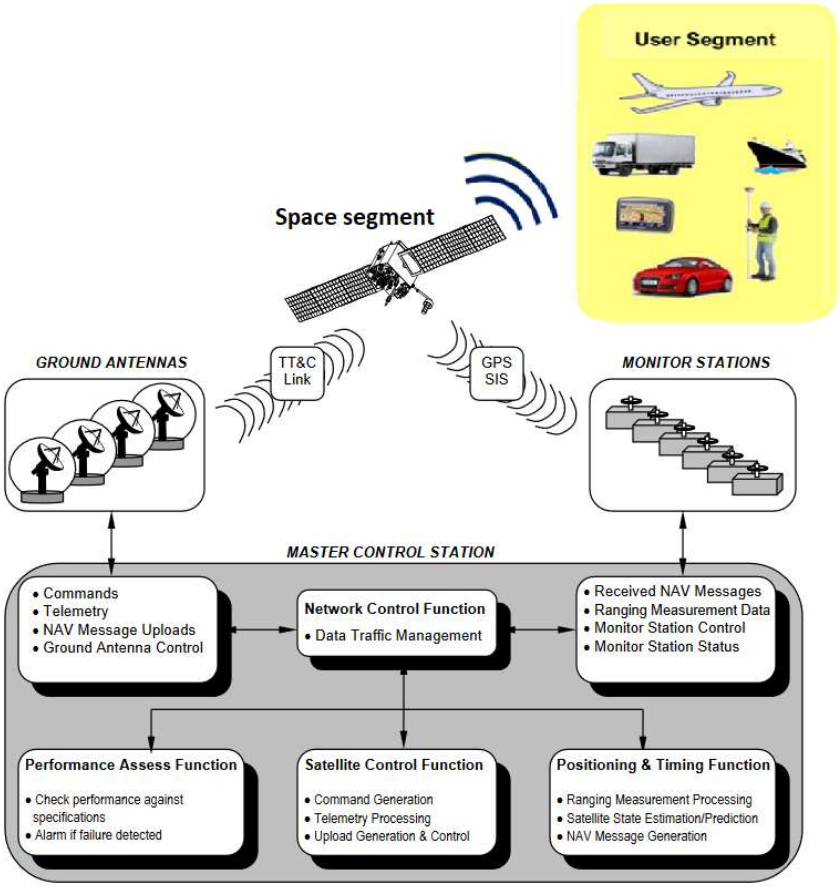

Source: Adapted from (MOOREFIELD, 2020)

maneuver must be performed. This information is transmitted to the space segment by uplink stations, which then broadcast them to the user segment.

The user segment consists of receivers that detect the GPS signals and convert them into observables, providing services that users are mainly interested in, such as estimation of their position, velocity, and time. This segment includes military and civilian users, also classified into authorized and unauthorized services. Currently, there are many generations of receivers available with different architectures, however, the basic components of a generic GPS receiver are (SEEBER, 2008): antenna; RF front-end section for identification and signal processing; microprocessor for receiver control, data sampling, and data processing; oscillator; power supply; memory for data storage; and user interface.

The antenna is responsible for detecting the electromagnetic waves coming from SVs, transforming their energy into electrical current, and handing the signal to receivers electronics. The RF front-end section converts the GPS signal into a lower frequency by combining it with

a sinusoidal signal generated by an internal oscillator. The microprocessor plays the role of controlling all operations, which includes the acquisition of signals, signal processing, decoding of the broadcast navigation message, differential corrections (when applied), input command from the user (user interface), data flow through communication port (when included), among other operations. Receivers usually are equipped with internal rechargeable batteries in addition to an external power input. Finally, for post-processing purposes, all data have to be stored on internal or external memory devices.

2.4 GPS Signals

The GPS is classified into a passive one-way downlink ranging system, which means that SVs emit modulated signals from space to Earth (one-way downlink) that allow users to derive ranges passively, i.e, receivers do not emit signals back to satellites. The emitted SV signals can be described by a three-layer model, composed of a data-link layer, ranging code layer, and physical layer (HOFMANN-WELLENHOF; LICHTENEGGER; WASLE, 2008). The physical layer characterizes the physical properties of the transmitted signals. The ranging code layer is based on a continuous but periodic modulated signal, and its periodicity is strictly synchronized to SV's time system and data message. The data-link layer contains parameters, such as time of transmission, ephemeris, satellite's health, etc., that allow users to estimate their position.

As mentioned earlier, GPS has gone through a modernization program, which, consequently, had its impact on GPS signal structure. For this reason, it is common to refer to the signals that precede the modernization program as legacy GPS signals, and those that have been included over the years, as modernized signals. The legacy signals include two carrier frequencies, link 1 (L1) and link 2 (L2), modulated by two PRN-codes (C/A code and P code), and by a navigation message. All navigation signals are based on the fundamental frequency $f_0 = 10.23$ MHz, which is coherently derived from AFS. The carrier frequencies are 1575.42 MHz ($154 f_0$) and 1227.6 MHz ($120 f_0$) for L1 and L2, respectively, and the corresponding wavelengths are approximately 19 cm and 24.4 cm. The large gap between L1 and L2 frequencies was designed so that user equipment can estimate the ionosphere delays (MCCARTHY; PETIT, 2004).

The C/A-code is embedded only onto the L1 carrier frequency by the biphase modulation (i.e., BPSK), and it is associated with the SPS service, available for civilian use as it was intended to provide a less accurate position. It is a PRN taken from a family of Gold code (GOLD, 1967), consisting of a chip sequence (rectangular pulses with an amplitude of ± 1)

with length of 1023 chips, chipping rate of 1.023 Mchips/s, and period of 1 ms. Each satellite is assigned a unique PRN code. The cross-satellite interference is small since Gold codes have bounded small cross-correlation within a set, thus, the SV signals can be separated and detected, even though they are transmitted at the same carrier frequencies. This technique is referred to as CDMA. The P-code, in turn, is embedded onto both L1 and L2 frequencies. It has a length of 23547×10^{14} chips and chipping rate of 10.23 Mchips/s. The P-code is partitioned into 37 unique code segments, and each GPS satellite is assigned a different 1-week repeating segment of this code (period T = 1 week) (SPILKER, 1996). The P-code is publicly available, however, GPS satellites normally broadcast the encrypted P(Y)-code, which is only available for licensed PPS users since it was intended for military purposes and acts as an AS measure.

The legacy navigation message (NavData) is added to the C/A-code and the P-code via modulo 2 adder, forming the binary modulating, and then they are embedded onto carrier frequencies L1 and L2 via BPSK modulation. The NavData is a bitstream running at a 50-bps rate that contains, among other auxiliary data, the information necessary to compute the precise locations of each visible satellite and time of transmission for each navigation signal (GREWAL; ANDREWS; BARTONE, 2013). Some of the information of the navigation data stream comprises:

- Satellite almanac data, that contains the approximate ephemeris parameters, clock calibration, and health of the entire satellite constellation;
- Satellite ephemeris data, which is the data of a particular satellite that enables a more accurate determination of that SV position and clock errors;
- Signal timing data, which is the time tagging needed to determine the satellite-to-user propagation delay;
- Ionosphere delay data, which comprises eight coefficients of the ionosphere propagation delay correction model (Klobuchar model) for single-frequency users;
- Satellite health message, which indicates the current status of the signals and navigation message, so that the receiver can ignore that satellite if it is not operating properly.

The data format of the GPS navigation message consists of 25 frames with length of 1500 bits. Each frame is subdivided into five 300 bit subframes of six seconds duration, comprising ten data words of 30 bit, which incorporates a parity check in the last 6 bits of each

word. It takes 30 s to transmit one frame, and the transmission of the full 25-frame NavData requires 750 s. Each subframe begins with a TLM, a fixed 8-bit pattern intended to assist the user equipment in locating the beginning of each subframe. The second word in each subframe is the HOW, which is transmitted every 6 s, and aids PPS user equipment in the transition from C/A-code to P(Y)-code by providing the number of 1.5-second P(Y)-code periods that have occurred thus far in the week. Subframe 1 includes clock correction data, satellite's health, and predicted accuracy. Subframes 2 and 3 provide satellite ephemeris data. Subframes 4 and 5 provide less important data, including almanac, health data of the entire constellation, and ionosphere delay corrections. Since subframes 1-3 consist of critical data, they are repeated in every frame of NavData, while subframes 4 and 5 are cycled through 25 pages each. It means that in each cycle, the SV broadcasts 1 page out of 25 comprised in these subframes. The receiver takes 750 *s* to read the entire set of data, which means that during this period the critical clock and ephemeris data will be received 25 times within subframes 1-3 (TEUNISSEN; MONTENBRUCK, 2017). Figure 2.3 depicts the NavData format.

Figure 2.3 – Legacy navigation message format

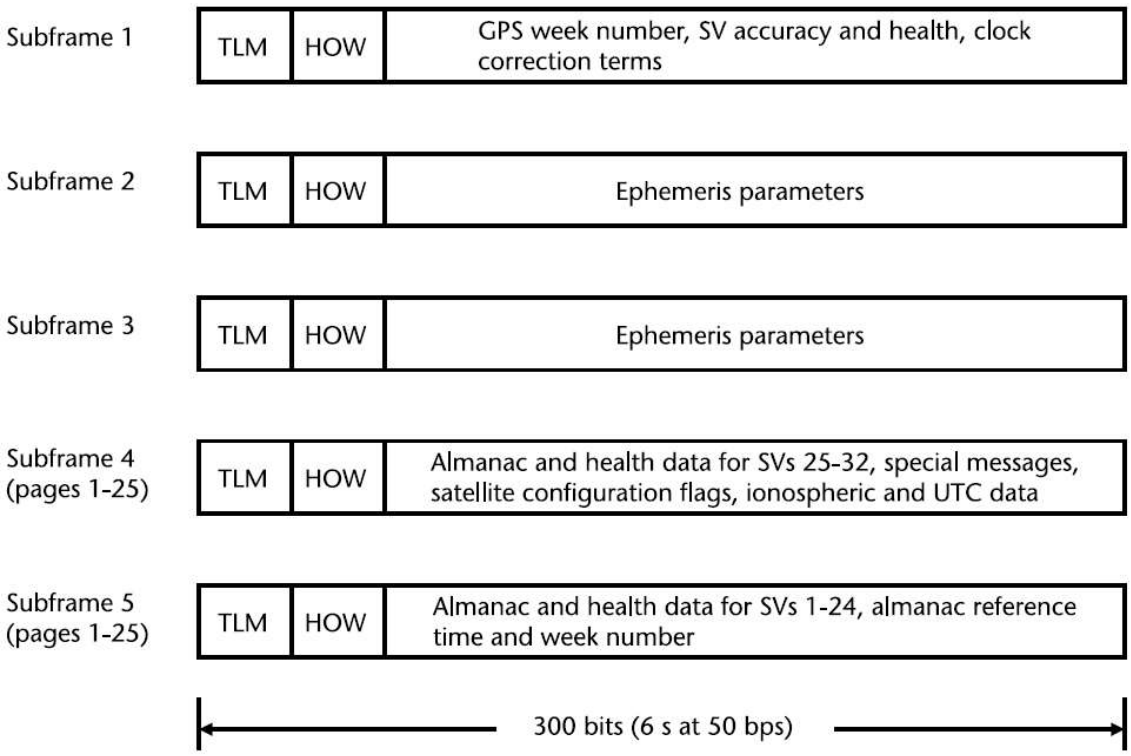

Source: (KAPLAN; HEGARTY, 2005)

The modernization program aimed, among other things, to provide signal redundancy and improve positioning accuracy, signal availability, and system integrity (EL-RABBANY,

2002). Some of the signals introduced in GPS structure in the last 20 years are: a new military signal on L1 and L2 referred to as the M-code; a second civil signal on L2 referred to as L2C; a third civil signal on a new carrier frequency referred to as L5; a fourth civil signal referred to as L1C on the L1 carrier (AMERICA, 2022).

2.5 GPS Satellite Position

Information about the position of satellites plays a fundamental role in the process of computing the user position. The ideal satellite motion may be characterized by the classic two-body, central force-field problem developed by Johannes Kepler and Isaac Newton, respectively (MISRA; ENGE, 2006). Kepler's three laws of planetary motion applied to the Earth-orbiting satellite are stated as follows (TEUNISSEN; MONTENBRUCK, 2017):

1. The orbit of a satellite is an ellipse with the Earth located in one of its *foci*;
2. The radius vector covers a constant area per unit time interval;
3. The square of the orbital period increases proportionally with the third power of the mean distance from the center of the Earth.

The first law implies that to compute an accurate position of the satellite, the eccentricity of the orbit must be accounted for. The second law, known as the law of equal areas, states that the speed of the satellite is not constant along the orbit, moving faster when it is closer to the Earth, and slowing down as it moves away. The third law was proved by Newton, who showed that the constant of proportionality is related to the masses of both bodies and the gravitational constant, as follows (TEUNISSEN; MONTENBRUCK, 2017).

$$T^2 = \frac{4\pi^2}{G(M+m)} r^3, \tag{2.4}$$

where G is the universal constant of gravity, T is the orbital period and r is the mean orbital radius, M is the Earth's mass and m is the satellite's mass.

The motion of the satellite is governed by Newton's laws of motion. For a simple analysis, we can assume that the only force acting on the satellite is the Earth's gravitational force of attraction. Let us model the Earth as a point mass $M_{\oplus}$, and denote the position of the satellite with respect to the center of Earth by the vector $\mathbf{r}$, and its respective distance as $\|\mathbf{r}\| = r$. From

Newton's second law, we obtain the second-order differential equation of the satellite position vector relative to the center of Earth, namely (MISRA; ENGE, 2006):

$$\ddot{\mathbf{r}} + \frac{GM_{\oplus}}{r^3}\mathbf{r} = 0, \tag{2.5}$$

where $GM_{\oplus} = 3.986004415 \cdot 10^{14}\ m^3 s^{-2}$ is the Earth's gravitational constant, also represented as μ. The mass of the satellite was neglected in (2.5) since the mass of Earth is about 20 orders larger.

It should be noticed that performing the double integration of (2.5) will provide the instantaneous velocity and position of the satellite for a given time, introducing six constants of integration. It means that providing the initial condition of velocity and position for a time t_0, the orbit can be completely described for any time t. Alternatively, these six parameters can be characterized geometrically by Kepler's elements, of which three are used to describe the satellite orbit within the orbital plane, and the other three elements describe the orientation of the orbit with respect to the Earth (MISRA; ENGE, 2006).

As mentioned earlier, the satellites have an elliptical motion in the orbital plane, as depicted in Figure 2.4. The size of an ellipse is defined by its semi-major axis, a, and its semi-minor axis, b, while its shape is defined by the eccentricity, e_o. The Earth is placed in one of its *foci*, with distance ae_o from the ellipse center along the semi-major axis. The orbit closest point to the Earth's center of mass is the perigee, located along the semi-major axis. The direction of perigee points from the center of the ellipse passing through the center of the Earth. The satellite location is described by the true anomaly, ν, the angle formed counterclockwise from the direction of perigee to the SV's line of sight. Since ν does not vary linearly in time, two other parameters are used to represent satellite location, which are the eccentric anomaly, E, and the mean anomaly, M. The former is the angle measured from the center of the ellipse and the projection of satellite location in a circumscribed circle around the elliptical orbit (see Figure 2.4). The latter is a mathematical abstraction of the mean angular satellite motion, n (HOFMANN-WELLENHOF; LICHTENEGGER; WASLE, 2008). The relationship between theses three anomalies is given by:

$$M = M_0 + n(t^s_{st,a} - t_{oe}), \tag{2.6}$$

$$E = M + e_o \sin E, \tag{2.7}$$

$$\nu = \arctan_2 \left[\left(\frac{\sqrt{1-e_o^2}\sin E}{1-e_o \cos E} \right), \left(\frac{\cos E - e_o}{1-e_o \cos E} \right) \right], \tag{2.8}$$

where M_0 is the mean anomaly in the reference time of ephemeris t_{oe} and $n = \sqrt{\mu/a^3}$. Equation (2.7) is known as Kepler's equation, which is obtained from the analytical integration of (2.5), where a four-quadrant arctangent function must be used.

Figure 2.4 – Satellite orbit description, according to the Kepler's definitions.

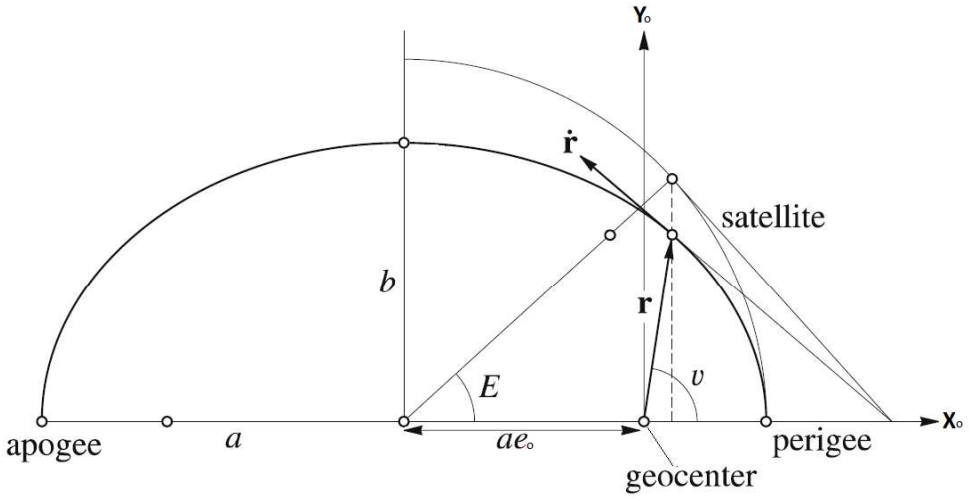

Source: Adapted from (HOFMANN-WELLENHOF; LICHTENEGGER; COLLINS, 2012)

The orientation of the orbital plane is illustrated in Figure 2.5 and it is characterized by the remaining Kepler's parameters. The inclination of the orbit, i, is the dihedral angle between the orbital plane and equatorial plane. According to Kaplan and Hegarty (2005), the orbital plane crosses the equatorial plane in two points, the ascending node and the descending node. The right ascension, Ω, is the angle between the direction of the ascending node and the Earth x-axis, which for an ECEF frame corresponds to the longitude of the ascending node at the reference time since ECEF rotates. Finally, the argument of perigee, ω, is the counterclockwise angle from the ascending node to the perigee.

In practice, however, satellite orbits are not a pure Keplerian motion due to disturbing accelerations coming from third-body gravitation forces (Sun and Moon), solar radiation pressure, magnetic field forces, relativistic effects, etc. These perturbations are treated as temporal variances in the six Kepler's parameters, introducing time dependence. Furthermore, the Earth's

Figure 2.5 – Satellite orbit orientation description according to the Kepler's definitions.

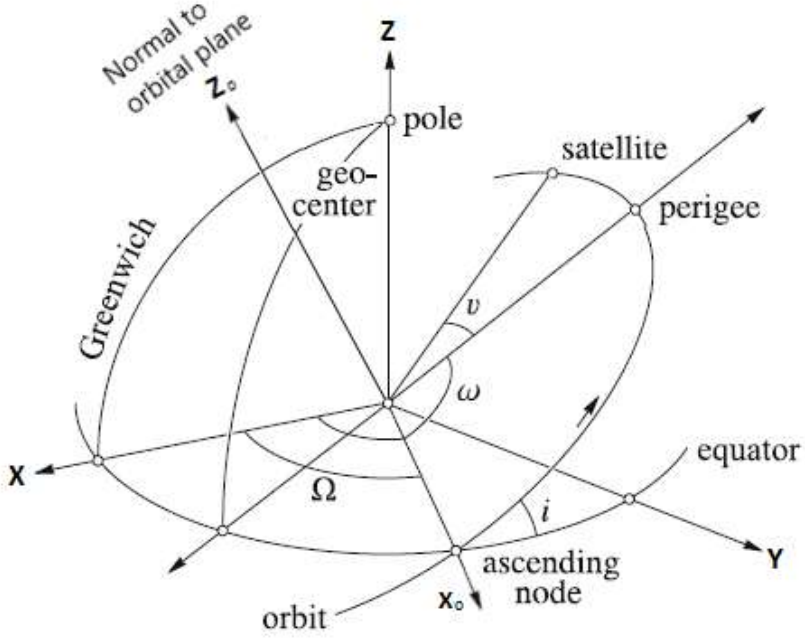

Source: Adapted from (HOFMANN-WELLENHOF; LICHTENEGGER; COLLINS, 2012)

gravitational field is not uniform and it is modeled by a spherical harmonic series in terms of satellite position. For this reason, an expanded set of *quasi-Kaplerian parameters* is introduced, consisting of 16 elements. The additional parameters are: reference time, three pairs of amplitude terms from the harmonic series model, rate of the right ascension, rate of the inclination, and correction to the mean motion (MISRA; ENGE, 2006).

According to Groves (2013), the task of determining the position of the satellite can be divided into two steps. First, we determine the position within the orbital coordinated frame, with its origin at the center of Earth, x^o- axis aligned with the direction of ascending node, z^o- axis normal to the orbital plane, and y^o- axis completing the orthogonal set (see Figure 2.5). The second step is a transformation of coordinates from orbital frame to ECEF.

The first step to compute the GPS satellite position in a given epoch is to determine the elapsed time from the reference time of ephemeris, t_{oe}, to the signal transmission time, $t^s_{st,a}$, which is given by:

$$\Delta t = t^s_{st,a} - t_{oe}. \tag{2.9}$$

In a pure Keplerian motion, the mean anomaly can be calculated to the time of the signal transmission using (2.6). As this is not the case, a correction of the mean motion, Δn, is broadcast in the navigation message, and should be considered during the computation of mean anomaly. The corrected mean anomaly, then, may be calculated as:

$$M = M_0 + (n + \Delta n)\Delta t. \tag{2.10}$$

Next, the eccentric anomaly is obtained from Kepler's equation (2.7), which does not have a closed-form solution. Thus, it must be solved iteratively. Teunissen and Montenbruck (2017) suggests an initial approximation of $E_0 = M$, where refined values can be obtained by Newton's method. Finally, the true anomaly is obtained using (2.8).

Having determined the true anomaly and the eccentric anomaly, we can find an expression for the satellite position vector expressed in polar coordinates (Equation 2.11), in terms of the radius, r^o_{os}, and argument of latitude, Φ, defined as the sum of the argument of perigee and true anomaly.

$$\Phi = \omega + \nu. \tag{2.11}$$

According to Groves (2013), the orbital radius varies as a function of eccentric anomaly, where second harmonic perturbations are applied as corrections to both terms. Thus, the corrected orbit radius and argument of latitude, u^o_{os}, are given by:

$$\begin{aligned} r^o_{os} &= a(1 - e_o \cos E) + C_{rs} \sin 2\Phi + C_{rc} \cos 2\Phi. \\ u^o_{os} &= \Phi + C_{us} \sin 2\Phi + C_{uc} \cos 2\Phi. \end{aligned} \tag{2.12}$$

where C_{rs}, C_{rc}, C_{us}, and C_{uc} are harmonic coefficients broadcast into navigation message.

Therefore, the position vector of the satellite expressed in polar coordinates referenced into orbital frame is:

$$x^o_{os} = r^o_{os} \cos u^o_{os}, \qquad y^o_{os} = r^o_{os} \sin u^o_{os}, \qquad z^o_{os} = 0. \tag{2.13}$$

Since the orbital and the ECEF frames have the same origin by definition, the transformation of coordinates may be obtained with the direction cosine matrix C^e_o, defined by the Euler angle rotation sequence from the ECEF to the orbital frame. For this scenario, the Euler rotation comprises a yaw rotation through the longitude of the ascending node, followed by a

roll rotation through the inclination angle. Then, the rotation matrix, C_o^e, for $\psi_{eo} = \Omega$, $\phi_{eo} = i$, and $\theta_{eo} = 0$ is:

$$C_o^e = \begin{pmatrix} \cos\Omega & -\cos i \sin\Omega & \sin i \sin\Omega \\ \sin\Omega & \cos i \cos\Omega & -\sin i \cos\Omega i \\ 0 & \sin i & \cos\Omega \end{pmatrix}, \tag{2.14}$$

where Ω and i are values at the time of signal transmission. For GPS system, these values are corrected with parameters broadcast in the navigation message as follows,

$$\Omega = \Omega_0 + (\dot{\Omega}_d - \omega_{ie})\Delta t + \omega_{ie} t_{oe}. \tag{2.15}$$

$$i = i_0 + \dot{i}_d \Delta t + C_{is} \sin 2\Phi + C_{ic} \cos 2\Phi. \tag{2.16}$$

where Ω_0 is the right ascension of the ascending node of the orbital plane at the weekly epoch, ω_{ie} is the Earth-rotation rate, $\dot{\Omega}_d$ is the rate of change of the longitude of the ascending node at the reference time (all transmitted as part of the navigation message), i_0 is the inclination angle at the reference time, $\dot{i}_d$ is the rate of inclination, and C_{is} and C_{ic} are amplitude terms of the harmonic series (all transmitted as part of the navigation message).

Therefore, the position vector of the GPS satellite referenced and resolved on the ECEF frame is:

$$\mathbf{r}_{es}^e = \begin{pmatrix} x_{os}^o \cos\Omega - y_{os}^o \cos i \sin\Omega \\ x_{os}^o \sin\Omega + y_{os}^o \cos i \cos\Omega \\ y_{os}^o \sin i \end{pmatrix}. \tag{2.17}$$

According to Groves (2013), velocity is defined as the rate of change of position with respect to a frame of reference, whether its change is a translation or a rotation. Hence, the following relation is valid:

$$\mathbf{v}_{es}^e = \dot{\mathbf{r}}_{es}^e \tag{2.18}$$

It means that by the differentiation of the position with respect to $t^s_{st,a}$, we can obtain the satellite velocity. Thus, differentiating (2.7), (2.8), (2.11), (2.12), and (2.13) gives the satellite position in an orbital frame,

$$\begin{aligned}
\dot{x}^o_{os} &= \dot{r}^o_{os}\cos u^o_{os} - r^o_{os}\dot{u}^o_{os}\sin u^o_{os} \\
\dot{y}^o_{os} &= \dot{r}^o_{os}\sin u^o_{os} + r^o_{os}\dot{u}^o_{os}\cos u^o_{os} \\
\dot{z}^o_{os} &= 0
\end{aligned} \tag{2.19}$$

$$\begin{aligned}
\dot{r}^o_{os} &= (ae_o\sin E)\dot{E} + 2(C_{rs}\cos 2\Phi - C_{rc}\sin 2\Phi) \\
\dot{u}^o_{os} &= (1 + 2C_{us}\cos 2\Phi - C_{uc}\sin 2\Phi)\dot{\Phi}
\end{aligned} \tag{2.20}$$

$$\dot{E} = \frac{n+\Delta n}{1-e_o\cos E} \tag{2.21}$$

$$\dot{\Phi} = \frac{\sin\nu}{\sin E}\dot{E} \tag{2.22}$$

Differentiating (2.15) and (2.16) gives

$$\dot{\Omega} = \dot{\Omega}_d - \omega_{ie} \tag{2.23}$$

$$\dot{i} = \dot{i}_d + 2(C_{is}\cos 2\Phi - C_{ic}\sin 2\Phi)\dot{\Phi} \tag{2.24}$$

Finally, differentiating (2.17) gives the ECEF-frame satellite velocity,

$$\mathbf{v}^e_{es} = \begin{pmatrix} \dot{x}^o_{os}\cos\Omega - \dot{y}^o_{os}\cos i\sin\Omega + i\dot{y}^o_{os}\sin i\sin\Omega \\ \dot{x}^o_{os} + \dot{y}^o_{os}\cos i\cos\Omega - i\dot{y}^o_{os}\sin i\cos\Omega \\ \dot{y}^o_{os}\sin i + i\dot{y}^o_{os}\cos i \end{pmatrix} + (\omega_{ie} - \dot{\Omega}_d)\begin{pmatrix} x^o_{os}\sin\Omega + y^o_{os}\cos i\cos\Omega \\ -x^o_{os}\cos\Omega + y^o_{os}\cos i\sin\Omega \\ 0 \end{pmatrix} \tag{2.25}$$

2.6 Error Sources

GNSS signals have very low power, and hence they are prone to several sources of errors. These errors have a significant deteriorating effect on GNSS positioning. Therefore, in order to obtain a better user position accuracy, these errors need to be addressed. According to

Lachapelle (1991), the pseudorange measurement is corrupted by seven main types of errors, namely: satellite orbital (ephemeris) error (E^s), satellite clock bias ($\delta\rho_c^s$), ionospheric delay (I^s), tropospheric delay (T^s), multipath error (M_a^s), receiver clock bias ($\delta\rho_c^a$), and receiver noise (η_a^s). The pseudorange observable model taking into account these errors may be expressed as

$$\rho_a^s = r_{as} + \delta\rho_c^a - \delta\rho_c^s + I^s + T^s + E^s + M_a^s + \eta_a^s, \tag{2.26}$$

where the true range between the EFEC receiver location $\mathbf{r}_{ea}^e$ and the EFEC satellite location $\mathbf{r}_{es}^e$ is

$$r_{as} = \left|\mathbf{C}_e^I \mathbf{r}_{es}^e - \mathbf{r}_{ea}^e\right|, \tag{2.27}$$

where $\mathbf{C}_e^I$ is the DCM that transforms the position vector $\mathbf{r}_{es}^e$ from ECEF coordinate frame to ECI frame, which is necessary to compensate the error in user position due to Earth's rotation during signal transit time, known as the Sagnac or Earth-rotation effect. Let I indicates the ECI frame synchronized with the ECEF frame at the time of signal arrival, then $\mathbf{C}_e^I$ is computed as

$$\mathbf{C}_e^I(t) = \begin{pmatrix} \cos\omega_{ie}(t-t_{sa}) & -\sin\omega_{ie}(t-t_{sa}) & 0 \\ \sin\omega_{ie}(t-t_{sa}) & \cos\omega_{ie}(t-t_{sa}) & 0 \\ 0 & 0 & 1 \end{pmatrix} \tag{2.28}$$

where ω_{ie} is the Earth rotation rate.

According to Kaplan and Hegarty (2005), the errors in (2.26) may be classified as those originated at satellites, those originated at the receiver, and those that are due to signal propagation. Another classification groups the latter into CME and NCME (FARRELL, 2008). The former are the spatially and timely correlated errors, i.e, the errors experienced by all receivers in the same vicinity and time frame. The latter are the errors that differ for each receiver. CME comprises the ephemeris error, satellite clock bias, ionospheric and tropospheric delay, and NCME comprises the receiver clock bias, multipath error and receiver noise. In the following subsections, a brief discussion of these errors will be provided.

2.6.1 Common-Mode Errors

GPS receivers calculate satellite position at the time of signal transmission based on the *quasi-Keplerian* parameters included in the navigation message, which are updated every

2 hours. These parameters are estimated at the control segment on the basis of measurements collected at the monitor stations. The orbit parameters estimates differ from true orbit since satellites are subjected to perturbations. This introduces some errors in the estimated satellite positions, known as *ephemeris errors*. An ephemeris error for a particular satellite is identical to all GNSS users worldwide, and it can be mitigated if global or local network corrections for the satellite position are available (KAPLAN; HEGARTY, 2005).

Time plays a core role into GNSS systems, since receivers generate measurements based mainly on measuring time. For this reason, satellites are equipped with very precise atomic clocks. Despite their accuracy, satellite clocks still drifts slightly from GNSS time. This deviation is known as *satellite clock error*, and is due to relativistic effects and accumulated effect of oscillator noise. The latter is mostly corrected for using three calibration coefficients broadcast in the navigation message. Despite their corrections, there are still residual satellite clock and ephemeris error, and their combined accuracy in terms of the annual root-mean-square signal-in-space range error is about 0.7 m for the GPS constellation (TEUNISSEN; MONTENBRUCK, 2017).

GNSS signals travel through the Earth's atmosphere towards receivers on or near the ground. When they travel through ionosphere (the upper ionized part of the atmosphere), they are refracted, i.e., there is a change in the signal propagation speed that causes a significant error in GNSS positioning (up to 45 m). This effect, known as *ionospheric delay*, is one of the most significant error sources, which, however, can be mitigated by linearly combining simultaneous measurements (either pseudoranges or carrier phases) on two frequencies. Alternatively, single-frequency receivers can use models to estimate the ionosphere propagation delay, such as Klobuchar model, which has its parameters transmitted in the GPS satellite navigation message (EL-RABBANY, 2002). According to Moorefield (2020), the value for residual ionospheric delays, averaged over the globe ranges from 9.8 m to 19.6 m.

GNSS signals are also refracted in the troposphere (the lower part of the Earth's atmosphere), effect known as *tropospheric delay*. The troposphere is a nondispersive medium, so all GNSS signals are delayed equally and are frequency independent. The tropospheric delay depends on the temperature, pressure, and humidity along the signal path through the troposphere. Typically, at sea level, zenith delay is about 2.4 m, rising to more than 24 m at an elevation angle of 5º (angle between local horizontal plane and satellite line-of-sight). There

are different analytical models used to estimate the tropospheric delays, such as Saastamoinen model and Hopfield model (MISRA; ENGE, 2006).

2.6.2 Noncommon-Mode Errors

GNSS receivers, in contrast to satellites, are equipped with inexpensive crystal clocks for commercial reasons, which are much less accurate when compared to satellite clocks. Consequently, the errors introduced in the pseudorange measurements due to *receiver clock error* are much larger than those due to satellite clock error. There are three ways to handle this issue. The first option, and less usual, is to use an external clock with better performance, such as cesium or rubidium clocks. As they are very expensive, this make their commercialization unaffordable for civilian users. The second solution, which is more common, is to estimate this error as an additional unknown parameter in the position estimation process. The third and last option is to differ measurements between satellites, creating the so called single-differenced observations. Since any two observations from a given receiver made at the same time have the same receiver clock errors, differencing these observables will eliminate the receiver clock bias from the new formed observables (EL-RABBANY, 2002).

GNSS signals are also subjected to reflection and diffraction like any other type of electromagnetic wave. This results in the so called *multipath error*, which is the reception of multiple reflected or diffracted replicas of the desired signal, along with the direct path signal. Multipath errors are highly location dependent, and most signal reflections occur within the surrounding environment, such as the ground, buildings, vehicles, or trees, where the signals may bounce off objects in vicinity, taking longer path than the direct signal. It results in an error in pseudorange measurements and thus affects the position estimation accuracy. To decrease the effects of multipath, the user can take some precautions, such as selecting an antenna with low gain at small elevations, and changing receiver settings to avoid using satellites at low elevation (KOS; MARKEZIC; POKRAJCIC, 2010).

Receiver noise error, finally, consists mostly of thermal noise intercepted by the antenna or produced by the internal components of the receiver. The magnitude of the ranging errors due to receiver noise is different for each tracking channel and depends on the signal-to-noise ratio of the signal assigned to the channel. The receiver noise is usually modeled as white and independent between both satellites and channels (FARRELL, 2008).

2.7 Receiver Position Estimation

As mentioned in Section 2.1, in order to provide the user with its three-dimensional position and the receiver clock bias, it is necessary the observation of at least four pseudorange measurements, resulting in a system of four or more nonlinear equations. These nonlinear equations can be solved for the unknowns employing a closed-form solution (LEVA, 1996), iterative techniques based on linearization, or filtering. In this Section, three common methods used for standalone GNSS positioning are presented.

2.7.1 Iterated Least Squares

The ILS method is commonly used for receiver position computation from pseudoranges (BORRE et al., 2007). It comes from the fact that the user position problem is characterized by a nonlinear and overdetermined system since there are generally more pseudorange measurements originated from different satellites than unknowns. Furthermore, the main goal is to find the position solution which is most consistent with the measurement stream, therefore, the ILS method presents itself as a good candidate for this optimization problem.

As discussed in Section 2.6, the pseudorange measurements are affected by different sources of errors. Corrections may be applied for some known errors, and the corrected pseudorange measurement can be written as:

$$\tilde{\rho}^{s}_{a,C} = \sqrt{[\mathbf{C}^{I}_{e}(\tilde{t}^{s}_{st,a})\hat{\mathbf{r}}^{e}_{es}(\tilde{t}^{s}_{sta}) - \hat{\mathbf{r}}^{e}_{ea}(t^{s}_{sa,a})]^{T}[\mathbf{C}^{I}_{e}(\tilde{t}^{s}_{st,a})\hat{\mathbf{r}}^{e}_{es}(\tilde{t}^{s}_{st,a}) - \hat{\mathbf{r}}^{e}_{ea}(t^{s}_{sa,a})]} + \delta\hat{\rho}^{a}_{c}(t^{s}_{sa,a}) + \delta\rho^{s+}_{a,\varepsilon}, \tag{2.29}$$

where $\delta\rho^{s+}_{a,\varepsilon}$ is the residual measurement, defined as the difference between the measured pseudorange and that predicted from the position solution.

The Equation (2.29) is nonlinear in the first term, so a linearization is made by generating a predicted ($^{-}$) receiver position, $\hat{\mathbf{r}}^{e-}_{ea}(\tilde{t}^{s}_{sa,a})$, and its clock bias, $\delta\hat{\rho}^{a-}_{c}$, from which a predicted pseudorange can be obtained as follows,

$$\tilde{\rho}^{s-}_{a,C} = \sqrt{[\mathbf{C}^{I}_{e}(\tilde{t}^{s}_{st,a})\hat{\mathbf{r}}^{e}_{e,s}(\tilde{t}^{s}_{st,a}) - \hat{\mathbf{r}}^{e-}_{e,a}(\tilde{t}^{s}_{sa,a})]^{T}[\mathbf{C}^{I}_{e}(\tilde{t}^{s}_{st,a})\hat{\mathbf{r}}^{e}_{e,s}(\tilde{t}^{s}_{st,a}) - \hat{\mathbf{r}}^{e-}_{e,a}(\tilde{t}^{s}_{sa,a})]} + \delta\hat{\rho}^{a-}_{c}. \tag{2.30}$$

The unknown user position and receiver clock offset are considered to consist of an predicted value and an incremental component,

$$\begin{aligned} x^e_{e,a} &= \hat{x}^{e-}_{e,a} + \Delta x \\ y^e_{e,a} &= \hat{y}^{e-}_{e,a} + \Delta y \\ z^e_{e,a} &= \hat{z}^{e-}_{e,a} + \Delta z \\ \delta\rho^a_c &= \delta\hat{\rho}^{a-}_c + \Delta\rho^a_c. \end{aligned} \tag{2.31}$$

Applying a first-order Taylor expansion about the predicted user position gives:

$$\rho^s_{a,C} = \hat{\rho}^{s-}_{a,C} - u^e_{as,x}\Delta x - u^e_{as,y}\Delta y - u^e_{as,z}\Delta z. \tag{2.32}$$

The Equation 2.32 is the pseudorange linearized about the receiver predicted position, and Δx, Δy, Δz, and $\Delta\rho^a_c$ are the unknowns to be determined. For a number of m simultaneous pseudorange measurements from satellites available to a given receiver, there will be m linear equations to solve the user position estimation problem, which can be written in a matrix format as follows

$$\overbrace{\begin{pmatrix} \tilde{\rho}^1_{a,C} - \hat{\rho}^{1,-}_{a,C} \\ \tilde{\rho}^2_{a,C} - \hat{\rho}^{2,-}_{a,C} \\ \vdots \\ \tilde{\rho}^m_{a,C} - \hat{\rho}^{m,-}_{a,C} \end{pmatrix}}^{\mathbf{Y}} = \overbrace{\begin{pmatrix} -u^e_{a1,x} & -u^e_{a1,y} & -u^e_{a1,z} & 1 \\ -u^e_{a2,x} & -u^e_{a2,y} & -u^e_{a2,z} & 1 \\ \vdots & \vdots & \vdots & \vdots \\ -u^e_{am,x} & -u^e_{am,y} & -u^e_{am,z} & 1 \end{pmatrix}}^{\mathbf{H^e_G}} \overbrace{\begin{pmatrix} \Delta x \\ \Delta y \\ \Delta z \\ \Delta\rho^a_c \end{pmatrix}}^{\mathbf{X}} + \overbrace{\begin{pmatrix} \rho^{1+}_{a,\varepsilon} \\ \rho^{2+}_{a,\varepsilon} \\ \vdots \\ \rho^{m+}_{a,\varepsilon} \end{pmatrix}}^{\xi} \tag{2.33}$$

where $\mathbf{H^e_G}$ is the geometric matrix, which characterizes the user-satellite geometry. Its terms are components of the line-of-sight unit vector, the vector that describes the direction from which the satellite signal arrives at the user antenna. The line-of-sight unit vector from the user antenna, a, to satellite, s, resolved about ECEF-frame axes, is:

$$\mathbf{u}^e_{as} \approx \frac{\mathbf{r}^e_{es}(t^s_{st,a}) - \mathbf{r}^e_{ea}(t^s_{sa,a})}{\left|\mathbf{r}^e_{es}(t^s_{st,a}) - \mathbf{r}^e_{ea}(t^s_{sa,a})\right|}. \tag{2.34}$$

The main goal is to find a solution for the set of linear equations in (2.33) which best fits the measurements, i.e., to find values for increments Δx, Δy, Δz, and $\Delta\rho^a_c$ that minimizes the

residual measurements. The criterion of Least Squares is used, which results in the minimum squared residual between the measurement vector $\mathbf{Y}$ and the estimated measurement matrix $\mathbf{H}_G^e$ based upon the estimate of $\mathbf{X}$ (KAPLAN; HEGARTY, 2005). In equations, the solution of this linear system is given by:

$$\hat{\mathbf{X}} = (\mathbf{H}_G^{e\,T}\mathbf{H}_G^e)^{-1}\mathbf{H}_G^{e\,T}\mathbf{Y}. \tag{2.35}$$

Once Δx, Δy, Δz, and $\Delta\rho_c^a$ have been properly determined with (2.35), they can be used to update ($^+$) the user position and clock bias estimates. Therefore, the position solution for the user is:

$$\begin{pmatrix} \hat{x}_{ea}^{e+} \\ \hat{y}_{ea}^{e+} \\ \hat{z}_{ea}^{e+} \\ \delta\hat{\rho}_c^{a+} \end{pmatrix} = \begin{pmatrix} \hat{x}_{ea}^{e-} \\ \hat{y}_{ea}^{e-} \\ \hat{z}_{ea}^{e-} \\ \delta\hat{\rho}_c^{a-} \end{pmatrix} + (\mathbf{H}_G^{e\,T}\mathbf{H}_G^e)^{-1}\mathbf{H}_G^{e\,T} \begin{pmatrix} \tilde{\rho}_{a,C}^1 - \hat{\rho}_{a,C}^{1,-} \\ \tilde{\rho}_{a,C}^2 - \hat{\rho}_{a,C}^{2,-} \\ \vdots \\ \tilde{\rho}_{a,C}^m - \hat{\rho}_{a,C}^{m,-} \end{pmatrix}. \tag{2.36}$$

2.7.2 Iterated Weighted Least Squares

According to Kaplan and Hegarty (2005), the effective uncertainty of the pseudorange measurement which is termed User Equivalent Range Error (UERE), comprises the statistical sum of the contributions from each of the error sources associated with the observable. The GNSS position uncertainty, in turn, is also affected by the effect of signal geometry, which is quantified using the Dilution of Precision (DOP) concept (FARRELL, 2008). Hence, the uncertainty of the position/time solution determined by GNSS is given by the error covariance matrix $\mathbf{P}$, which is expressed as:

$$\mathbf{P} = (\mathbf{H}_G^{e\,T}\mathbf{H}_G^e)^{-1}\sigma_\rho^2, \tag{2.37}$$

where σ_ρ^2 is the UERE variance and $(\mathbf{H}_G^{e\,T}\mathbf{H}_G^e)^{-1}$ is the matrix that contains in its diagonal elements, the terms D_x^2, D_y^2, D_z^2 and D_t^2, which are the square of the individual channel position and time DOPs, respectively.

The UERE varies according to the satellite elevation angle (between the satellite line-of-sight and the local horizontal plane). Satellites with small elevation angles have larger uncertainties if compared with satellites at zenith, as the signals travel a longer distance through the

ionosphere and troposphere and are corrupted for residual errors that were not properly compensated for. To minimize the effects of pseudorange measurements with large uncertainties, the Iterated Weighted Least Squares (IWLS) approach can be used to estimate the user position and receiver clock error. The IWLS position solution is:

$$\begin{pmatrix} \hat{x}_{ea}^{e+} \\ \hat{y}_{ea}^{e+} \\ \hat{z}_{ea}^{e+} \\ \delta\hat{\rho}_{c}^{a+} \end{pmatrix} = \begin{pmatrix} \hat{x}_{ea}^{e-} \\ \hat{y}_{ea}^{e-} \\ \hat{z}_{ea}^{e-} \\ \delta\hat{\rho}_{c}^{a-} \end{pmatrix} + (\mathbf{H}_G^{e\,T}\mathbf{C}_\rho^{-1}\mathbf{H}_G^{e})^{-1}\mathbf{H}_G^{e\,T}\mathbf{C}_\rho^{-1} \begin{pmatrix} \tilde{\rho}_{a,C}^{1} - \hat{\rho}_{a,C}^{1,-} \\ \tilde{\rho}_{a,C}^{2} - \hat{\rho}_{a,C}^{2,-} \\ \vdots \\ \tilde{\rho}_{a,C}^{m} - \hat{\rho}_{a,C}^{m,-} \end{pmatrix}, \tag{2.38}$$

where the diagonal elements of the measurement error covariance matrix, $\mathbf{C}_\rho$, are the predicted variances of each pseudorange error and the off-diagonal terms account for any correlations between the pseudorange measurement. Smaller variances in a measurement stream indicate greater reliability in that specific measurement. A commonly used simplifying assumption is that the components of the measurement error covariance matrix are identically distributed and independent, i.e.:

$$\mathbf{C}_\rho = \begin{bmatrix} \sigma_{\rho 1}^2 & 0 & \cdots & 0 \\ 0 & \sigma_{\rho 2}^2 & \cdots & 0 \\ \vdots & \vdots & \ddots & \vdots \\ 0 & 0 & \cdots & \sigma_{\rho m}^2 \end{bmatrix}. \tag{2.39}$$

A suitable model that is elevation-dependent to predict the pseudorange measurements uncertainties, $\sigma_{\rho j}$, is:

$$\sigma_{\rho j} = \frac{\sigma_{\rho Z}}{\sin(\theta_{nu}^{aj})}, \tag{2.40}$$

where $\sigma_{\rho Z}$ is a constant empirical UERE value for the pseudorange uncertainty when satellite is at zenith, and θ_{nu}^{aj} is the satellite j elevation angle.

The IWLS, as the ILS, should also be iterated in order to obtain a better estimation for position. A drawback of both approaches is that they are single-epoch (pointwise or yet, snapshot) navigation solutions, i.e., they use only the current set of ranging processor measurement to compute the user position and receiver clock bias, ignoring the past measurements, which may lead to noisy navigation estimates. To overcome this issue, the filtered navigation solution is presented in Section 2.7.3.

2.7.3 Extended Kalman Filter

So far, the methods described to determine user position and receiver clock error were of the type snapshot, according to which the parameter estimates are derived from the whole set of measurement data without prior estimates. A more sophisticated method for computing user position is the Kalman-filter-based estimation algorithm.

According to Groves (2013), the Kalman filter is an estimator that uses knowledge of the deterministic and statistical properties of the system parameters and measurements to obtain optimal estimates given the information available. The optimal weighting of the data in the Kalman filter is due to a set of uncertainties in its estimates and a measure of the correlations between them that is carried forward alongside the parameter estimates.

According to Farrell et al. (1996), the Kalman filter consists of two steps: I. system propagation (or prediction), where a dynamic model for the system and uncertainties are defined to predict how they will change over time; II. measurement update, where a received measurement stream is used to compute the measurement innovation (the difference between the true measurement vector and that computed from the state vector estimate), which updates the state vector.

In the GNSS filtered approach, the navigation solution comprises the Kalman filter state vector, whose definition varies according to the application. In general, there are eight states to be estimated, which encompass the user antenna position and velocity, the receiver clock offset and drift. Therefore, the following state vector is defined:

$$\mathbf{x}^e = [(\mathbf{r}^e_{ea})^T, (\mathbf{v}^e_{ea})^T, \delta\rho^a_c, \delta\dot{\rho}^a_c]^T \in \mathbb{R}^n, \tag{2.41}$$

where $n = 8$, $\mathbf{v}^e_{ea}$ is the rover velocity, and $\delta\dot{\rho}^a_c$ is the antenna clock drift.

The system model describes how the states are propagated forward to account for the user motion and receiver clock dynamics between the interval of received measurements. For GNSS navigation in an ECEF frame, the derivative of the position is the velocity, while the time derivative of the clock offset is the clock drift. Since velocity and clock drift are not functions of any other state, their time derivatives are zero. Therefore, the system model is given by

$$\begin{aligned} \dot{\mathbf{r}}^e_{ea} &= \mathbf{v}^e_{ea}, \qquad & \frac{\partial}{\partial t}\delta\rho^a_c &= \delta\dot{\rho}^a_c \\ \dot{\mathbf{v}}^e_{ea} &= 0, \qquad & \frac{\partial}{\partial t}\delta\dot{\rho}^a_c &= 0. \end{aligned} \tag{2.42}$$

The main sources of increased uncertainty on the state estimates are due to user motion, random walk on the receiver clock drift, and phase noise on the clock bias. The system noise, which represents the uncertainties in the Kalman filter's deterministic system model, for small propagation intervals is given by:

$$\mathbf{Q}_{k-1}^{e} = \begin{bmatrix} 0_{3,3} & 0_{3,3} & 0_{3,1} & 0_{3,1} \\ 0_{3,3} & \mathbf{S}_{a}^{e}\tau_s & 0_{3,1} & 0_{3,1} \\ 0_{1,3} & 0_{1,3} & S_{c\phi}^{a}\tau_s & 0 \\ 0_{1,3} & 0_{1,3} & 0 & S_{cf}^{a}\tau_s \end{bmatrix}. \tag{2.43}$$

where $\mathbf{S}_{a}^{e}$ is the acceleration Power Spectral Density (PSD) matrix, composed by horizontal (S_{aH}) and vertical (S_{aV}) acceleration PSDs, as expressed in (2.44), $S_{c\phi}^{a}$ and S_{cf}^{a} are the clock phase and frequency PSDs, respectively, and τ_s is the propagation interval.

$$\mathbf{S}_{a}^{e} = (\mathbf{C}_{e}^{n})^{T} \begin{pmatrix} S_{aH} & 0 & 0 \\ 0 & S_{aH} & 0 \\ 0 & 0 & S_{aV} \end{pmatrix} \mathbf{C}_{e}^{n} \tag{2.44}$$

where $\mathbf{C}_{e}^{n}$ is the ECEF to North-East-Down (NED) coordinate transformation matrix.

These PSD values depends on the dynamics of each specific application, and it rely on the designer's knowledge on the given problem to perform a suitable choice. According to Groves (2013), typical values for S_{aH} are around 1 $\mathrm{m^2\ s^{-3}}$ for a pedestrian or ship, 10 $\mathrm{m^2\ s^{-3}}$ for a car, and 100 $\mathrm{m^2\ s^{-3}}$ for a military aircraft. Typical values for temperature-compensated crystal oscillator, a common type of clock used in GNSS receivers, are $S_{cf}^{a} \approx 0.04\ \mathrm{m^2\ s^{-3}}$ and $S_{cf}^{a} \approx 0.01\ \mathrm{m^2\ s^{-1}}$.

The GNSS filtered navigation requires a non-zero initialization of the state estimates, therefore the states may be initialized using the ILS or WLS single-epoch navigation solution, as described in Sections 2.7.1 and 2.7.2, respectively.

Equations (2.42) and (2.43) represent the dynamic model of the Kalman filter that governs the prediction step of the navigation filter. For the update step, the measurement model is defined as in (2.29), and the measurement vector comprises the pseudoranges output by the GNSS ranging processor. Thus, for m satellites tracked:

$$\mathbf{z}_G = [\tilde{\rho}_{a,C}^{1}, \tilde{\rho}_{a,C}^{2}, \ldots \tilde{\rho}_{a,C}^{m}]^{T}, \tag{2.45}$$

where G denotes GNSS measurements and the subscript C indicates that the pseudoranges have been partially corrected (for the common mode errors).

Since the pseudoranges measurements are not linear functions of the states, a linearization of the filter's dynamic is performed aiming at making the measurements innovations linear functions of the state residuals. This transforms the filter in an Extended Kalman Filter (EFK), whose measurement innovation vector is given by

$$\delta \mathbf{z}_{G,k}^{-} = \mathbf{z}_{G,k} - h_g(\hat{\mathbf{x}}_k^{-}) \tag{2.46}$$

where h_g is the nonlinear pseudorange estimate function, which is based on the predicted state vector $\hat{\mathbf{x}}_k^{-}$:

$$h_g(\hat{\mathbf{x}}_k^{-}) = [\hat{\rho}_{a,C}^{1-}, \hat{\rho}_{a,C}^{2-}, ... \hat{\rho}_{a,C}^{m-}]^T. \tag{2.47}$$

The predicted pseudorange between rover a and satellite j is computed as in (2.30).

The measurement matrix $\mathbf{H}_G^e$, which is the geometric matrix that characterizes the user-satellite geometry is defined as:

$$\mathbf{H}_G^e = \begin{bmatrix} -u_{a1,x}^e & -u_{e}a1,y & -u_{a1,z}^e & 0 & 0 & 0 & 1 & 0 \\ -u_{a2,x}^e & -u_{a2,y}^e & -u_{a2,z}^e & 0 & 0 & 0 & 1 & 0 \\ \vdots & \vdots & \vdots & \vdots & \vdots & \vdots & \vdots & \vdots \\ -u_{am,x}^e & -u_{am,y}^e & -u_{am,z}^e & 0 & 0 & 0 & 1 & 0 \end{bmatrix}, \tag{2.48}$$

where $\mathbf{u}_{aj}^e$ is the rover-to-satellite j line-of-sight unit vector.

The measurement noise covariance matrix, which is used to weight the uncertainties of the pseudorange observables, is given by:

$$\mathbf{R} = \begin{bmatrix} \sigma_{\rho 1}^2 & 0 & \cdots & 0 \\ 0 & \sigma_{\rho 2}^2 & \cdots & 0 \\ \vdots & \vdots & \ddots & \vdots \\ 0 & 0 & \cdots & \sigma_{\rho m}^2 \end{bmatrix}, \tag{2.49}$$

where $\sigma_{\rho j}^2$ should take into account the satellite j elevation angle, since pseudorange uncertainty is expected to be larger for satellites with low elevation angle. Therefore, a suitable model for $\sigma_{\rho j}$ is the same as in (2.40).

2.8 Advanced Positioning Techniques

The positioning accuracy of the standalone GPS positioning is about 5 m to 10 m (MOOREFIELD, 2020). However, there are many applications that demand higher levels of accuracy, requiring advanced GNSS positioning techniques. Some of them are described in sequence.

2.8.1 Differential GNSS

The error sources discussed in Section 2.6 are responsible for limiting the accuracy attainable using GNSS. The errors with most significant impact on the pseudorange measurements are the common-mode errors, which are spatially and temporally correlated. One of the most common techniques used to mitigate these errors, and consequently improve the positioning accuracy, is the Differential GNSS (DGNSS) (TEUNISSEN, 1991). According to Farrell et al. (1996), this technique has the potential to reduce the spherical position error deviation to a submeter level.

The basic concept behind DGNSS relies on the high correlation between the errors corrupting the user (sometimes referred to as rover) equipment and a nearby reference (base) station, i.e., the fact that two or more receivers at the same vicinity essentially experiences the same common-mode errors (SEEBER, 2008). Since these errors change slowly in time and distance, if they can be estimated for a known location (reference station), this information can greatly benefit the nearby end user.

All DGNSS approaches consist of at least one reference or base station, which is a pre-surveyed facility equipped with both high quality receiver and communication link (e.g. radio frequency, internet, etc.). Due to the fact that the antenna location is stationary and its location known, the reference station tracks data of all satellites in view and can estimate differential corrections that are transmitted via communication link to the rover. The rover corrects its data, enabling significant enhancement on its position estimation accuracy, provided its receiver is sufficiently close to the reference station and the corrections are received in a timely fashion (TEUNISSEN; MONTENBRUCK, 2017). Figure 2.6 depicts this concept.

According to Seeber (2008), the common-mode error correlation decreases with base station (baseline) separation, i.e, the accuracy of DGNSS navigation solution decreases as the rover moves away from the reference station. Corrections are also time correlated, which means that the latency of the calibration data (difference time between the time-of-applicability and the time that is actually used by the rover) affects the quality of the corrections. In summary, higher

Figure 2.6 – Differential GNSS scenario with GNSS signals indicated by solid lines and DGNSS correction signals indicated by dashed lines.

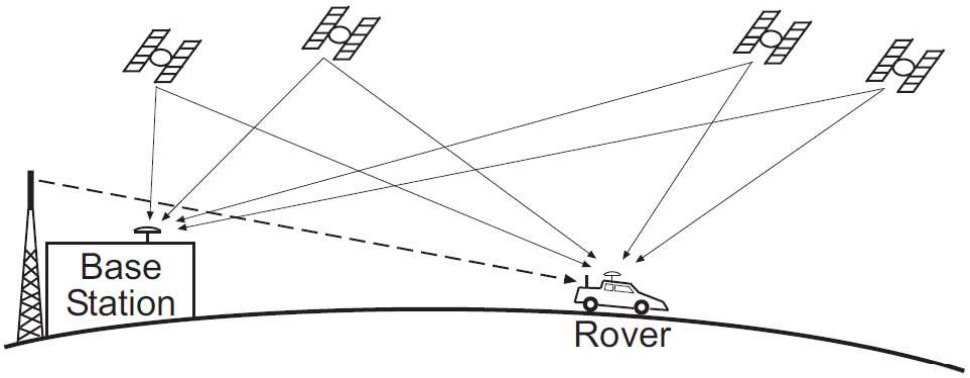

Source: (FARRELL, 2008)

accuracy is obtained with short baseline separation and high transmission rate of calibration data.

According to Kaplan and Hegarty (2005), DGNSS techniques may be categorized in different ways: as local-area and regional-area, and as code-based or carrier-based. The former category refers to the geographic area that they are intended to serve. The latter category refers to the type of DGNSS observable the DGNSS relies on, whether it is code pseudorange (code-based) or carrier phase (carrier-based). In the following subsections, code-base local-area and regional-area DGNSS will be discussed.

2.8.2 Local-area DGNSS

In a code-based, LADGNSS, a single reference station provides error corrections to rovers within its transmission range. There are two methods to generate these corrections. The first method, known as position correction, consists of computing coordinate differences (in latitude, longitude, and geodetic height) between the reference station surveyed position and the position estimated from GNSS measurements. The second and most common method consists of determining pseudorange corrections for each visible satellite. DGNSS concept using pseudorange corrections is explained in detail in the following mathematical treatment.

In order to generate DGNSS corrections, the reference station must have accurate knowledge of its own position. For a local base station at position $(x^e_{eb}, y^e_{eb}, z^e_{eb})$, the computed geometric distance, $\hat{r}_{bs}$, from the reference station b to a satellite s is:

$$\hat{r}_{bs} = \sqrt{(\hat{x}^e_{es} - x^e_{eb})^2 + (\hat{y}^e_{es} - y^e_{eb})^2 + (\hat{z}^e_{es} - z^e_{eb})^2}, \tag{2.50}$$

where $(\hat{x}^e_{es}, \hat{y}^e_{es}, \hat{z}^e_{es})$ is the satellite position computed using ephemeris data.

The reference station makes a pseudorange measurement, $\tilde{\rho}^s_b$, to the same satellite s, which contains the true geometric range, r_{bs}, along with the previously discussed errors:

$$\tilde{\rho}^s_b = r_{bs} + \delta\rho^b_c - \delta\rho^s_c + I^s + T^s + E^s + M^s_b + \eta^s_b, \tag{2.51}$$

The reference station then computes the differential correction by subtracting the pseudorange measurement from the computed geometric range:

$$\nabla\rho^s_{dc} = \hat{r}_{bs} - \tilde{\rho}^s_b. \tag{2.52}$$

Applying (2.51) in (2.52) yields the differential correction model, given by:

$$\nabla\rho^s_{dc} = -\delta\rho^b_c + \delta\rho^s_c - I^s - T^s - E^s - M^s_b - \eta^s_b. \tag{2.53}$$

The correction, defined in (2.53), is broadcast to all rovers near the reference station where it is added to the user receiver's pseudorange measurement to the same satellite s. The differential corrected pseudorange measurement for a rover a in the vicinity, $\tilde{\rho}^s_{a,DC}$, is given by:

$$\tilde{\rho}^s_{a,DC} = \tilde{\rho}^s_a + \nabla\rho^s_{dc}. \tag{2.54}$$

Therefore, substituting (2.26) and (2.53) into (2.54) yields the differential corrected pseudorange model:

$$\tilde{\rho}^s_{a,DC} = r_{as} + \Delta\rho^{ba}_c + \Delta I^s + \Delta T^s + \Delta M^s_{ba} + \Delta\eta^s_{ba}, \tag{2.55}$$

where $\Delta\rho^{ba}_c$ is the rover clock offset relative to the reference station clock, ΔI^s and ΔT^s are the difference in ionosphere and troposphere delays, respectively, as experienced at rover and reference station, and ΔM^s_{ba} and $\Delta\eta^s_{ba}$ are the difference in multipath and receiver noise errors, which are not common to rover and reference station.

Analyzing (2.55), one can see that ephemeris and satellite clock errors are canceled out since reference station and rover are using the same satellite to obtain pseudorange measurements. The terms ΔI^s and ΔT^s are expected to be negligible when the latency between computation and the effective application of correction is short, and when the baseline distance between rover and reference station is small, so that both receivers should experience same ef-

fects in ionosphere and troposphere delays. Finally, it should be noted that the multipath errors and receiver noise combinations of both rover and base station directly affect the computed correction and cannot be mitigated in differential mode, thus, other techniques must be applied to mitigate these effects since they are not common to the receivers. Therefore, considering a baseline distance between receivers to be close enough so that ionospheric and tropospheric delay may be canceled out, the differential pseudorange model can be expressed as (time dependency of the variables has been omitted, for brevity):

$$\rho^s_{a,DC} = \left|\mathbf{C}^I_e \mathbf{r}^e_{es} - \mathbf{r}^e_{ea}\right| + \Delta\rho^{ba}_c + \Delta M^s_{ba} + \Delta\eta^s_{ba}. \tag{2.56}$$

After applying the differential corrections, the rover position may be determined with corrected pseudorange measurements from all satellites available in place of original measurements, applying the same methods as for standalone GNSS positioning discussed in subsection 2.7. For DGNSS positioning estimation using EKF, the position solution is obtained as described in Section 2.7.3, where the state vector is still composed by eight states to be estimated, namely: three-dimensional user position, three-dimensional user velocity, differential receiver clock bias and differential receiver clock drift. The system is still governed by the dynamic model defined in (2.42), as the uncertainties in the deterministic system model are based on the same PSDs as defined in (2.43) and (2.44). The measurement vector now comprises the differential corrected pseudoranges:

$$\mathbf{z}_G = [\rho^1_{a,DC}, \rho^2_{a,DC}, ..., \rho^m_{a,DC}]^T. \tag{2.57}$$

The measurement innovation vector is defined as in (2.46), where the nonlinear pseudorange estimate function is based on the predicted differential corrected pseudoranges:

$$h_g(\hat{\mathbf{x}}^-_k) = [\hat{\rho}^{1-}_{a,DC}, \hat{\rho}^{2-}_{a,DC}, ...\hat{\rho}^{m-}_{a,DC}]^T. \tag{2.58}$$

Finally, the geometric matrix, $\mathbf{H}^e_G$, and measurement noise covariance matrix, $\mathbf{R}$, are still given as in (2.48) and (2.49), respectively.

The clock offset produced by the EKF position solution is the difference between the rover's clock error and the reference station clock error. Therefore, if accurate time of rover clock is desirable, the reference station clock offset may be estimated using standard position solution techniques and then removed from the correction. Since DGNSS corrections are spa-

tially correlated, the improvement in positioning accuracy is restricted, theoretically, to small baseline distances when Local-area DGNSS is used. To overcome this problem, Regional-area DGNSS system is a candidate.

2.8.2.1 Regional-area DGNSS

To extend the coverage over which LADGNSS corrections can be used without the decorrelation of errors due to spatial separation between rover and reference station, the RADGNSS approach may be applied. It has the same principle of LADGNSS, but instead of employing only one reference station, three or more bases are distributed along the perimeter of the covered region. This network of reference stations generates corrections and broadcasts them for an extended area.

Since errors in the broadcast corrections grow as the distance from the station increase, the main idea is to penalize the corrections originated from bases that are farther from the rover, as they tend to be less effective. This is made by adding weights to the corrections, which are inversely proportional to the geometric distance between rover and station, so that the largest weight is given to the closest station, and the smallest weight, to the farthest base. In equations, the corrections ($\nabla\rho_{dc}$) from multiple reference stations combined are given by:

$$\nabla\rho^{s}_{dc} = \sum_{i} W_i \nabla\rho^{s}_{dc,i}, \quad \sum_{i} W_i = 1. \tag{2.59}$$

where W_i is the weight for the i^{th} station.

The error introduced by each reference station is thus diluted by its weight, allowing the rover to have greater accuracy in its position solution when compared to the LADGNSS approach.

An alternative user's position estimation using multiple reference station is presented by Lapucha and Huff (1992). The user position is determined individually with pseudorange corrections coming from each base. Then, the final user position is computed using a weighted average of the individual position estimates, allowing an equally accurate estimate of the position.

2.8.3 Relative RGNSS

The basic idea behind Relative GNSS (RGNSS) is to determine the user's position with respect to another reference point. Therefore, RGNSS approach still needs a reference station equipped with a high quality GNSS receiver, but unlike DGNSS positioning, which computes corrections in pseudoranges to be broadcast, in RGNSS positioning, the reference station broadcasts measurements (raw observables) of all satellites in view. The rover, in sequence, forms differences between its own measurements and those received from the reference station, which are used in position estimation algorithms, so that the rover position relative to the reference station can be determined, instead of the rover absolute position. Basically, in relative positioning, the vector between the user and the reference station, known as baseline, is estimated, instead of the rover absolute position. As, in general, the coordinates of the reference station are well known, the absolute position of the rover can also be obtained.

According to Teunissen and Montenbruck (2017), the differenced observables used in RGNSS can be classified in three different ways: I. single-differences, which are formed by taking the difference of the measurements between receivers and satellites at the same epoch; II. double-differences, which are formed by subtracting the single differences from two different satellites; III. triple-differences, which are formed by subtracting two double differences at different epochs. In this work, only single and double-differenced observables are discussed.

2.8.3.1 Single-Differenced RGNSS

Single differences between receivers are formed by subtracting the measurements from two GNSS receivers simultaneously tracking a same satellite. For short baselines between receivers, satellite-related and atmospheric-related pseudorange errors are similar, allowing the effect of these errors to be reduced or removed significantly with this linear combination, as depicted in Fig. 2.7.

Let the GNSS pseudorange observables from satellite s, measured simultaneously at the reference b and rover a, be modeled, respectively, as:

$$\tilde{\rho}_b^s = r_{bs} + \delta\rho_c^r - \delta\rho_c^s + I^s + T^s + E^s + M_b^s + \eta_b^s, \tag{2.60}$$

$$\tilde{\rho}_a^s = r_{as} + \delta\rho_c^a - \delta\rho_c^s + I^s + T^s + E^s + M_a^s + \eta_a^s. \tag{2.61}$$

Figure 2.7 – Atmospheric effect on GNSS signals for between-receivers single difference

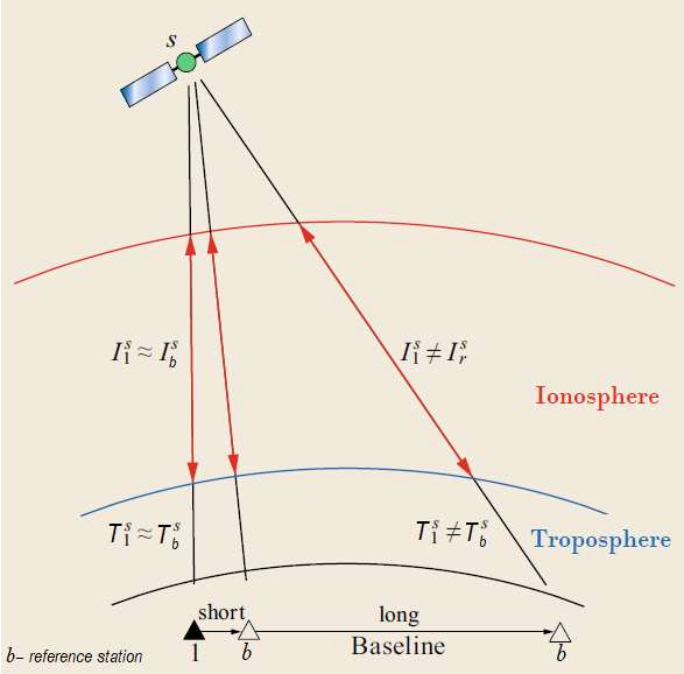

Source: adapted from (TEUNISSEN; MONTENBRUCK, 2017)

If the reference station broadcast its absolute pseudorange measurements, the rover in the vicinity can compute the following single-differenced observables:

$$\Delta\tilde{\rho}_{ba}^{s} = \tilde{\rho}_{a}^{s} - \tilde{\rho}_{b}^{s}. \tag{2.62}$$

Substituting (2.60) and (2.61) into (2.62), and assuming the user and reference station are close enough to each other, the single-differenced pseudorange model is given by:

$$\Delta\tilde{\rho}_{ba}^{s} = -u_{as}^{e} r_{ba}^{e} + \Delta\hat{\rho}_{c}^{ba} + \Delta M_{ba}^{s} + \Delta\eta_{ba}^{s}. \tag{2.63}$$

Analyzing (2.63), it can be noticed that when relative positioning is applied, the GNSS common-mode errors ($\delta\rho_c^s, I^s, T^s, E^s$) are canceled out, as in differential positioning. However, this cancellation is valid solely when the rover's latency to access the reference station measurements is short, and when the physical separation (baseline) between the latter is within a certain range so that the relative terms of ionosphere, troposphere and Sagnac corrections can be assumed negligible. The same methods discussed in Section 2.7 may be applied to compute rover's position estimate based on single-differenced pseudorange observables. Nevertheless,

RGNSS deals with relative positioning, thus, for position estimation using EKF, the state vector is defined as:

$$\mathbf{x}^e = [(\mathbf{r}^e_{ba})^T, (\mathbf{v}^e_{ba})^T, \Delta\rho^{ba}_c, \Delta\dot{\rho}^{ba}_c]^T \in \mathbb{R}^n, \tag{2.64}$$

where $n = 8$, $\mathbf{r}^e_{ba}$ is the rover position relative to the reference station, $\mathbf{v}^e_{ba}$ is the rover velocity relative to the reference station, and $\delta\dot{\rho}^{ba}_c$ is the rover clock drift relative to the reference station.

The same state model adopted in Section 2.7.3 for GNSS positioning can be applied for RGNSS purposes, i.e, the dynamic of state variables in (2.64) is governed by equations in (2.42). The acceleration PSD matrix in (2.44) is also the same for this approach.

The EFK measurement vector now comprises single-differenced pseudoranges:

$$\mathbf{z}_G = [\Delta\tilde{\rho}^1_{ba,R}, \Delta\tilde{\rho}^2_{ba,R}, ...\Delta\tilde{\rho}^m_{ba,R})]^T. \tag{2.65}$$

The measurement innovation vector is defined as in (2.46), where the single-differenced pseudorange estimate is now function of satellite ($\hat{\mathbf{r}}^{e-}_{ej}$), rover ($\hat{\mathbf{r}}^{e-}_{ea}$) and reference station ($\hat{\mathbf{r}}^{e-}_{eb}$) estimated positions, namely:

$$\Delta\hat{\rho}^{j-}_{ba} = \left|\mathbf{C}^I_e\hat{\mathbf{r}}^{e-}_{ej} - \hat{\mathbf{r}}^{e-}_{ea}\right| - \left|\mathbf{C}^I_e\hat{\mathbf{r}}^{e-}_{ej} - \hat{\mathbf{r}}^{e-}_{eb}\right| + \Delta\hat{\rho}^{ba-}_c. \tag{2.66}$$

The measurement matrix, H^e_G, is still given as in (2.48), and the measurement noise covariance matrix is two times as that given in (2.49), since it is performed a differentiation between observables. This shows that single-differences are still uncorrelated among themselves.

The EKF-based RGNSS position solution can be accomplished with higher accuracy since the only errors left in the model (2.63) are the errors due to receiver noise and multipath. However, the position solution will be the rover's position with respect to the reference station, $\hat{\mathbf{r}}^e_{ba}$. When the Earth's relative position is required and the reference station position is known, it is straightforward to compute the former as the sum of the reference position and the estimated relative position vector.

2.8.3.2 Double-Differenced RGNSS

Double differences, in turn, can be formed by subtracting, from the single-differenced observables from all satellites, the single-differenced pseudorange of a specific satellite p, re-

ferred to as pivot satellite (generally the one with highest elevation angle), as depicted in Fig. 2.8.

Figure 2.8 – Double difference of observations from receiver *a* and reference station *b* and satellites *s* and *p*.

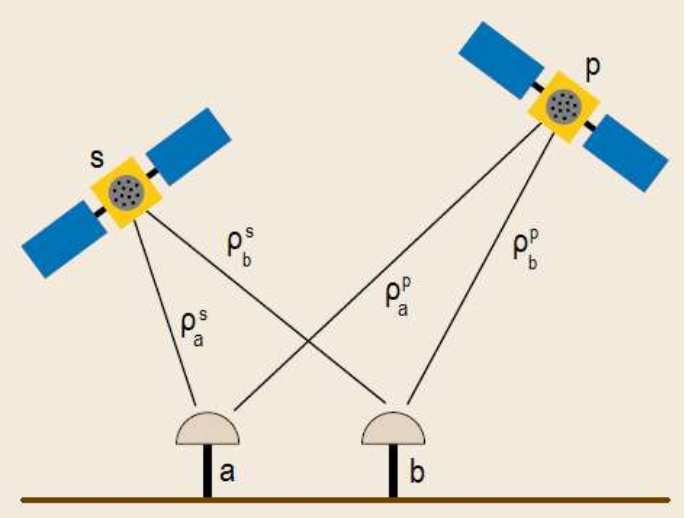

Source: adapted from (TEUNISSEN; MONTENBRUCK, 2017)

Therefore, the DD pseudorange may be defined as follows:

$$\nabla\Delta\tilde{\rho}_{ba}^{ps} = \tilde{\rho}_{a}^{s} - \tilde{\rho}_{b}^{s} + \tilde{\rho}_{b}^{p} - \tilde{\rho}_{a}^{p}. \tag{2.67}$$

Substituting (2.60) and (2.61) into (2.67), yields the double-differenced pseudorange model:

$$\nabla\Delta\rho_{ba}^{ps} = -(\mathbf{u}_{as}^{e} - \mathbf{u}_{ap}^{e})^{T}\mathbf{r}_{ba}^{e} + \nabla\Delta M_{ba}^{ps} + \nabla\Delta\eta_{ba}^{ps}. \tag{2.68}$$

Analyzing (2.68), note that the common-mode errors were canceled out due to between-receiver single-difference operation, and the receiver clock error has been removed due the single-difference between satellites operation. At least three double-differenced observables are required to estimate the user position, therefore, as in standalone approach, four satellites are still required. Equation (2.68) can be solved using the approaches discussed in Section 2.7. For EKF solution, the state vector now comprises only six states to be estimated (which are the three-dimensional relative position and three-dimensional relative velocity), defined as:

$$\mathbf{x}^{e} = [(\mathbf{r}_{ba}^{e})^{T}, (\mathbf{v}_{ba}^{e})^{T}]^{T} \in \mathbb{R}^{n}, \tag{2.69}$$

where $n = 6$.

The dynamic model is given by:

$$\dot{\mathbf{r}}_{ba}^{e} = \mathbf{v}_{ba}^{e}, \quad \dot{\mathbf{v}}_{ba}^{e} = 0. \tag{2.70}$$

The same acceleration PSD matrix of (2.44) is the one used for this approach. The EFK measurement vector now comprises double-differenced pseudoranges:

$$\mathbf{z}_{G} = [\nabla\Delta\tilde{\rho}_{ba,R}^{p1}, \nabla\Delta\tilde{\rho}_{ba,R}^{p2}, ...\nabla\Delta\tilde{\rho}_{ba,R}^{pm})]^{T}, \tag{2.71}$$

The measurement innovation vector is defined again as in (2.46), where the double-differenced pseudorange estimate are now function of satellite:

$$\begin{aligned}\Delta\nabla\hat{\rho}_{ra,R}^{s-} = &\left\|\mathbf{C}_{e}^{I}\hat{\mathbf{r}}_{es}^{e-} - \hat{\mathbf{r}}_{ea}^{e-}\right\| - \left\|\mathbf{C}_{e}^{I}\hat{\mathbf{r}}_{ep}^{e-} - \hat{\mathbf{r}}_{ea}^{e-}\right\| \\ &- \left\|\mathbf{C}_{e}^{I}\hat{\mathbf{r}}_{es}^{e-} - \hat{\mathbf{r}}_{er}^{e-}\right\| + \left\|\mathbf{C}_{e}^{I}\hat{\mathbf{r}}_{ep}^{e-} - \hat{\mathbf{r}}_{er}^{e-}\right\|.\end{aligned} \tag{2.72}$$

The geometric matrix, $\mathbf{H}_G^e$, now contains rows defined by $(\mathbf{u}_{aj}^e - \mathbf{u}_{ap}^e)$, $j \in 1,...,m$. In contrast to GNSS solution, $\mathbf{H}_G^e$ does not include a column for the receiver clock bias and drift, as these terms are canceled out during double-difference operation. Then,

$$\mathbf{H}_G^e = -\begin{bmatrix} (u_{a1,x}^e - u_{ap,x}^e) & (u_{a1,y}^e - u_{ap,y}^e) & (u_{a1,z}^e - u_{ap,z}^e) & 0 & 0 & 0 \\ (u_{a2,x}^e - u_{ap,x}^e) & (u_{a2,y}^e - u_{ap,y}^e) & (u_{a2,z}^e - u_{ap,z}^e) & 0 & 0 & 0 \\ \vdots & \vdots & \vdots & \vdots & \vdots & \vdots \\ (u_{am,x}^e - u_{ap,x}^e) & (u_{am,y}^e - u_{ap,y}^e) & (u_{am,z}^e - u_{ap,z}^e) & 0 & 0 & 0 \end{bmatrix}. \tag{2.73}$$

Finally, since the satellite p is used as pivot by subtracting its single-differenced observables from all satellites in view, this results in the double-differenced pseudoranges having cross-correlated noise processes. Therefore, the measurement noise covariance matrix, which is used to weight the uncertainties of the double-differenced pseudorange observables, is given by:

$$\mathbf{R} = \begin{bmatrix} 4\sigma_{\rho 1}^2 & 2\sigma_{\rho 1} * \sigma_{\rho 2} & \cdots & 2\sigma_{\rho 1} * \sigma_{\rho n} \\ 2\sigma_{\rho 2} * \sigma_{\rho 1} & 4\sigma_{\rho 2}^2 & \cdots & 2\sigma_{\rho 2} * \sigma_{\rho n} \\ \vdots & \vdots & \ddots & \vdots \\ 2\sigma_{\rho m} * \sigma_{\rho 1} & 2\sigma_{\rho m} * \sigma_{\rho 2} & \cdots & 4\sigma_{\rho m}^2 \end{bmatrix}. \tag{2.74}$$

Although double-differenced RGNSS is effective in removing common-mode errors along with receiver clock errors, it cannot remove the non-common mode errors, which are the double-differenced multipath and receiver tracking noise error. The main advantages of double-differencing techniques is that clock modeling is no longer required and various small receiver error terms are removed. The drawbacks are the processing of cross-correlated measurements, and the increase in range noise.

3 CONCLUSION

Location information is essential to our everyday lives. From home addresses, to transport systems that allow us to travel, accurate location information is fundamental. In the first part of this work, a brief introduction including the scope wherein this work is inserted, its relevance, organization, and the summary of the main contributions, has been provided. A short review on fundamental topics in Global Navigation Satellite Systems (GNSS) positioning was introduced. These systems allow the user equipped with proper receiver to estimate its own position at global coverage in a affordable way. The basic concepts of GNSS position estimation and its architecture were discussed. Furthermore, the main constellations that compose the GNSSs and their features were presented, namely: GPS (USA), GLONASS (Russia), Galileo (Europe), and BeiDou (China). Next, the main types of error that corrupt the GNSS positioning accuracy were introduced. They can be classified into Common-Mode Errors (CME) or Noncommon-Mode Errors (NCME). The former is related to the errors experienced by all receivers in the same vicinity and time frame, and the latter has an individual degradation effect for each receiver.

As of some applications require more accurate position estimates, the errors that corrupt GNSS positioning needs to be addressed. Two Advanced positioning techniques that mitigate the common-mode errors (the type of error that have the most impact in positioning accuracy) were presented, namely Differential GNSS (DGNSS) and Relative GNSS (RGNSS). Both approaches take advantage of the temporal and spatial correlation of the CME, so that the accuracy of the user's final position estimate can be improved. The main focus of this work was to provide a comprehensive analysis of how the communication latency and baseline separation between receivers impacts on the accuracy of RGNSS positioning in order to obtain a final position estimate at submetric level.

The second part of this work presents experimental results where real GNSS data was used during the experiment. The first analysis was a brief comparison between DGNSS and RGNSS techniques. The second analysis consisted in the study of the impact of baseline separation between two high-performance GNSS receivers in a stationary scenario. Next, again a high-performance GNSS receiver was used in a stationary scenario but now the focus was the impact of communication latency on the final user's position estimate. Finally, the last analysis was focused on the impact of both factors (baseline separation and communication latency) on the position estimate of a moving rover equipped with low-cost GNSS receiver.

In Paper I, simulated tests were conducted with GNSS, DGNSS and RGNSS algorithms, such that simulated GNSS data were generated and purposely corrupted in order to evaluate and compare their performances. We verified that RGNSS and DGNSS performed better in comparison to GNSS, as expected, since these approaches mitigate the effect of the common-mode errors present in pseudorange measurements . In sequence, DGNSS results were compared with RGNSS solution, and the latter has showed a better performance over DGNSS in terms of position accuracy for all error criteria established in this work. The RGNSS accuracy for total position estimation was 3 m at 99.7 % of probability (3σ), while DGNSS accuracy for the same criteria was 5.78 m at 99.7% of probability (3σ).

Paper II presents an experimental test, such that real GNSS data collected on stations belonging to RBMC were used with RGNSS algorithm to examine the degradation effects on positioning accuracy as functions of baseline separation distance between two GNSS receivers in a stationary scenario. Results demonstrated that horizontal position estimation accuracy is achievable at 1 meter level at 68% of probability (3σ) using Double-Differenced RGNSS approach with a reference station spaced at up to 2157 km. This shows that RGNSS is effective to correct common-mode errors for receivers in a wide range, differently from what the literature suggests.

Paper III conducts a similar experiment using real GNSS data belonging to RBMC to evaluate how communication latency between rover and reference station affect position estimation accuracy on RGNSS positioning approach with stationary receivers. Results demonstrated that horizontal position estimation accuracy is achievable at 1 meter level (1 σ) with latency up to 1500 s. This shows that RGNSS is effective to correct common-mode errors and it has proven to be more robustness than Differential GNSS (DGNSS) in terms of latency sensitivity.

Finally, Paper IV addressed the effect of both baseline separation and communication latency between a moving rover and reference station receivers, two common degradation factors of Relative Global Navigation System (RGNSS) position accuracy. A radio-controlled robot was equipped with a low-cost GNSS receiver to evaluate the performance of RGNSS technique in a dynamic scenario. Results showed that the Society of Automotive Engineers (SAE) J2945 standard that specifies horizontal accuracy of 1.5 m at 1 σ is achievable for latency up to 3000 s and baseline separation of 1441.826 km.

As suggestions for future works, the authors plan to investigate Real-Time Precise Point Positioning (RT-PPP), which consists of using precise corrections of common-mode errors pro-

duced by specialized institutions, such as International GNSS Service (IGS). Another topic of interest is the integration between Inertial Navigation Systems (INSs) and GNSSs as they are complementary in terms of advantages/drawbacks.

REFERENCES

AKOS, D. et al. GNSS album: Images and spectral signatures of the new GNSS signals. **Inside GNSS**, v. 1, n. 4, p. 46–56, 2006.

AMERICA, U. S. of. **Control Segment Elements**. 2021. <https://www.gps.gov/systems/gps/control/>. GPS is operated and maintained by the U.S. Air Force. GPS.gov is maintained by the National Coordination Office for Space-Based Positioning, Navigation, and Timing. Accessed: 2022-02-10.

AMERICA, U. S. of. **Current and Future Satellite Generations**. 2022. <https://www.gps.gov/systems/gps/space/>. GPS is operated and maintained by the U.S. Air Force. GPS.gov is maintained by the National Coordination Office for Space-Based Positioning, Navigation, and Timing. Accessed: 2022-04-18.

BORRE, K. et al. **A software-defined GPS and Galileo receiver: a single-frequency approach**. [S.l.]: Springer Science & Business Media, 2007.

CARVALHO, G. S.; SILVA, F. O. Performance analysis of relative gps positioning as function of communication latency. In: IEEE. **2021 Latin American Robotics Symposium (LARS), 2021 Brazilian Symposium on Robotics (SBR), and 2021 Workshop on Robotics in Education (WRE)**. [S.l.], 2021. p. 252–257.

CARVALHO, G. S. et al. Performance analysis of code-based relative gps positioning as function of baseline separation. In: IEEE. **2020 Latin American Robotics Symposium (LARS), 2020 Brazilian Symposium on Robotics (SBR) and 2020 Workshop on Robotics in Education (WRE)**. [S.l.], 2020. p. 1–6.

CHINA, P. R. of. **Development of the BeiDou Navigation Satellite System**. 2019. <http://en.beidou.gov.cn/SYSTEMS/Officialdocument/>. Beidou is operated and maintained by the China Satellite Navigation Office. Accessed: 2022-01-25.

COMMISSION, E. **Galileo**. <https://www.esa.int/Applications/Navigation/Galileo>, year = 2022, note = Galileo is operated by European GNSS Agency and maintained by European Space Agency. Accessed: 2022-04-15.

DORIDES, C. **GNSS user technology report**. 2018. <https://www.gsa.europa.eu/european-gnss/gnss-market/gnss-user-technology-report>. Accessed: 2020-01-15.

DORSEY, A. et al. **GPS system segments**. [S.l.]: Understanding GPS—principles and applications, 2nd edn. Artech House, Norwood, 2006. 67–112 p.

EL-RABBANY, A. **Introduction to GPS: the global positioning system**. [S.l.]: Artech house, 2002.

FARRELL, J. **Aided navigation: GPS with high rate sensors**. [S.l.]: McGraw-Hill, Inc., 2008.

FARRELL, J. et al. Differential GPS with latency compensation for autonomous navigation. In: IEEE. **Proceedings of the 1996 IEEE International Symposium on Intelligent Control**. [S.l.], 1996. p. 20–24.

FEAIRHELLER, S.; CLARK, R. **Other satellite navigation systems**. [S.l.: s.n.], 2006. 595–634 p.

GOLD, R. Optimal binary sequences for spread spectrum multiplexing (corresp.). **IEEE Transactions on information theory**, IEEE, v. 13, n. 4, p. 619–621, 1967.

GRAAS, F. V.; BRAASCH, M. S. Selective availability. **Global Positioning System: Theory and applications.**, v. 1, p. 601–621, 1996.

GREWAL, M. S.; ANDREWS, A. P.; BARTONE, C. G. **Global navigation satellite systems, inertial navigation, and integration**. 3rd. ed. [S.l.]: John Wiley & Sons, 2013.

GROVES, P. D. **Principles of GNSS, inertial, and multisensor integrated navigation systems**. 2nd. ed. [S.l.]: Artech house, 2013.

HEIN, G. W. **From GPS and GLONASS via EGNOS to Galileo–Positioning and Navigation in the Third Millennium**. [S.l.]: Springer, 2000. v. 3. 39–47 p.

HOFMANN-WELLENHOF, B.; LICHTENEGGER, H.; COLLINS, J. **Global positioning system: theory and practice**. [S.l.]: Springer Science & Business Media, 2012.

HOFMANN-WELLENHOF, B.; LICHTENEGGER, H.; WASLE, E. **GNSS–global navigation satellite systems: GPS, GLONASS, Galileo, and more**. [S.l.]: Springer Science & Business Media, 2008.

KAPLAN, E.; HEGARTY, C. **Understanding GPS: principles and applications**. [S.l.]: Artech house, 2005.

KOS, T.; MARKEZIC, I.; POKRAJCIC, J. Effects of multipath reception on GPS positioning performance. In: IEEE. **Proceedings ELMAR-2010**. [S.l.], 2010. p. 399–402.

LACHAPELLE, G. **GPS observables and error sources for kinematic positioning**. [S.l.]: Springer, 1991. 17–26 p.

LAPUCHA, D.; HUFF, M. Multi-site real-time dgps system using starfix link; operational results. In: **Proceedings of the 5th International Technical Meeting of the Satellite Division of The Institute of Navigation (ION GPS 1992)**. [S.l.: s.n.], 1992. p. 581–588.

LEVA, J. L. An alternative closed-form solution to the GPS pseudo-range equations. **IEEE Transactions on Aerospace and Electronic Systems**, IEEE, v. 32, n. 4, p. 1430–1439, 1996.

MCCARTHY, D. D.; PETIT, G. IERS conventions (2003)(IERS technical note; 32). **Verlag des Bundesamtes für Kartographie und Geodäsie, Frankfurt am Main**, 2004.

MCDONALD, K. D. Global positioning system: Origins, early concepts, development, and design success. **Success Stories in Satellite Systems**, p. 239, 2008.

MISRA, P.; ENGE, P. **Global Positioning System: signals, measurements and performance**. 2nd. ed. [S.l.]: Ganga-Jamuna Press, 2006. v. 206.

MOLIN, J. P.; AMARAL, L. R. do; COLAÇO, A. **Agricultura de precisão**. [S.l.]: Oficina de textos, 2015.

MONICO, J. F. G. **Posicionamento pelo Navstar-GPS**. [S.l.]: Unesp, 2000.

MONTEIRO, L. S.; MOORE, T.; HILL, C. What is the accuracy of dgps? **The Journal of Navigation**, Cambridge University Press, v. 58, n. 2, p. 207, 2005.

MOOREFIELD, F. D. J. **GPS Standard Positioning Service ((SPS) Performance Standard**. 2020. <https://www.gps.gov/technical/ps/2020-SPS-performance-standard.pdf>. GPS is operated and maintained by the U.S. Air Force. GPS.gov is maintained by the National Coordination Office for Space-Based Positioning, Navigation, and Timing. Accessed: 2022-03-20.

MOSCOW, R. Russian Institute of S. D. E. **Glonass interface control document**. [S.l.], 2008.

NOURELDIN, A.; KARAMAT, T. B.; GEORGY, J. **Fundamentals of inertial navigation, satellite-based positioning and their integration**. [S.l.]: Springer Science & Business Media, 2012.

PARKINSON, B. W. **Origins, evolution, and future of satellite navigation**. [S.l.: s.n.], 1997. v. 20. 11–25 p.

POLISCHUK, G. et al. **The global navigation satellite system GLONASS: Development and usage in the 21st century**. [S.l.: s.n.], 2002.

RAHMAN, F.; AGHAPOUR, E.; FARRELL, J. A. Vehicle ecef position accuracy and reliability in the presence of dgnss communication latency. **IEEE Intelligent Transportation Systems Magazine**, IEEE, 2020.

RAHMAN, F.; FARRELL, J. A. Earth-centered earth-fixed (ecef) vehicle state estimation performance. In: IEEE. **2019 IEEE Conference on Control Technology and Applications (CCTA)**. [S.l.], 2019. p. 27–32.

REVNIVYKH, S. et al. Glonass status, performance and perspectives. In: **Proceedings ION GNSS**. [S.l.: s.n.], 2005. p. 13–16.

SEEBER, G. **Satellite geodesy: foundations, methods, and applications**. [S.l.]: Walter de gruyter, 2008.

SPILKER, J. **GPS Signal Structure and Theoretical Performance. Global Positioning System: Theory and Applications, Volume I. American Institute of Aeronautics and Astronautics**. [S.l.: s.n.], 1996.

SPILKER, J.; PARKINSON, B. W. **Overview of GPS operation and design**. [S.l.: s.n.], 1996. v. 1. 29–55 p.

TEUNISSEN, P. **Differential GPS: Concepts and quality control**. [S.l.]: Netherlands Institution of Navigation, Amsterdam, 1991. v. 10. 48–60 p.

TEUNISSEN, P.; MONTENBRUCK, O. **Springer handbook of global navigation satellite systems**. [S.l.]: Springer, 2017.

Parte II

Second Part: Results & Published Works

PAPER I - A Comparative Study between Differential and Relative GNSS Performance

Paper written for final assessment in the "Advanced Navigation System" course and to be submitted at XXI Postgraduate Congress at UFLA. (Preliminary Version)

A Comparative Study between Differential and Relative GNSS Performance

Gustavo S. Carvalho,[1] Felipe O. Silva,[2]

***Abstract*— Few decades after the first Global Navigation Satellite System (GNSS) be available to civilians, it has become the main navigation technology due to its global coverage, low cost and versatility in different modern-day applications. GNSS positioning accuracy lies in a range up to 10 m. Differential GNSS (DGNSS) and Relative GNSS (RGNSS) are two techniques that improves positioning accuracy by correcting common-mode errors present in GNSS observables. The main contribution of this paper is to provide a comparative analyzes in terms of performance of DGNSS and RGNSS approaches used to improve GNSS position accuracy. Results from simulated test show that the common-mode errors are effectively mitigated and confirm the robustness of RGNSS over DGNSS.**

I. INTRODUCTION

The human being has been concerned with the knowledge of his position on Earth's surface since the dawn of civilization, whether to map the environment, delimit borders or assist in navigation. The observation of celestial bodies (e.g. stars and planets) along with triangulation techniques have been used for hundreds of years in order to determine a specific location on Earth. Since these techniques were affected by considerable errors in celestial object position estimation (reaching hundreds of meters), they did not allow to obtain precise information about the final desired location. With the start of the space age and, consequently, the advent of new technologies, it was possible to develop high precision positioning and navigation systems at a global level, via both optical techniques (which employed the visible part of the electromagnetic spectrum) and radio techniques, e.g., the Navy Navigation Satellite System (NNSS) and Global Positioning System (GPS) [1].

In full operation capability since 1995 [2], the GPS quickly became the dominant navigation system, leading to the development of hundreds of applications that would affect every aspect of modern life. Over the years, other systems have emerged, such as GLONASS (Russia), BeiDou (China), and Galileo (Europe). These four constellations form the current Global Navigation Satellite System (GNSS).

*This work was supported by the Coordination for the Improvement of Higher Education Personnel (CAPES), under grant 88881.169927/2018-01, the Brazilian Agricultural Research Corporation (EMBRAPA), under grant 212-20/2018, the Minas Gerais Research Foundation (FAPEMIG), under grant CAG-APQ-01449-17, and the National Council for Scientific and Technological Development (CNPq), under grant 313160/2019-8

[1]Gustavo S. Carvalho is with the Department of Automatics, Federal University of Lavras, MG gustavo.carvalho8@estudante.ufla.br

[2]Felipe O. Silva is with the Department of Automatics, Federal University of Lavras, MG felipe.oliveira@ufla.br

GNSSs are based on observations of signals transmitted from satellites, which provides three types of measurements, known as observables: pseudorange (distance between the satellite and the receiver during the transmission and reception of the GNSS signal), Doppler shifts (associated with the speed of a moving receiver), and carrier phase (distance between satellite and receiver expressed in cycles of the carrier wave).

GNSS signals have very low power, hence they are prone to several sources of errors, which have a big deteriorating effect on the GNSS positioning. Pseudorange measurement (the main GNSS observable) is primarily corrupted by seven types of errors [3], [4], which can be classified into two categories [5]:

- *Common-mode errors* are spatially and timely correlated errors, i.e, they are experienced by all receivers in the same vicinity and time frame. They are comprised of ephemeris error, satellite clock bias, ionospheric and tropospheric delays.
- *Noncommon-mode errors* are the errors that are different for each receiver, being comprised of receiver clock bias, multipath error and receiver tracking noise.

A number of solutions are available to reduce the effect of common-mode errors on GNSS position estimation. A well known technique is the Differential GNSS (DGNSS), which has been largely employed by the civilian community over the last decades [4]–[7]. DGNSS operation involves a receiver at a surveyed location (reference station), a rover in an unknown and possibly changing location, and a communication link between the latter. Corrections (common-mode error estimates) are computed at reference station and then broadcast to the rover in the vicinity, allowing it to compensate its pseudorange measurements, which increases position estimation accuracy.

Alternatively, Relative GNSS (RGNSS) positioning has also been employed in the last few years as a mean of mitigating GNSS common-mode errors [8], [9]. RGNSS technique still needs a reference station, but instead of computing corrections to be broadcast, the rover has access to the reference station raw observables, which are differenced from its own measurements. The differenced observations are used in position estimation algorithms, so that the rover position relative to the reference station is obtained. Once the reference station location is precisely known, the absolute rover position can be computed.

In face of the aforementioned methods widely employed to mitigate the effects of common-mode errors in GNSS positioning, this paper aims to investigate DGNSS and RGNSS

algorithms for comparison purposes. Simulated GNSS observables are used to test the performance of both algorithms. The main contribution of this work is a comprehensive analysis of DGNSS and RGNSS approaches, showing that the latter is more robust in correcting the common-mode errors.

This paper is organized as follows. Section II presents notation and background on GNSS position estimation. Section III introduces the concept of DGNSS positioning, where differential corrections are computed to minimize the common-mode errors that effect position accuracy. Section IV introduces the concept of RGNSS positioning, another methodology to mitigate common-mode errors. Section V describes how simulated GNSS observables were implemented to analyze performance of Standalone GNSS, DGNSS and RGNSS and presents simulation results. Section VI, lastly, summarizes the paper and presents final thoughts and conclusions.

II. STANDALONE GNSS POSITION ESTIMATION

The pseudorange measurement between a rover a and a satellite s, taking into account the errors cited in Section I, can be modeled as:

$$\rho^s_{a,R} = r_{as} + \delta\rho^a_c - \delta\rho^s_c + \delta\rho^s_{I,a} + \delta\rho^s_{T,a} + \delta\rho^s_E + \delta\rho^s_{M,a} + w^s_{p,a}, \tag{1}$$

where subscript *R* denotes raw measurement, and the true range between rover location $\mathbf{r}^e_{ea}$ and the satellite location $\mathbf{r}^e_{es}$ is defined in (2):

$$r_{as} = \left|\mathbf{C}^I_e \mathbf{r}^e_{es} - \mathbf{r}^e_{ea}\right|, \tag{2}$$

where $\mathbf{C}^I_e$ is the Direct Cosine Matrix (DCM) compensating for ECEF rotation during signal propagation [10].

The term $\delta\rho^a_c$ represents the receiver clock bias, $\delta\rho^s_c$ is the satellite clock bias, $\delta\rho^s_{I,a}$ is the ionospheric delay, $\delta\rho^s_{T,a}$ is the tropospheric delay, $\delta\rho^s_E$ is the ephemeris error, $\delta\rho^s_{M,a}$ is the multipath error, and $w^s_{p,a}$ is the receiver tracking noise.

The Least Squares (LS) algorithm is commonly used for receiver position computation from pseudoranges [11]. Kalman-filter-based estimation algorithm presents itself as a more robust method for position solution estimation, since it makes use of information derived from previous measurements. For standalone GNSS positioning estimation using an Extended Kalman Filter (EKF) algorithm, the following state vector is defined:

$$\mathbf{x}^e = [(\mathbf{r}^e_{ea})^T, (\mathbf{v}^e_{ea})^T, \delta\rho^a_c, \delta\dot{\rho}^a_c]^T \in \mathbb{R}^n, \tag{3}$$

where $n = 8$, $\mathbf{v}^e_{ea}$ is the rover velocity, and $\delta\dot{\rho}^a_c$ is the antenna clock drift.

The dynamic model that describes how the states in (3) are propagated forward in time is given by:

$$\begin{aligned} \dot{\mathbf{r}}^e_{ea} &= \mathbf{v}^e_{ea}, \quad \frac{\partial}{\partial t}\delta\rho^a_c = \delta\dot{\rho}^a_c \\ \dot{\mathbf{v}}^e_{ea} &= 0 \quad \frac{\partial}{\partial t}\delta\dot{\rho}^a_c = 0 \end{aligned} \tag{4}$$

The main sources of increased uncertainty on the states estimates are due to user motion, random walk on the receiver clock drift, and phase noise on the clock bias. The acceleration Power Spectral Density (PSD) matrix is:

$$S^e_a = (C^n_e)^T \begin{pmatrix} S_{aH} & 0 & 0 \\ 0 & S_{aH} & 0 \\ 0 & 0 & S_{aV} \end{pmatrix} C^n_e, \tag{5}$$

where C^n_e is the Earth-Centered Earth-Fixed (ECEF) to North-East-Down (NED) coordinate transformation matrix and S_{aH} and S_{aV} are the horizontal and vertical acceleration PSDs, respectively. For dynamic applications such as a moving vehicle, S_{aH} and S_{aV} can be typically tuned as $10\ m^2s^{-3}$. The receiver clock frequency-drift PSD and clock phase-drift PSD, in turn, can be tuned as $S^a_{cf} \approx 0.04\ m^2s^{-3}$ and $S^a_{c\phi} \approx 0.01\ m^2s^{-1}$, respectively [12].

Equations (4) and (5) represent the dynamic model of the Kalman Filter that governs the prediction step of the navigation filter. For the measurement step, the measurement vector (for m satellites tracked) defined in (6) is considered:

$$\mathbf{z}_G = [\rho^1_{a,C}, \rho^2_{a,C}, ...\rho^m_{a,C}]^T, \tag{6}$$

where G denotes GNSS measurements, and the subscript C indicates that the pseudoranges have been partially corrected for common-mode errors, using for instance: Klobuchar model [13] to mitigate ionosphere delay, UNB3 model [14] for tropospheric delay, and satellite clock corrections transmitted in the GPS navigation message [15]. It should be noted, however, that these pseudorange measurements still contain residual components of common-mode errors that are not totally compensated for by aforementioned models.

The measurement innovations vector that is effectively processed by the EKF is:

$$\delta\mathbf{z}^-_{G,k} = \mathbf{z}_{G,k} - h_g(\hat{\mathbf{x}}^-_k), \tag{7}$$

where k is the iteration index and h_g is the non-linear pseudorange estimate based on the predicted state vector $\hat{\mathbf{x}}^-_k$, given by:

$$h_g(\hat{\mathbf{x}}^-_k) = [\hat{\rho}^{1-}_{a,C}, \hat{\rho}^{2-}_{a,C}, ...\hat{\rho}^{m-}_{a,C}]^T, \tag{8}$$

The pseudorange estimation between rover a and satellite j is computed as follows:

$$\hat{\rho}^{j-}_{a,C,k} = \sqrt{[C^I_e\hat{\mathbf{r}}^e_{ej,k} - \hat{\mathbf{r}}^{e-}_{ea,k}]^T[C^I_e\hat{\mathbf{r}}^e_{ej,k} - \hat{\mathbf{r}}^{e-}_{ea,k}]} + \delta\hat{\rho}^{a-}_{c,k}, \tag{9}$$

where $\hat{\mathbf{r}}^e_{ej}$ is the estimated satellite position, $\hat{\mathbf{r}}^{e-}_{ea,k}$ is the estimated rover position, and $\delta\hat{\rho}^{a-}_{c,k}$ is the estimated receiver clock bias.

The measurement matrix is defined as:

$$H^e_G = \begin{bmatrix} -u^e_{a1,x} & -u_{e}a1,y & -u^e_{a1,z} & 0 & 0 & 0 & 1 & 0 \\ -u^e_{a2,x} & -u^e_{a2,y} & -u^e_{a2,z} & 0 & 0 & 0 & 1 & 0 \\ \vdots & \vdots & \vdots & \vdots & \vdots & \vdots & \vdots & \vdots \\ -u^e_{am,x} & -u^e_{am,y} & -u^e_{am,z} & 0 & 0 & 0 & 1 & 0 \end{bmatrix}, \tag{10}$$

where $\mathbf{u}^e_{aj}$ is the the rover-to-satellite j line-of-sight unit vector.

The measurement noise covariance matrix, which is used to weight the uncertainties of the pseudorange observables, is given by:

$$R = \begin{bmatrix} \sigma^2_{p1} & 0 & \cdots & 0 \\ 0 & \sigma^2_{p2} & \cdots & 0 \\ \vdots & \vdots & \ddots & \vdots \\ 0 & 0 & \cdots & \sigma^2_{pm} \end{bmatrix}, \tag{11}$$

where σ^2_{pj} should take into account the satellite j elevation angle, since pseudorange uncertainty is expected to be larger for satellites with low elevation angle. A suitable model for σ^2_{pj} is:

$$\sigma^2_{pj} = \frac{\sigma^2_{pZ}}{\sin^2(\theta^{aj}_{nu})}, \tag{12}$$

where σ^2_{pZ} is a constant empirical value for the pseudorange uncertainty when satellite is at zenith, and θ^{aj}_{nu} is the satellite j elevation angle.

Given the system and measurement models described above, standalone GNSS EKF can be implemented using the traditional discrete equations presented in standard literature. For more information, see [10], [12].

III. DGNSS POSITION ESTIMATION

As mentioned in Section I, in order to generate DGPS corrections, the reference station must have accurate knowledge of its own position, so the geometric range between base station and satellite can be computed. Similar to (1), the pseudorange taken at a reference station *r* can be modeled as:

$$\begin{aligned} \rho^s_{r,R} = r_{rs} + \delta\rho^r_c - \delta\rho^s_c + \delta\rho^s_{I,r} + \delta\rho^s_{T,r} + \delta\rho^s_E \\ + \delta\rho^s_{M,r} + w^s_{p,r}, \end{aligned} \tag{13}$$

The idea behind the differential positioning is to compute differential corrections (estimations of common-mode errors) by subtracting the pseudorange measurement taken at reference station ($\rho^s_{r,R}$) from the computed geometric range ($\hat{r}_{rs}$). Therefore, the differential correction computed at the reference station is:

$$\nabla\rho^s_{DC} = \hat{r}_{rs} - \tilde{\rho}^s_{r,R} \tag{14}$$

The corrections in (14) are broadcast to rovers in vicinity of the base station. To obtain rover's differentially corrected pseudo-range, these corrections are applied as follows:

$$\rho^s_{a,DC} = \rho^s_{a,R} + \nabla\rho^s_{DC} \tag{15}$$

Applying (1) and (14) into (15) yields the differential single-differenced pseudorange model:

$$\rho^s_{a,DC} = \left|\mathbf{C}^I_e\mathbf{r}^e_{es} - \mathbf{r}^e_{ea}\right| + \Delta\rho^{ra}_c + \Delta\rho^s_{M,ra} + \Delta w^s_{p,ra}, \tag{16}$$

where $\Delta\rho^{ra}_c$ is the rover clock offset relative to the reference station clock, and $\Delta\rho^s_{M,ra}$ and $\Delta w^s_{p,ra}$ are the single-differenced multipath and receiver tracking noise errors, respectively.

By analyzing (16), it should be noted that when differential GNSS positioning is applied, the GNSS common-mode errors are canceled out. However, this cancellation is valid solely when the latency between computation and the effective application of correction is short, and when the physical separation (baseline) between reference and user is within a certain range.

After applying differential corrections, the rover may use these single-differenced observables in place of original measurements to determine its position solution using the EKF approach as described in Section II for standalone GNSS. As a difference, the navigation processor solves for the relative clock offset and drift between the user and reference instead of the user receiver clock bias.

IV. RGNSS POSITION ESTIMATION

As mentioned in Section I, to compute position using RGNSS approach, the rover needs to access the reference station raw observables. The pseudorange taken at a reference station *r* can be modeled as in 13.

The idea behind the relative positioning is to form differences between the receivers absolute GNSS measurements (the so called, single-differenced observables), so that common-mode errors can be removed or considerably reduced. Therefore, the single-differenced pseudorange between the rover *a* and reference station *r*, for satellite *s* is

$$\nabla\rho^s_{ra,R} = \rho^s_{a,R} - \rho^s_{r,R}, \tag{17}$$

Applying (1) and (13) into (17) yields the single differenced pseudorange model

$$\begin{aligned} \nabla\rho^s_{ra,R} = \left|\mathbf{C}^I_e\mathbf{r}^e_{es} - \mathbf{r}^e_{ea}\right| - \left|\mathbf{C}^I_e\mathbf{r}^e_{es} - \mathbf{r}^e_{eb}\right| + \Delta\rho^{ra}_c \\ + \Delta\rho^s_{M,ra} + \Delta w^s_{p,ra}, \end{aligned} \tag{18}$$

By analyzing (18), it should be noted that when relative positioning is applied, the GNSS common-mode errors are canceled out. However, this cancellation is valid solely when the rover's latency to access the reference station measurements is short, and when the physical separation (baseline) between the latter is within a certain range. Studies of latency effect in GPS position accuracy are presented in [16], [17].

In Section II, the standalone GNSS position estimation algorithm was defined. RGNSS, in turn, deals with relative positioning, thus, the EFK state vector is defined as

$$\mathbf{x}^e = [(\mathbf{r}^e_{ra})^T, (\mathbf{v}^e_{ra})^T, \Delta\rho^{ra}_c, \Delta\dot{\rho}^{ra}_c]^T \in \mathbb{R}^n, \tag{19}$$

where $n = 8$, $\mathbf{r}^e_{ra}$ is the rover position relative to the reference station, $\mathbf{v}^e_{ea}$ is the rover velocity relative to the reference station, and $\delta\dot{\rho}^{ra}_c$ is the rover clock drift relative to the reference station.

The same state model adopted in Section II is also applied for RGNSS purposes, i.e, the dynamic of state variables in

(19) is governed by equations in (4). The PSDs matrices in (5) are also the same.

The EFK measurement vector now comprises single-differenced pseudoranges, as defined in (20):

$$\mathbf{z}_G = [\nabla\rho^1_{ra,R}, \nabla\rho^2_{ra,R}, ...\nabla\rho^m_{ra,R})]^T, \tag{20}$$

The measurement innovation vector is defined as in (7), where the single differenced pseudorange estimate now is function of satellite ($\hat{\mathbf{r}}^e_{ej}$), rover ($\hat{\mathbf{r}}^{e-}_{ea}$) and reference station ($\hat{\mathbf{r}}^{e-}_{er}$) estimated positions, namely

$$\nabla\hat{\rho}^{j-}_{ra,R} = \left|\hat{\mathbf{r}}^{e-}_{ej} - \hat{\mathbf{r}}^{e-}_{ea}\right| - \left|\hat{\mathbf{r}}^{e-}_{ej} - \hat{\mathbf{r}}^{e-}_{er}\right| + \Delta\hat{\rho}^{ra-}_{c}. \tag{21}$$

The measurement matrix, H^e_G, is still given as in (10), and the measurement noise covariance matrix is two times as that given in (11), since it is performed a differentiation between observables.

V. SIMULATION RESULTS

To confirm whether DGNSS and RGNSS navigation algorithms were running properly, and to compare their performances in the expected scenario, a simulation test was conducted. The test consisted of simulating a moving vehicle with initial position located at latitude 50 deg, longitude 0 deg and altitude 10 m. The reference station baseline from initial user position, in the North-East-Down (NED) navigation frame, was simulated at 5000 m North, 1000 m East and -100 m Down. The vehicle was supposed to be equipped with a GNSS receiver. During simulation, in the NED frame, the vehicle moves towards East for 40 s, makes a 90 deg turn towards South, and keeps moving for 20 s. Then, it slides 30 degrees towards South-East, keeps moving for 40 s, and makes another 30 deg turn, back to the South direction, moving for 30 s. Finally, the vehicle makes another 90 deg turn, back to the East direction, slowing down until completely stop after 45 s. Figure 1 depicts the described trajectory.

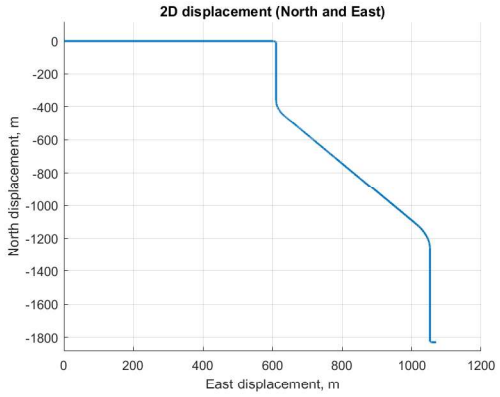

Fig. 1. Simulated vehicle's trajectory.

The GNSS was simulated as an ensemble of 30 regularly distributed satellites, orbiting Earth in six circular orbits equally spaced, each of radius 26561.750 km and inclination angle of 55 deg (w.r.t. Earth's axis of rotation). Code-based observables were generated from each satellite to the antenna, supposing a single frequency carrier-wave of 1575.42 MHz. The observables were supposed to be available to the receiver at a rate of 2 Hz, i.e., a GNSS solution was computed every 0.5 s, and they were purposely corrupted by range errors due to atmospheric propagation (ionospheric and tropospheric) delays, ephemeris errors, receiver/satellite clock delays/drifts, multipath errors (modeled as first order Gauss-Markov processes) and white Gaussian noise, as indicated in (1). The main error parameters in the simulation are summarized in Table I, where PSD is Power Spectral Density, and SD is Standard Deviation.

TABLE I
SIMULATED GNSS ERROR PARAMETERS

Error parameter	Numerical value
Receiver clock delay (at t = 0)	10000 [m]
Receiver clock drift	100 [m/s]
Satellite clock delay SD	0.5 [m]
Ephemeris SD	0.5 [m]
Zenith tropospheric delay SD	0.2 [m]
Zenith ionospheric delay SD	4 [m]
Multipath error SD	0.5 [m]
Multipath error correlation time	10 [s]
Code tracking SD	1 [m]

To assess the performance of navigation solution approaches, three criteria were considered: individual channel position error (e_{ic}), defined in (22); horizontal position error (e_h), defined in (23); and total position error (e_t), defined in (24).

$$e_{ic,N,E,D} = \mathbf{r}^n_{ea,N,E,D} - \hat{\mathbf{r}}^n_{ea,N,E,D}, \tag{22}$$

$$e_h = \left\| \begin{bmatrix} 1 & 0 & 0 \\ 0 & 1 & 0 \end{bmatrix} (\mathbf{r}^n_{ea} - \hat{\mathbf{r}}^n_{ea}) \right\|, \tag{23}$$

$$e_t = \left\| \begin{bmatrix} 1 & 0 & 0 \\ 0 & 1 & 0 \\ 0 & 0 & 1 \end{bmatrix} (\mathbf{r}^n_{ea} - \hat{\mathbf{r}}^n_{ea}) \right\|, \tag{24}$$

where $\mathbf{r}^n_{ea}$ is the ground-truth position provided by vehicle's dynamic profile, and $\hat{\mathbf{r}}^n_{ea}$ is the estimated position during simulation. All position vectors are represented in the NED navigation frame.

A. Standalone GNSS Performance in Simulation

Before performing a comparison between DGNSS and RGNSS techniques, the user position solution was obtained by EKF-based standalone GNSS approach, presented in Section II, in order to analyze whether the navigation algorithm is running as expected with simulated data. For brevity, this approach will be referred to as SGNSS ensuing text. Fig. 2 shows the position errors as function of time in each individual channel (North, East, and Down) for SA-GNSS approach, and Table II presents statistics for positioning error criteria established in Section V.

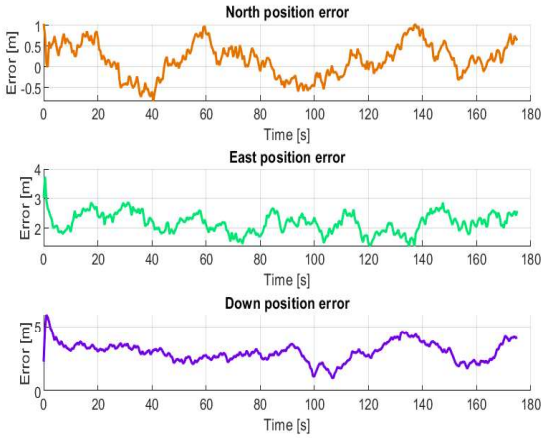

Fig. 2. Individual channel error over time obtained through simulation using SGNSS approach.

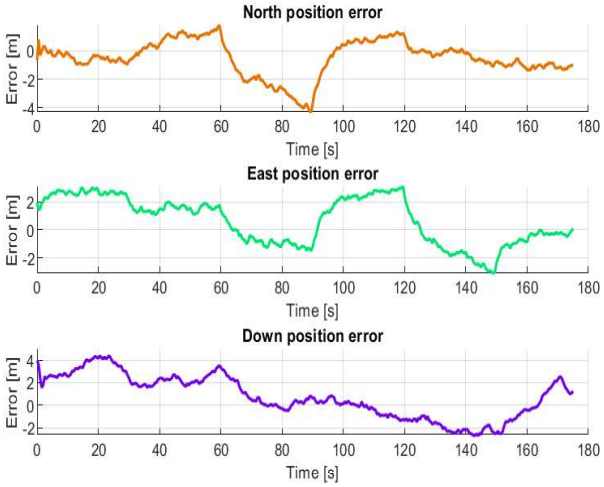

Fig. 3. Individual channel error over time obtained through simulation using DGNSS approach.

TABLE II
POSITION ERROR STATISTICS FOR SA-GNSS APPROACH

	Mean [m]	Std. dev [m]
North	0.168	0.408
East	2.189	0.343
Down	3.018	0.753
Horizontal	2.233	0.344
Total	3.785	0.675

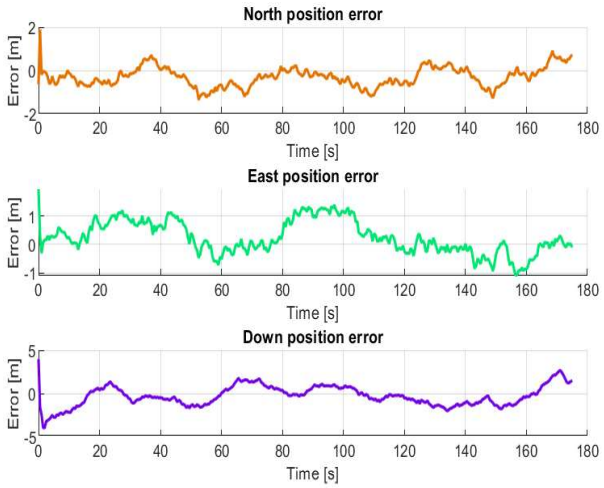

Fig. 4. Individual channel error over time obtained through simulation using RGNSS approach.

In qualitative terms, it can be seen in Fig. 2 that in all channels the error oscillates around a value different from zero. It occurs due to common-mode errors that, for a certain time interval and baseline distance between receivers, can be considered constants, acting as biases in the user position solution. In a quantitative perspective, it can be inferred from Table II that the total position error is less than 6 m at 99.7% of probability, which is in agreement with literature, where the error is expected to lie in a range of 5 m to 10 m [10]. It indicates that the GNSS observables generated during simulation are consistent with the pseudorange measurements we find in practice and the SGNSS algorithm presents satisfactory performance in terms of position solution.

B. DGNSS vs. RGNSS Performance

The main goal of this paper is to compare the performance of two techniques that mitigate common-mode errors in order to improve accuracy in a GNSS position solution. For this purpose, EKF-based Differential GNSS and EKF-based Single-Differenced Relative GNSS algorithms were implemented as described in Sections III and IV. The same scenario described in Section V was used in both approaches, where corrupted GNSS observables were generated for position estimation of the moving vehicle. Figures 3 and 4 present the individual channel errors through time for position solution provided by DGNSS and RGNSS, respectively.

A qualitative analyze of Figs. 2, 3 and 4 shows that errors in DGNSS and RGNSS are less biased, i.e., they have mean value closer to zero, indicating that the common-mode errors inserted during simulation were effectively mitigated.

For performance comparison purposes between DGNSS and RGNSS, the mean and standard deviation of the position error criteria are summarized in Table III. It can be seen that RGNSS presented a better performance over DGNSS, since its mean error for all criteria (i.e. north, east, down, horizontal, and total errors) are closer to zero, evidencing that this approach has mitigated the common-mode errors in a more effective way in comparison to DGNSS. Finally, RGNSS presented an accuracy in position of 3.03 m at 99.7% of probability, while DGNSS position accuracy was 5.79 m at 99.7% of probability (3σ), evidencing the superiority of RGNSS over the DGNSS.

TABLE III
POSITION ERROR STATISTICS FOR DGNSS AND RGNSS APPROACHES

	DGNSS		RGNSS	
	Mean [m]	Std. dev. [m]	Mean [m]	Std. dev. [m]
North	-0.487	1.246	-0.305	0.457
East	0.641	1.695	0.253	0.583
Down	0.727	1.908	-0.307	1.171
Horizontal	2.095	0.819	0.759	0.358
Total	2.877	0.970	1.362	0.557

To further analyze the performance between both techniques, Fig. 5 displays the distribution of the the individual channel position errors (North, East, and Down) and Fig. 6 displays the distribution of the horizontal and total errors in a boxplot. The first box in both figures corresponds to DGNSS approach, and in all cases it presented a larger interquartile range (larger box lengths), indicating that the errors are more variable when compared to RGNSS.

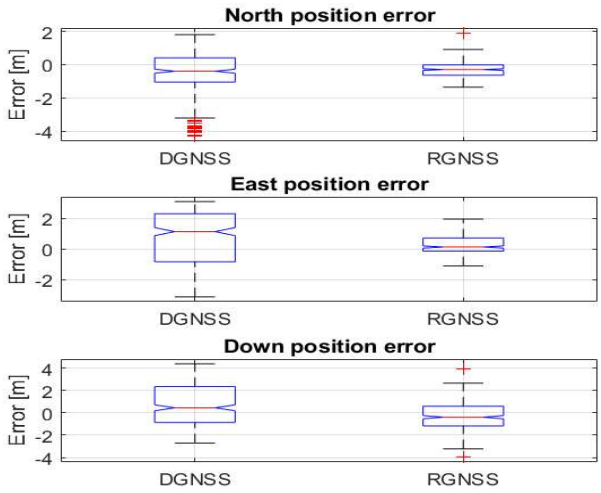

Fig. 5. Individual channel position error in NED-frame for DGNSS and RGNSS position estimation method.

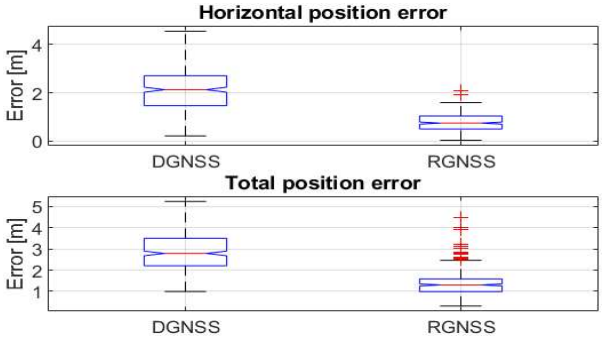

Fig. 6. Total and Horizontal position error in NED-frame for DGNSS and DD-RGNSS position estimation method.

VI. CONCLUSIONS AND FUTURE WORK

Accuracy in position estimation is of great interest in many commercial applications, specially for Precision Agriculture where the demand for this kind of technology has increased in the last few years. The main purpose of the investigations presented herein was to evaluate the performance of DGNSS and RGNSS techniques, responsible for mitigation of common-mode errors, a set of errors that most affect GNSS positioning accuracy. The experiment was conducted in a simulated environment, where GNSS observables were purposed corrupted and then submitted to both approaches to compare their performances. First, the position solution provided by standalone GNSS was compared to RGNSS and DGNSS solutions, and it was possible to verify that common-mode erros were effectivley mitigated. In sequence, DGNSS results were compared with RGNSS solution, and the latter has showed a better performance over DGNSS in terms of position accuracy for all error criteria established in this work. The RGNSS accuracy for total position estimation was 3 m at 99.7 % of probability, while DGNSS acuracy for the same criteria was 5.78 m at 99.7% of probability. For future studies, we intend to extend the same investigation using real GNSS data for a stationary scenario, and also for a dynamic test, where a receiver is attached to a moving vehicle.

ACKNOWLEDGMENT

The authors would like to thank the Graduate Program in Automation and Systems Engineering (PPGESISA) at Federal University of Lavras (UFLA) for supporting this study.

REFERENCES

[1] B. Hofmann-Wellenhof, H. Lichtenegger, and J. Collins, *Global positioning system: theory and practice*. Springer Science & Business Media, 2001.

[2] A. El-Rabbany, *Introduction to GPS: the global positioning system*. Artech house, 2002.

[3] G. Lachapelle, "Gps observables and error sources for kinematic positioning", in *Kinematic Systems in Geodesy, Surveying, and Remote Sensing*, Springer, 1991, pp. 17–26.

[4] P. Teunissen, "Differential gps: Concepts and quality control", *Netherlands Institution of Navigation, Amsterdam*, vol. 10, pp. 48–60, 1991.

[5] J. Farrell, M. Grewal, M. Djodot, and M. Barth, "Differential gps with latency compensation for autonomous navigation", in *Proceedings of the 1996 IEEE International Symposium on Intelligent Control*, IEEE, 1996, pp. 20–24.

[6] J. Farrell, M. Djodat, M. Barth, and M. Grewal, "Latency compensation for differential gps", *Navigation*, vol. 44, no. 1, pp. 99–107, 1997.

[7] Q. Ali and S. Montenegro, “A matlab implementation of differential gps for low-cost gps receivers”, *TransNav: International Journal on Marine Navigation and Safety of Sea Transportation*, vol. 8, no. 3, 2014.

[8] T. B. Karamat, M. M. Atia, and A. Noureldin, “Performance analysis of code-phase-based relative gps positioning and its integration with land vehicle’s motion sensors”, *IEEE Sensors Journal*, vol. 14, no. 9, pp. 3084–3100, 2014.

[9] W. Yang, Y. Liu, and F. Liu, “An improved relative gnss tracking method utilizing single frequency receivers”, *Sensors*, vol. 20, no. 15, p. 4073, 2020.

[10] J. Farrell, *Aided navigation: GPS with high rate sensors*. McGraw-Hill, Inc., 2008.

[11] Y. He, R. Martin, and A. M. Bilgic, “Approximate iterative least squares algorithms for gps positioning”, in *The 10th IEEE International Symposium on Signal Processing and Information Technology*, IEEE, 2010, pp. 231–236.

[12] P. D. Groves, *Principles of GNSS, inertial, and multisensor integrated navigation systems*, 2nd. Artech house, 2013.

[13] J. Klobuchar, “Global positioning system: Theory and applications”, *Vol. I, Cap*, vol. 12, pp. 485–515, 1996.

[14] D. Kaplan Elliott and J. Hegarty Christopher, *Understanding GPS: principles and applications*. Artech House, 2006.

[15] G. Navstar, “Space segment/navigation user interfaces, interface control document gps (200), no”, *ICD GPS*, vol. 200,

[16] F. Rahman and J. A. Farrell, “Earth-centered earth-fixed (ecef) vehicle state estimation performance”, in *2019 IEEE Conference on Control Technology and Applications (CCTA)*, IEEE, 2019, pp. 27–32.

[17] F. Rahman, E. Aghapour, and J. A. Farrell, “Vehicle ecef position accuracy and reliability in the presence of dgnss communication latency”, *IEEE Intelligent Transportation Systems Magazine*, 2020.

PAPER II - Performance Analysis of Code-Based Relative GPS Positioning as Function of Baseline Separation

Paper submitted, approved and presented at the "17th IEEE Latin American Robotics Symposium - LARS 2020"in August 31st, 2020.

Performance Analysis of Code-Based Relative GPS Positioning as Function of Baseline Separation*

Gustavo S. Carvalho,[1] Felipe O. Silva,[2] Rogério P. Menezes Filho[3] and Victor Hugo L. Pereira [4]

Abstract— **With the beginning of the space age and, consequently, the advent of new technologies, it was possible to develop low-cost positioning and navigation systems with global coverage, reaching accuracy up to 10 m. Nevertheless, many modern-day applications have arisen demanding navigation technologies able to provide sub-meter position accuracy, still at low-cost. Relative Global Navigation Satellite System (RGNSS) is a well-known technique used to correct common-mode errors present in GNSS observables. RGNSS is susceptible to two main degradation factors, namely, communication latency and baseline separation between the rover and reference. This paper investigates the sensitivity of position estimation accuracy as function of baseline separation between stationary Global Positioning System (GPS) receivers. As main contribution, we show that it is possible to achieve 1 m horizontal accuracy at 68% of probability with baselines up to 2100 km between rover and reference station. Experimental data collected from the Brazilian Network for Continuous Monitoring of GNSS (RBMC) are used to validate the analysis.**

I. INTRODUCTION

The human being has been concerned with the knowledge of his position on Earth's surface since the dawn of civilization, whether to map the environment, delimit borders or assist in navigation. The observation of celestial bodies (e.g. stars and planets) along with triangulation techniques have been used for hundreds of years in order to determine a specific location on Earth. Since these techniques were affected by considerable errors in celestial object position estimation (reaching hundreds of meters), they did not allow to obtain precise information about the final desired location. With the start of the space age and, consequently, the advent of new technologies, it was possible to develop high precision positioning and navigation systems at a global level, via both optical techniques (which used the visible part of the electromagnetic spectrum) and radio techniques, e.g., the Navy Navigation Satellite System (NNSS) and Global Positioning System (GPS) [1].

In full operation capability since 1995 [2], the GPS quickly became the dominant navigation system, leading to the development of hundreds of applications that would affect every aspect of modern life. Over the years, other systems have emerged, such as GLONASS (Russia), BeiDou (China), and Galileo (Europe). These four constellations together form the so called Global Navigation Satellite System (GNSS).

GNSSs are systems based on observations of signals transmitted from satellites, which provides three types of measurements, known as observables: pseudorange (distance between the satellite and the receiver during the transmission and reception of the GNSS signal), Doppler shifts (associated with the speed of a moving receiver), and carrier phase (distance between satellite and receiver expressed in unit cycles of the carrier wave).

GNSS signals have very low power, hence they are prone to several sources of errors, which have a big deteriorating effect on the GNSS positioning. Pseudorange measurement (the main GNSS observable) is primarily corrupted by seven types of errors [3], [4], which can be classified into two categories [5]:

- *Common-mode errors* are spatially and timely correlated errors, i.e, they are experienced by all receivers in the same vicinity and time frame. They are comprised of ephemeris error, satellite clock bias, ionospheric and tropospheric delays.
- *Noncommon-mode errors* are the errors that are different for each receiver, being comprised of receiver clock bias, multipath error and receiver tracking noise.

A number of solutions are available to reduce the effect of common-mode errors on GNSS position estimation. A well known technique is the Differential GNSS (DGNSS), which has been largely employed by the civilian community over the last decades [4]–[6]. DGNSS operation involves a receiver at a surveyed location (reference station), a rover in an unknowing and possibly changing location, and a communication link between the latter. Corrections (common-mode error estimates) are computed at reference station and then broadcast to the rover in the vicinity, allowing it to compensate its pseudorange measurements, which increases position estimation accuracy. Alternatively, Relative GNSS (RGNSS) positioning has also been employed in the last few years as a mean of mitigating GNSS common-mode errors [7], [8]. RGNSS technique still needs a reference station, but instead of computing corrections to be broadcast, the rover

*This work was supported by the Coordination for the Improvement of Higher Education Personnel (CAPES), under grant 88881.169927/2018-01, the Brazilian Agricultural Research Corporation (EMBRAPA), under grant 212-20/2018, the Minas Gerais Research Foundation (FAPEMIG), under grant CAG-APQ-01449-17, and the National Council for Scientific and Technological Development (CNPq), under grant 313160/2019-8

[1]Gustavo S. Carvalho is with the Department of Automatics, Federal University of Lavras, MG gustavo.carvalho8@estudante.ufla.br

[2]Felipe O. Silva is with the Department of Automatics, Federal University of Lavras, MG felipe.oliveira@ufla.br

[3]Rogério P. Menezes Filho is with the Department of Automatics, Federal University of Lavras, MG rogeriofilho03@gmail.com

[4]Victor Hugo L. Pereira is with the Department of Automatics, Federal University of Lavras, MG pereira.victor@estudante.ufla.br

978-0-7381-1153-7/20/$31.00 ©2020 IEEE

has access to the reference station raw observables, which are differenced from its own measurements. The differenced observations are used in position estimation algorithms, so that the rover position relative to the reference station is obtained. Once the reference station location is precisely known, the absolute rover position can be computed.

There are two main degradation factors to which DGNSS and RGNSS systems are prone to [9]: the baseline separation, which is the physical distance between reference station and rover, and the communication latency between the computed correction and actual time of use (for DGNSS) or the time it took to the rover to access the reference station raw observables (for RGNSS). Recent works have investigated the effects of communication latency on GPS position estimation accuracy [10], [11], demonstrating that with suitable algorithmic processing, positioning performance is insensitive to correction latency up to 500 s. This paper aims at analyzing the first aforementioned factor, i.e, the effect of baseline separation on GPS position estimation accuracy. The main contribution of this work is a comprehensive analysis relating the maximum baseline distance between reference station and rover, and the feasibility of RGNSS sub-meter position accuracy.

This paper is organized as follows. Section II presents notation and background on GNSS position estimation. Section III introduces the concept of RGNSS positioning. Section IV describes experimental data and discusses positioning performance of GNSS and RGNSS. Section V, lastly, summarizes the paper and presents final thoughts and conclusions.

II. STANDALONE GNSS POSITION ESTIMATION

The pseudorange measurement between a rover a and a satellite s, taking into account the errors cited in Section I, can be modeled as

$$\rho^s_{a,R} = r_{as} + \delta\rho^a_c - \delta\rho^s_c + \delta\rho^s_{I,a} + \delta\rho^s_{T,a} + \delta\rho^s_E + \delta\rho^s_{M,a} + w^s_{p,a}, \quad (1)$$

where subscript *R* denotes raw measurement, and the true range between rover location $\mathbf{r}^e_{ea}$ and the satellite location $\mathbf{r}^e_{es}$ is defined in (2):

$$r_{as} = \left|\mathbf{r}^e_{ea} - \mathbf{r}^e_{es}\right|, \quad (2)$$

The term $\delta\rho^a_c$ represents the receiver clock bias, $\delta\rho^s_c$ is the satellite clock bias, $\delta\rho^s_{I,a}$ is the ionospheric delay, $\delta\rho^s_{T,a}$ is the tropospheric delay, $\delta\rho^s_E$ is the ephemeris error, $\delta\rho^s_{M,a}$ is the multipath error, and $w^s_{p,a}$ is the receiver tracking noise.

The Least Squares (LS) algorithm is commonly used for receiver position computation from pseudoranges [12]. Kalman-filter-based estimation algorithm presents itself as a more robust method for position solution estimation, since it makes use of information derived from previous measurements. For standalone GNSS positioning estimation using an Extended Kalman Filter (EKF) algorithm, the following state vector is defined:

$$\mathbf{x}^e = [\mathbf{r}^e_{ea}, \mathbf{v}^e_{ea}, \delta\rho^a_c, \delta\dot{\rho}^a_c]^T \in \mathbb{R}^n, \quad (3)$$

where $n = 8$, $\mathbf{v}^e_{ea}$ is the rover velocity, and $\delta\dot{\rho}^a_c$ is the antenna clock drift.

The dynamic model that describes how the states in (3) are propagated forward in time is given by

$$\begin{aligned} \dot{\mathbf{r}}^e_{ea} &= \mathbf{v}^e_{ea}, \quad \frac{\partial}{\partial t}\delta\rho^a_c = \delta\dot{\rho}^a_c \\ \dot{\mathbf{v}}^e_{ea} &= 0 \quad \frac{\partial}{\partial t}\delta\dot{\rho}^a_c = 0 \end{aligned} \quad (4)$$

The main sources of increased uncertainty on the states estimates are due to user motion, random walk on the receiver clock drift, and phase noise on the clock bias. The acceleration Power Spectral Density (PSD) matrix is

$$S^e_a = (C^n_e)^T \begin{pmatrix} S_{aH} & 0 & 0 \\ 0 & S_{aH} & 0 \\ 0 & 0 & S_{aV} \end{pmatrix} C^n_e, \quad (5)$$

where C^n_e is the Earth-Centered Earth-Fixed (ECEF) to North-East-Down (NED) coordinate transformation matrix and S_{aH} and S_{aV} are the horizontal and vertical acceleration PSDs, respectively. For low dynamic applications (stationary receivers), S_{aH} and S_{aV} can be typically tuned as $0.01\ m^2s^{-3}$. The receiver clock frequency-drift PSD and clock phase-drift PSD, in turn, can be tuned as $S^a_{cf} \approx 0.04\ m^2s^{-3}$ and $S^a_{c\phi} \approx 0.01\ m^2s^{-1}$, respectively [13].

Equations (4) and (5) represent the dynamic model of the Kalman Filter that governs the prediction step of the navigation filter. For the measurement step, the measurement vector (for m satellites tracked) defined in (6) is considered:

$$\mathbf{z}_G = [\rho^1_{a,C}, \rho^2_{a,C}, ...\rho^m_{a,C}]^T, \quad (6)$$

where G denotes GNSS measurements, and the subscript C indicates that the pseudoranges have been partially corrected for common-mode errors, using for instance: Klobuchar model [14] to mitigate ionosphere delay, UNB3 model [15] for tropospheric delay, and satellite clock corrections transmitted in the GPS navigation message [16]. It should be noted, however, that these pseudorange measurements still contain residual components of common-mode errors that are not totally compensated for by aforementioned models.

The measurement innovations vector that is effectively processed by the EKF is

$$\delta\mathbf{z}^-_{G,k} = \mathbf{z}_{G,k} - h_g(\hat{\mathbf{x}}^-_k), \quad (7)$$

where k is the iteration index and h_g is the pseudorange estimate based on the predicted state vector $\hat{\mathbf{x}}^-_k$, given by

$$h_g(\hat{\mathbf{x}}^-_k) = [\hat{\rho}^{1-}_{a,C}, \hat{\rho}^{2-}_{a,C}, ...\hat{\rho}^{m-}_{a,C}]^T, \quad (8)$$

The pseudorange estimation between rover a and satellite j is computed as follows

This work, as [10], [11], focuses on results from GPS constellation only. Hence, the terms GPS and GNSS are used interchangeably hereinafter.

$$\hat{\rho}^{j-}_{a,C,k} = \sqrt{[C^I_e \hat{\mathbf{r}}^e_{ej} - \hat{\mathbf{r}}^{e-}_{ea,k}]^T [C^I_e \hat{\mathbf{r}}^e_{ej} - \hat{\mathbf{r}}^{e-}_{ea,k}]} + \delta\hat{\rho}^{a-}_{c,k}, \quad (9)$$

where C^I_e is the coordinate transformation matrix accounting for ECEF rotation during GNSS signal transit time, $\hat{\mathbf{r}}^e_{ej}$ is the estimated satellite position, $\hat{\mathbf{r}}^{e-}_{ea,k}$ is the estimated rover position, and $\delta\hat{\rho}^{a-}_{c,k}$ is the estimated receiver clock bias.

The measurement matrix is defined as

$$H^e_G = \begin{bmatrix} -u^e_{a1,x} & -u_{e}a1,y & -u^e_{a1,z} & 0 & 0 & 0 & 1 & 0 \\ -u^e_{a2,x} & -u^e_{a2,y} & -u^e_{a2,z} & 0 & 0 & 0 & 1 & 0 \\ \vdots & \vdots & \vdots & \vdots & \vdots & \vdots & \vdots & \vdots \\ -u^e_{am,x} & -u^e_{am,y} & -u^e_{am,z} & 0 & 0 & 0 & 1 & 0 \end{bmatrix}, \quad (10)$$

where $\mathbf{u}^e_{aj}$ is the the rover-to-satellite j line-of-sight unit vector.

The measurement noise covariance matrix, which is used to weight the uncertainties of the pseudorange observables, is given by

$$R = \begin{bmatrix} \sigma^2_{p1} & 0 & \cdots & 0 \\ 0 & \sigma^2_{p2} & \cdots & 0 \\ \vdots & \vdots & \ddots & \vdots \\ 0 & 0 & \cdots & \sigma^2_{pm} \end{bmatrix}, \quad (11)$$

where σ^2_{pj} should take into account the satellite j elevation angle, since pseudorange uncertainty is expected to be larger for satellites with low elevation angle. Therefore, σ^2_{pj} is

$$\sigma^2_{pj} = \frac{\sigma^2_{pZ}}{\sin^2(\theta^{aj}_{nu})}, \quad (12)$$

where σ^2_{pZ} is a constant empirical value for the pseudorange uncertainty when satellite is at zenith, and θ^{aj}_{nu} is the satellite j elevation angle.

Given the system and measurement models described above, standalone GNSS EKF can be implemented using the traditional discrete equations presented in standard literature. For more information, see [13], [17].

III. RGNSS POSITION ESTIMATION

As mentioned in Section I, to compute position using RGNSS approach, the rover needs to access the reference station raw observables. Similar to (1), the pseudorange taken at a reference station *r* can be modeled as

$$\rho^s_{r,R} = r_{rs} + \delta\rho^r_c - \delta\rho^s_c + \delta\rho^s_{I,r} + \delta\rho^s_{T,r} + \delta\rho^s_E + \delta\rho^s_{M,r} + w^s_{p,r}, \quad (13)$$

The idea behind the relative positioning is to form differences between the receivers absolute GNSS measurements (the so called, single-differenced observables), so that common-mode errors can be removed or considerably reduced. Therefore, the single-differenced pseudorange between the rover *a* and reference station *r* is

$$\nabla\rho^s_{ra,R} = \rho^s_{a,R} - \rho^s_{r,R}, \quad (14)$$

Applying (1) and (13) into (14) yields the single differenced pseudorange model

$$\nabla\rho^s_{ra,R} = |\mathbf{r}^e_{es} - \mathbf{r}^e_{ea}| - |\mathbf{r}^e_{es} - \mathbf{r}^e_{er}| + \Delta\rho^{ra}_c + \Delta\rho^s_{M,ra} + \Delta w^s_{p,ra}, \quad (15)$$

where $\Delta\rho^{ra}_c$ is the rover clock offset relative to the reference station clock, and $\Delta\rho^s_{M,ra}$ and $\Delta w^s_{p,ra}$ are the single-differenced multipath and receiver tracking noise errors, respectively.

By analyzing (15), it should be noted that when relative positioning is applied, the GNSS common-mode errors are canceled out. However, this cancellation is valid solely when the rover's latency to access the reference station measurements is short, and when the physical separation (baseline) between the latter is within a certain range. Studies of latency effect in GPS position accuracy are presented in [10], [11]. The main goal of this paper is to analyze to which extent the baseline separation allows this cancellation to be effective in RGNSS positioning accuracy.

In Section II, the standalone GNSS position estimation algorithm was defined. RGNSS, in turn, deals with relative positioning, thus, the EFK state vector is defined as

$$\mathbf{x}^e = [\mathbf{r}^e_{ra}, \mathbf{v}^e_{ra}, \Delta\rho^{ra}_c, \Delta\dot{\rho}^{ra}_c]^T \in \mathbb{R}^n, \quad (16)$$

where $n = 8$, $\mathbf{r}^e_{ra}$ is the rover position relative to the reference station, $\mathbf{v}^e_{ea}$ is the rover velocity relative to the reference station, and $\delta\dot{\rho}^{ra}_c$ is the rover clock drift relative to the reference station.

The same state model adopted in Section II is also applied for RGNSS purposes, i.e, the dynamic of state variables in (16) is governed by equations in (4). The PSDs matrices in (5) are also the same.

The EFK measurement vector now comprises single-differenced pseudoranges, as defined in (17):

$$\mathbf{z}_G = [\nabla\rho^1_{ra,R}, \nabla\rho^2_{ra,R}, ...\nabla\rho^m_{ra,R})]^T, \quad (17)$$

The measurement innovation vector is defined as in (7), where the single differenced pseudorange estimate now is function of satellite ($\hat{\mathbf{r}}^e_{ej}$), rover ($\hat{\mathbf{r}}^{e-}_{ea}$) and reference station ($\hat{\mathbf{r}}^{e-}_{er}$) estimated positions, namely

$$\nabla\hat{\rho}^{j-}_{ra,R} = \left|\hat{\mathbf{r}}^{e-}_{ej} - \hat{\mathbf{r}}^{e-}_{ea}\right| - \left|\hat{\mathbf{r}}^{e-}_{ej} - \hat{\mathbf{r}}^{e-}_{er}\right| + \Delta\hat{\rho}^{ra-}_c. \quad (18)$$

The measurement matrix, H^e_G, is still given as in (10), and the measurement noise covariance matrix is two times as that given in (11), since it is performed a differentiation between observables.

IV. EXPERIMENTAL RESULTS

This section discusses the data that was used to generate the experimental results. The experiment analyzes the degradation effect of baseline separation in RGNSS positioning accuracy. The main goal was to identify what is the maximum baseline separation between rover and reference

station that enables meter level accuracy in RGNSS positioning determination. For simplicity, a stationary scenario was considered.

A. Data Acquisition

The Brazilian Network for Continuous Monitoring of GNSS (RBMC) is the most precise geodetic reference structure in Brazil. It consists of 112 geodetic stations placed in well surveyed locations with coordinates established at high precision level. Each station is equipped with a high performance receiver that collects and stores GNSS observables and navigation data continuously. RBMC provides GNSS data in three different ways: real time, daily basis with sampling interval of $15\,s$, and at every $15\,min$ with sampling interval of $1\,s$. These data can be freely accessed in [18].

For position estimation, daily post-processed GNSS data of 14 RBMC base stations were used. The data were collected on June 25, 2020 and the selected time frame was chosen to comprise an interval of $600\,s$ (from $11:55\,am$ to $12:05\,pm$), where the ionospheric delay is expected to have its most significant impact on pseudorange measurements [19]. The bases chosen were EACH, POLI, SPBP, SPC1, MGIN, CHPI, EESC, SPJA, SJRP, SPFE, GOJA, MTLE, ROJI, and SAGA, where the selection was made according to their baseline separations (from EACH), in the range of $0\,km$ to $3416\,km$. Although some of these bases are equipped with multi-ferquency, multi-constellation receivers, only L1 pseudorange measurements for the GPS constellation were used for state estimation during the experimental tests.

To analyze the sensitivity of position estimation accuracy with respect to baseline separation between stationary receivers, the following procedure was adopted with two estimation approaches:

1) EKF-based standalone GNSS approach using pseudorange measurements. For brevity, this approach will be referred to as SA-GNSS ensuing text.
2) EKF-based RGNSS using single-differenced pseudorange measurements. This approach will be designated SD-RGNSS hereinafter.

To assess the performance of both approaches, three criteria were considered: individual channel position error (e_{ic}), defined in (19); horizontal position error (e_h), defined in (20); and total position error (e_t), defined in (21).

$$e_{ic,N,E,D} = \mathbf{r}^n_{ea,N,E,D} - \hat{\mathbf{r}}^n_{ea,N,E,D}, \tag{19}$$

$$e_h = \left\| \begin{bmatrix} 1 & 0 & 0 \\ 0 & 1 & 0 \end{bmatrix} (\mathbf{r}^n_{ea} - \hat{\mathbf{r}}^n_{ea}) \right\|, \tag{20}$$

$$e_t = \left\| \begin{bmatrix} 1 & 0 & 0 \\ 0 & 1 & 0 \\ 0 & 0 & 1 \end{bmatrix} (\mathbf{r}^n_{ea} - \hat{\mathbf{r}}^n_{ea}) \right\|, \tag{21}$$

where $\mathbf{r}^n_{ea}$ is the ground-truth base position provided by each RBMC station report, and $\hat{\mathbf{r}}^n_{ea}$ is the estimated position. All position vectors are represented in the North-East-Down (NED) navigation frame.

B. GNSS vs. RGNSS Performance Analysis

The EACH station was chosen as the main base to play the role of a stationary rover, whose position is to be estimated using the aforementioned approaches. The first approach, SA-GNSS, simply computes the standard position of the EACH base using its own raw pseudoranges contained in the data set described in subsection IV-A.

The second approach, SD-RGNSS, consists of RGNSS positioning, where the EACH base position was estimated by using POLI base as the reference station ($25\,km$ of baseline separation). Figs. 1 and 2 show the position errors as function of time in each individual channel (North, East, and Down) for GNSS and RGNSS approach, respectively, as defined in (19).

According to literature, the errors in standalone GNSS positioning are expected to lie in the range of $5\ m$ to $10\ m$ [17]. Analyzing Figs. 1 and 2, it is possible to see that, although SA-GNSS has good results in each individual channel (even better than expected), SD-RGNSS presented improved performance, as the position error of the channels have mean value closer to zero, indicating that the common errors were effectively mitigated.

Table I summarizes the mean and standard deviation of the position error criteria, evidencing the SD-RGNSS superiority in performance. Another outcome we should pay attention to on Fig. 1 is the fact that around the GPS Time of Week (TOW) $388800\ s$ ($12:00\ pm$) the satellite ephemerides were updated, what caused a slight decrease in the SA-GNSS position errors and, consequently, an improvement in accuracy positioning. This effect cannot be seen in Fig. 2, since ephemeris errors are adequately mitigated in RGNSS position, regardless of the ephemeris time-of-validity.

C. Baseline Separation Analysis

To further analyze the effect of baseline separation on positioning accuracy, the EACH position was re-estimated using

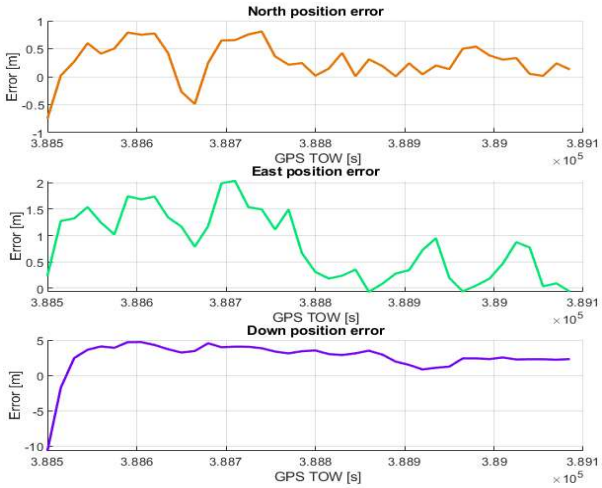

Fig. 1. Individual channel error over time for EACH base position estimation using GNSS standalone positioning.

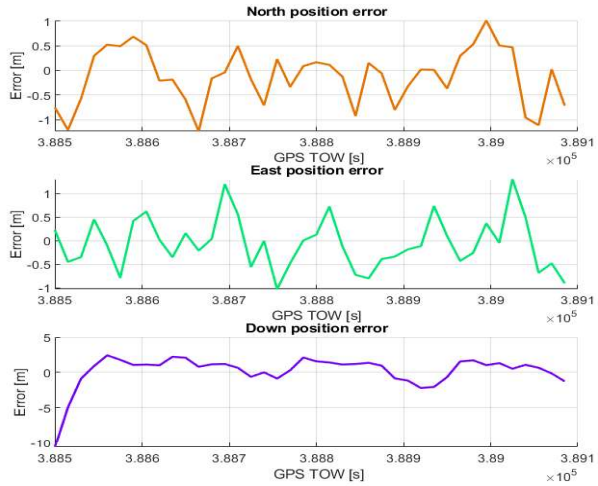

Fig. 2. Individual channel error over time for EACH base position estimation using RGNSS positioning with POLI as reference station.

TABLE I

POSITION ERROR STATISTICS

	SA-GNSS		SD-RGNSS	
	Mean [m]	Std. dev. [m]	Mean [m]	Std. dev. [m]
North	0.38	0.50	-0.12	0.56
East	0.89	0.69	-0.05	0.55
Down	2.06	2.07	0.21	2.28
Horizontal	0.94	0.61	0.70	0.36
Total	3.37	1.60	1.77	1.62

the same SA-GNSS and SD-RGNSS algorithms. For SD-RGNSS positioning,in particular, 13 different bases belonging to RBMC were selected as reference stations, gradually distanced towards North-Western direction from EACH station. Table II shows the individual distances between EACH base and the reference stations. Each algorithm processed the set of GNSS measurements (k = 1,...,*Nd*; *Nd* = 600 *s*) as if they were occurring in real-time (i.e., incrementally) to estimate the state vector at each time index *k*.

Fig. 3 displays the individual channel position errors (North, East, and Down) as function of baseline distance between receivers in a boxplot. The first box (at distance 0 m) is the interquartile range of EACH base position estimation error performed by SA-GNSS algorithm, whereas the remaining boxes represent the interquartile range of the errors obtained with SD-RGNSS algorithm. The error criteria defined in (20) and (21), i.e., the horizontal error and the total error, were also used to analyze the performance of position estimation. Fig. 4 displays a boxplot with the aforementioned criteria. Table II summarizes measures of horizontal position accuracy, in particular.

By analyzing Table II and Fig. 3, it is possible to see the improvement in position accuracy when using SD-RGNSS over SA-GNSS. Fig. 4 shows that the box lengths get larger when reference stations located at distances starting from 1200 km from EACH are used, indicating that the position

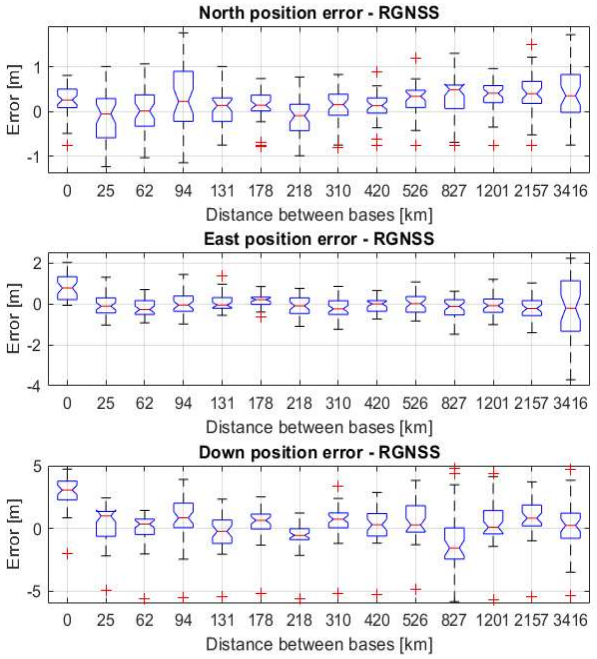

Fig. 3. Individual channel position error as function of baseline separation using RGNSS positioning. For distance 0 km (main station) the position estimation was performed by SA-GNSS algorithm.

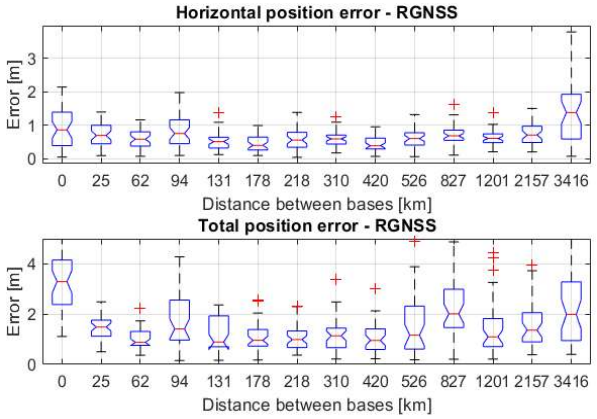

Fig. 4. Total and Horizontal position error as function of baseline separation using RGNSS positioning. For distance 0 km (main station) the position estimation was performed by SA-GNSS algorithm.

errors variability is greater as baseline distance increases.

Table II also shows that SD-RGNSS was effective to correct common-mode errors for reference station baseline distances up to 2157 km, where horizontal position accuracy of 1 m at 68% of probability was reached. At greater distances, SD-RGNSS performance becomes similar to SA-GNSS (or even worse), and the errors variability becomes greater, as indicated in Figs. 3 and 4.

TABLE II
HORIZONTAL ERROR STATISTICS

Reference Station	EACH (SA-GNSS)	POLI	SPBP	SPC1	MGIN	CHPI	EESC	SPJA	SJRP	SPFE	GOJA	MTLE	ROJI	SAGA
Distance from EACH $[km]$	0	25	62	94	131	178	218	310	420	526	827	1201	2157	3416
Mean $[m]$	0.94	0.70	0.60	0.86	0.51	0.45	0.58	0.58	0.45	0.60	0.71	0.61	0.75	1.40
Std. Dev. $[m]$	0.61	0.36	0.28	0.50	0.27	0.25	0.33	0.24	0.23	0.30	0.31	0.24	0.33	0.88

V. CONCLUSIONS AND FUTURE WORK

Accuracy in position estimation is of great interest in many commercial applications. The purpose of the investigations presented herein was to evaluate how baseline separation between rover and reference station affect position estimation accuracy with stationary receivers. Standalone GNSS and Relative GNSS (RGNSS) approaches were discussed, and the results demonstrated that horizontal position estimation accuracy is achievable at 1 meter level at 68% of probability by using Single-Differenced (SD) RGNSS approach with reference station distanced up to $2157\ km$. This shows that SD-RGNSS is effective to correct common-mode errors for receivers in a great range, differently from what some literatures suggest.

For future studies, we intend to extend the same investigation for moving platforms equipped with low-cost, real-time RGNSS. Although some works focused on the communication latency effect on RGNSS have already been proposed in the literature, this is a topic that deserves further attention and should also be investigated in the future.

ACKNOWLEDGMENT

The authors would like to thank the Graduate Program in Automation and Systems Engineering (PPGESISA) at Federal University of Lavras (UFLA) for supporting this study.

REFERENCES

[1] B. Hofmann-Wellenhof, H. Lichtenegger, and J. Collins, *Global positioning system: theory and practice*. Springer Science & Business Media, 2012.

[2] A. El-Rabbany, *Introduction to GPS: the global positioning system*. Artech house, 2002.

[3] G. Lachapelle, "Gps observables and error sources for kinematic positioning", in *Kinematic Systems in Geodesy, Surveying, and Remote Sensing*, Springer, 1991, pp. 17–26.

[4] P. Teunissen, "Differential gps: Concepts and quality control", *Netherlands Institution of Navigation, Amsterdam*, vol. 10, pp. 48–60, 1991.

[5] J. Farrell, M. Grewal, M. Djodot, and M. Barth, "Differential gps with latency compensation for autonomous navigation", in *Proceedings of the 1996 IEEE International Symposium on Intelligent Control*, IEEE, 1996, pp. 20–24.

[6] J. Farrell, M. Djodat, M. Barth, and M. Grewal, "Latency compensation for differential gps", *Navigation*, vol. 44, no. 1, pp. 99–107, 1997.

[7] T. B. Karamat, M. M. Atia, and A. Noureldin, "Performance analysis of code-phase-based relative gps positioning and its integration with land vehicle's motion sensors", *IEEE Sensors Journal*, vol. 14, no. 9, pp. 3084–3100, 2014.

[8] W. Yang, Y. Liu, and F. Liu, "An improved relative gnss tracking method utilizing single frequency receivers", *Sensors*, vol. 20, no. 15, p. 4073, 2020.

[9] L. S. Monteiro, T. Moore, and C. Hill, "What is the accuracy of dgps?", *The Journal of Navigation*, vol. 58, no. 2, p. 207, 2005.

[10] F. Rahman and J. A. Farrell, "Earth-centered earth-fixed (ecef) vehicle state estimation performance", in *2019 IEEE Conference on Control Technology and Applications (CCTA)*, IEEE, 2019, pp. 27–32.

[11] F. Rahman, E. Aghapour, and J. A. Farrell, "Vehicle ecef position accuracy and reliability in the presence of dgnss communication latency", *IEEE Intelligent Transportation Systems Magazine*, 2020.

[12] Y. He, R. Martin, and A. M. Bilgic, "Approximate iterative least squares algorithms for gps positioning", in *The 10th IEEE International Symposium on Signal Processing and Information Technology*, IEEE, 2010, pp. 231–236.

[13] P. D. Groves, *Principles of GNSS, inertial, and multisensor integrated navigation systems*, 2nd. Artech house, 2013.

[14] J. Klobuchar, "Global positioning system: Theory and applications", *Vol. I, Cap*, vol. 12, pp. 485–515, 1996.

[15] D. Kaplan Elliott and J. Hegarty Christopher, *Understanding GPS: principles and applications*. Artech House, 2006.

[16] G. Navstar, "Space segment/navigation user interfaces, interface control document gps (200), no", *ICD GPS*, vol. 200,

[17] J. Farrell, *Aided navigation: GPS with high rate sensors*. McGraw-Hill, Inc., 2008.

[18] IBGE, *Rede brasileira de monitoramento contínuo dos sistemas gnss - rbmc*, `https://bit.ly/2YsldI3`, Accessed: 2020-08-01, 2020.

[19] T. Hada and T. Tanaka, "Study on ionospheric delay in gps standard positioning service", in *SICE 2004 Annual Conference*, IEEE, vol. 1, 2004, pp. 226–229.

PAPER III - Performance Analysis of Relative GPS Positioning as Function of Communication Latency

Paper submitted, approved and presented at "18^{th} IEEE Latin American Robotics Symposium - LARS 2021"in August 9^{th}, 2021.

Performance Analysis of Relative GPS Positioning as Function of Communication Latency*

Gustavo S. Carvalho,[1] Felipe O. Silva[2]

***Abstract*— GNSS has become the main navigation system around the world, providing position accuracy up to 10 m. Due its low-cost and versatility, many segments have benefited from it, such as surveying & mapping, agriculture, aviation, marine, and recreation. Nevertheless, many other modern-day applications have arisen demanding navigation technologies able to provide submeter position accuracy, still at low-cost. Relative Global Navigation Satellite System (RGNSS) is a well-known technique used to correct common-mode errors present in GNSS observables. RGNSS is susceptible to two main degradation factors, namely, communication latency and baseline separation between two GNSS receivers. This paper investigates the sensitivity of position estimation accuracy as function of communication latency between stationary Global Positioning System (GPS) receivers. As main contribution, we show that it is possible to achieve 1 m horizontal accuracy at 68% of probability with latency up to 1500 s. Experimental data collected from the Brazilian Network for Continuous Monitoring of GNSS (RBMC) are used to validate the analysis.**

I. INTRODUCTION

The Global Positioning System (GPS) reached its Full Operational Capability (FOC) in 1995 [1], and after civilian segment had open access to this technology (even though its signals have been purposefully degraded in the early stages), the GPS quickly became the dominant navigation system, leading to the development of hundreds of applications that would affect every aspect of modern life. Over the years other systems have emerged, and currently there are three global systems in FOC, beyond GPS: GLONASS (Russia), BeiDou (China), and Galileo (Europe). These four constellations together form the so called Global Navigation Satellite Systems (GNSSs).

GNSSs are based on the transmission of signals from satellites, which provides three types of measurements, known as observables [2]–[5]: pseudoranges (distances between satellites and receiver during the transmission and reception of the GNSS signals), Doppler shifts (associated with the speed of a moving receiver), and carrier phases (distances between satellites and receiver expressed in unit cycles of the carrier wave).

*This work was supported by the Brazilian Agricultural Research Corporation (EMBRAPA), under grant 212-20/2018, the Minas Gerais Research Foundation (FAPEMIG), under grant CAG-APQ-01449-17, and the National Council for Scientific and Technological Development (CNPq), under grant 313160/2019-8

[1]Gustavo Carvalho is with the Department of Automatics, Federal University of Lavras gustavo.carvalho8@estudante.ufla.br

[2]Felipe O. Silva is with the Department of Automatics, Federal University of Lavras, MG felipe.oliveira@ufla.br

978-1-6654-0761-8/21/$31.00 ©2021 IEEE

GNSS signals are susceptible to numerous types of errors since they have very low power, and as consequence, the position accuracy is deteriorated. GPS Standard Position Service (SPS), for instance, provides horizontal and vertical accuracy of 9 m and 15 m, respectively [6]. Pseudorange measurements (the main GNSS observables), are primarily corrupted by seven types of errors [7], [8], which can be classified into two categories [9]:

- *Common-mode errors* are spatially and timely correlated errors, i.e, they are experienced by all receivers in the same vicinity and time frame. They are comprised of ephemeris error, satellite clock bias, ionospheric and tropospheric delays.
- *Noncommon-mode errors* are the errors that are different for each receiver, comprising the receiver clock bias, multipath error and receiver tracking noise.

A number of solutions are available to reduce the effect of common-mode errors on GNSS position estimation. A well known technique is the Differential GNSS (DGNSS), which has been largely employed by the civilian community over the last decades [8]–[10]. DGNSS operation involves a receiver at a surveyed location (reference station), a rover in an unknowing and possibly changing location, and a communication link between the latter. Corrections (common-mode error estimates) are computed at reference station and then broadcast to the rover in the vicinity, allowing it to compensate its pseudorange measurements by removing or considerably reducing the common-mode errors, which increases position estimation accuracy.

Alternatively, Relative GNSS (RGNSS) positioning has also been employed in the last few years as a mean of mitigating GNSS common-mode errors [11], [12]. RGNSS technique still needs a reference station, but instead of computing corrections to be broadcast, the rover has access to the reference station raw observables, which are differenced from its own measurements. The differenced observations are used in position estimation algorithms, so that the rover position relative to the reference station is obtained. Once the reference station location is precisely known, the absolute rover position can be computed.

In reference stations-based GNSSs (like RGNSS and DGNSS), two main degradation factors are responsible for the position accuracy deterioration [13]: the baseline separation, which is the physical distance between receivers, and the communication latency between the computed correction and actual time of use (for DGNSS) or the time it took to the rover to access the reference station raw

observables (for RGNSS). A recent work investigated the effects of baseline separation on RGNSS position accuracy [14], where horizontal position errors were showed to remain at submeter level (1 σ) for baseline distances up to 2100 km. Communication latency on DGPS position estimation accuracy has also been investigated [15], [16], demonstrating that with suitable algorithmic processing, DPGS positioning performance is insensitive to correction latency up to 600 s. This paper aims at analyzing the second aforementioned factor, i.e, the effect of communication latency on Relative GPS position estimation accuracy. The main contribution of this work is a comprehensive analysis concerning the maximum latency time frame that allows RGNSS position accuracy at submeter level.

This paper is organized as follows. Section II presents notation and background on RGNSS position estimation with Single-Differenced (SD) pseudorange measurements. Section III describes experimental data and discusses positioning performance of SD-RGNSS. Section IV, lastly, summarizes the paper and presents final thoughts and conclusions.

II. RELATIVE GNSS POSITION ESTIMATION

Let the GNSS pseudorange measurements from satellite s, measured simultaneously at rover a and reference r, taking into account the errors cited in Section I, be modeled as, respectively

$$\rho^s_{a,R} = r_{as} + \delta\rho^a_c - \delta\rho^s_c + \delta\rho^s_{I,a} + \delta\rho^s_{T,a} + \delta\rho^s_E + \delta\rho^s_{M,a} + w^s_{\rho,a}, \quad (1)$$

$$\rho^s_{r,R} = r_{rs} + \delta\rho^r_c - \delta\rho^s_c + \delta\rho^s_{I,r} + \delta\rho^s_{T,r} + \delta\rho^s_E + \delta\rho^s_{M,r} + w^s_{\rho,r}, \quad (2)$$

where the time index *t* has been omitted for simplicity, the subscript *R* denotes raw measurement, and $r_{is}, i \in \{a, r\}$ is the range (Euclidean distance) from the true Earth-Centered-Earth-Fixed (ECEF) position of satellite s ($\mathbf{r}^e_{es}$) to the true ECEF position of rover ($\mathbf{r}^e_{ea}$) or reference station ($\mathbf{r}^e_{re}$), defined as

$$r_{is} = \left\| \mathbf{C}^I_e \mathbf{r}^e_{es} - \mathbf{r}^e_{ei} \right\|, \qquad i \in \{a, r\} \quad (3)$$

where $\mathbf{C}^I_e$ is the Direct Cosine Matrix (DCM) compensating for ECEF rotation during signal propagation [5].

The term $\delta\rho^i_c$ represents the receiver clock bias, $\delta\rho^s_c$ is the satellite clock bias, $\delta\rho^s_{I,i}$ is the ionospheric delay, $\delta\rho^s_{T,i}$ is the tropospheric delay, $\delta\rho^s_E$ is the ephemeris error, $\delta\rho^s_{M,i}$ is the multipath error, and $w^s_{\rho,i}$ is a white Gaussian-like measurement noise representing the lumped effects of tracking noise and unmodeled residual errors.

This work, as [16], [17], focuses on results from GPS constellation only. Hence, the terms GPS and GNSS are used interchangeably hereinafter.

In the paper, the ECEF frame is represented by the superscript e, and is defined with its z_e axis pointing along the Earth's axis of rotation, x_e axis pointing from the center of Earth to the intersection of the equator with the Convention Zero Meridian (CZM), and y_e axis completing the rigth-hand orthogonal set.

Be the generic case where m satellites are in view of the receivers at reference station r and rover a. The same number m of observables (pseudoranges, carrier-phases, and eventually, Doppler-shifts) is expected to be tracked. This work focuses on GPS pseudorange measurements, therefore, Single-Differenced (SD) pseudoranges may be obtained by subtracting the observables of reference station r from those received by the rover a. In equation,

$$\begin{cases} \nabla\rho^{(1)}_{ra,R} = \rho^{(1)}_{a,R} - \rho^{(1)}_{r,R} = \left\| C^I_e \mathbf{r}^e_{e(1)} - \mathbf{r}^e_{ea} \right\| - \left\| C^I_e \mathbf{r}^e_{e(1)} - \mathbf{r}^e_{er} \right\| \\ \qquad\qquad + \Delta\rho^{ra}_c + \Delta\rho^{(1)}_{M,ra} + \Delta w^{(1)}_{\rho,ra} \\ \qquad\qquad \vdots \\ \nabla\rho^{(m)}_{ra,R} = \rho^{(m)}_{a,R} - \rho^{(m)}_{r,R} = \left\| C^I_e \mathbf{r}^e_{e(m)} - \mathbf{r}^e_{ea} \right\| - \left\| C^I_e \mathbf{r}^e_{e(m)} - \mathbf{r}^e_{er} \right\| \\ \qquad\qquad + \Delta\rho^{ra}_c + \Delta\rho^{(m)}_{M,ra} + \Delta w^{(m)}_{\rho,ra} \end{cases} \quad (4)$$

where $\Delta\rho^{ra}_c = \delta\rho^a_c - \delta\rho^r_c$, $\Delta\rho^{(s)}_{M,ra} = \delta\rho^{(s)}_{M,a} - \delta\rho^{(s)}_{M,r}$, and $\Delta w^{(s)}_{\rho,ra} = \delta w^{(s)}_{\rho,a} - \delta w^{(s)}_{\rho,r}$ with $s \in \{1, ..., m\}$, are the SD receiver clock delay, multipath and white Gaussian-like measurement noise for satellite s, respectively.

A quick inspection at (4) indicates that the SD pseudorange measurements are direct function of the baseline vector ($\mathbf{r}^e_{ra} = \mathbf{r}^e_{ea} - \mathbf{r}^e_{er}$) in the ECEF frame, and are no longer corrupted by the common-mode errors ($\delta\rho^{(s)}_c, \delta\rho^{(s)}_{I,i}, \delta\rho^{(s)}_{T,i}, \delta\rho^{(s)}_E$), since they were canceled out during the differencing process. However, this cancellation is valid solely when the rover's latency to access the reference station measurements is in a delimited time frame, and when the physical separation (baseline) between the latter is within a certain range.

Equation 4 is clearly cast into a Least Squares (LS) problem, which is an approach commonly used for receiver position computation from pseudoranges [18]–[20]. Alternatively, Kalman-filter-based estimation algorithm presents itself as a more robust method for position solution estimation, since it makes use of information derived from previous measurements. The Extended Kalman Filter (EKF) is one of the most used filters for this kind of application ([3]–[5], [14], [16], [17]) because of its reliability and relatively low computational cost. For RGNSS positioning estimation using an EKF algorithm, the following state vector comprising n = 8 states is defined

$$\mathbf{x}^e = [(\mathbf{r}^e_{ra})^T, (\mathbf{v}^e_{ra})^T, \Delta\rho^{ra}_c, \Delta\dot{\rho}^{ra}_c]^T \in \mathbb{R}^n, \quad (5)$$

where $\mathbf{v}^e_{ea}$ is the rover velocity relative to the reference station, and $\delta\dot{\rho}^{ra}_c$ is the rover clock drift relative to the reference station.

The dynamic model that describes how the states in (5) are propagated forward in time is given by

$$\begin{aligned} \dot{\mathbf{r}}^e_{ea} &= \mathbf{v}^e_{ea}, \quad \frac{\partial}{\partial t}\Delta\rho^{ra}_c = \Delta\dot{\rho}^a_c \\ \dot{\mathbf{v}}^e_{ea} &= 0 \quad \frac{\partial}{\partial t}\Delta\dot{\rho}^{ra}_c = 0 \end{aligned} \quad (6)$$

The main sources of increased uncertainty on the states estimates are due to user motion, random walk on the receiver clock drift, and phase noise on the clock bias. The acceleration Power Spectral Density (PSD) matrix is

$$S_a^e = (C_e^n)^T \begin{pmatrix} S_{aH} & 0 & 0 \\ 0 & S_{aH} & 0 \\ 0 & 0 & S_{aV} \end{pmatrix} C_e^n, \tag{7}$$

where C_e^n is the ECEF to North-East-Down (NED) DCM and S_{aH} and S_{aV} are the horizontal and vertical acceleration PSDs, respectively. For a scenario where receivers are stationary (low dynamic applications), S_{aH} and S_{aV} can be typically tuned as $0.01\ m^2s^{-3}$. The receiver clock frequency-drift PSD and clock phase-drift PSD, in turn, can be tuned as $S_{cf}^a \approx 0.04\ m^2s^{-3}$ and $S_{c\phi}^a \approx 0.01\ m^2s^{-1}$, respectively [4].

For the EKF measurement step, the measurement vector (for m satellites tracked) comprises the SD pseudoranges and can be described as,

$$\mathbf{z}_G = [\nabla\rho_{ra,R}^{(1)}, \nabla\rho_{ra,R}^{(2)}, ...\nabla\rho_{ra,R}^{(m)}]^T, \tag{8}$$

where G denotes GNSS measurements.

The measurement innovations vector that is effectively processed by the EKF is

$$\delta\mathbf{z}_{G,k}^- = \mathbf{z}_{G,k} - h_g(\hat{\mathbf{x}}_k^-), \tag{9}$$

where k is the iteration index and h_g is the SD pseudorange estimates based on the predicted (superscript -) state vector $\hat{\mathbf{x}}_k^-$, given by

$$h_g(\hat{\mathbf{x}}_k^-) = [\nabla\hat{\rho}_{ra,R}^{(1)-}, \nabla\hat{\rho}_{ra,R}^{(2)-}, ..., \nabla\hat{\rho}_{ra,R}^{(m)-}]^T, \tag{10}$$

The SD pseudorange estimation between rover *a* and satellite *s* is function of satellite ($\hat{\mathbf{r}}_{es}^{e-}$), rover ($\hat{\mathbf{r}}_{ea}^{e-}$), reference station ($\hat{\mathbf{r}}_{er}^{e-}$) estimated position, and SD clock delay. In equations,

$$\nabla\hat{\rho}_{ra,R}^{s-} = \left\| \mathbf{C}_e^I\hat{\mathbf{r}}_{es}^{e-} - \hat{\mathbf{r}}_{ea}^{e-} \right\| - \left\| \mathbf{C}_e^I\hat{\mathbf{r}}_{es}^{e-} - \hat{\mathbf{r}}_{er}^{e-} \right\| + \Delta\hat{\rho}_c^{ra-}. \tag{11}$$

The measurement matrix, $\mathbf{H}_G^e$, which is the geometric matrix that characterizes the user-satellite geometry, is defined as

$$\mathbf{H}_G^e = \begin{bmatrix} -u_{a,x}^{(1)} & -u_{a,y}^{(1)} & -u_{a,z}^{(1)} & 0_{1,3} & 1 & 0 \\ -u_{a,x}^{(2)} & -u_{a,y}^{(2)} & -u_{a,z}^{(2)} & 0_{1,3} & 1 & 0 \\ \vdots & \vdots & \vdots & \vdots & \vdots & \vdots \\ -u_{a,x}^{(m)} & -u_{a,y}^{(m)} & -u_{a,z}^{(m)} & 0_{1,3} & 1 & 0 \end{bmatrix}, \tag{12}$$

where $\mathbf{u}_a^{(s)} \approx \frac{\mathbf{r}_{es}^e - \mathbf{r}_{ea}^e}{r_{as}}$, $s \in \{1, ..., m\}$ is the unitary line-of-sight vector from the satellite s to the rover a.

The measurement noise covariance matrix, which is used to weight the uncertainties of the SD pseudorange observables, is

$$R = \begin{bmatrix} 2\sigma_{\rho 1}^2 & 0 & \cdots & 0 \\ 0 & 2\sigma_{\rho 2}^2 & \cdots & 0 \\ \vdots & \vdots & \ddots & \vdots \\ 0 & 0 & \cdots & 2\sigma_{\rho m}^2 \end{bmatrix}, \tag{13}$$

where the factor 2 arises from the SD process, and the variance $\sigma_{\rho s}^2$ should take into account the satellite s elevation angle, as pseudorange uncertainty is expected to be larger for satellites with low elevation angle. A suitable model for $\sigma_{\rho s}^2$ is given by

$$\sigma_{\rho s}^2 = \frac{\sigma_{\rho Z}^2}{\sin^2(\theta_{nu}^{as})}, \tag{14}$$

where $\sigma_{\rho Z}^2$ is a constant empirical value for the pseudorange uncertainty when satellite is at zenith (typically 5m) , and θ_{nu}^{as} is the satellite s elevation angle.

Given the system and measurement models described above, the EKF-based RGNSS algorithm can be implemented using the traditional discrete equations presented in standard literature. For more information, see [4], [5].

III. EXPERIMENTAL RESULTS

This section presents results analyzing experimental performance. The experiment was designed considering the degradation effect of communication latency between rover and reference station data on positioning accuracy, to verify the extend to which of RGNSS estimation algorithm is able to achieve one-meter level accuracy specification in presence of latency. For simplicity, the experiment was conducted in a stationary scenario.

A. Experimental Data Acquisition

The Brazilian Network for Continuous Monitoring of GNSS (RBMC) is the most precise geodetic reference structure in Brazil, operated and maintained by the Brazilian Institute of Geography and Statistics (IBGE). It consists of 112 geodetic stations spread around the country, placed in well surveyed locations with coordinates established at high precision level. Each station is equipped with a high performance receiver that collects and stores, continuously, GNSS observables and navigation data. RBMC provides GNSS data in three different ways: real time through the NTRIP "caster" server [21], 15-seconds tracking interval in RINEX 2 and RINEX 3 formats, and 1-second tracking interval files in RINEX 3 format [22]. These data can be freely accessed by all users in [23].

For position estimation, daily post-processed GNSS data with 15-seconds tracking interval of two stations belonging to RBMC were used: MGLA, located in Lavras-MG, and MGV1, located in Varginha-MG. The data were collected on June 16^{th}, 2021 and the selected time frame was chosen to comprise an interval of 3600 s (240 epochs), from 12:00 pm to 1:00 pm (GMT-3), when the ionospheric delay is expected to have its most significant impact on pseudorange measurements [24]. Although both bases are equipped with multi-frequency, multi-constellation receivers, only L1

Coarse Acquisition (C/A) pseudorange measurements from the GPS constellation were used for state estimation during the experimental tests.

B. Position Estimation Algorithm

To analyze the sensitivity of position estimation accuracy with respect to communication latency between stationary receivers, the EKF-based RGNSS approach using SD pseudorange measurements was adopted.

The EKF algorithm was used to process the entire batch of GNSS measurements ($k = 1, ..., N_d$; $N_d = 240$ epochs, where 1 epoch corresponds to 15 seconds) as if they were occurring in real-time i.e., incrementally, to estimate the state vector at each time index k for a given value of the latency l, using the SD pseudorange $\nabla\rho^s_{ra,R}(k; k-l)$. The experiment is repeated for latency values of $l = 0, ..., 100$ epochs, corresponding to 1500 seconds.

To assess the estimation performance of the RGNSS, three criteria were considered: individual channel position error ($e_{ic_{k,l}}$), defined in (15); horizontal position error ($e_{h_{k,l}}$), defined in (16); and total position error ($e_{t_{k,l}}$), defined in (17).

$$e_{ic_{k,l},N,E,D} = \mathbf{r}^n_{ea,N,E,D} - \hat{\mathbf{r}}^n_{ea_{k,l},N,E,D}, \tag{15}$$

$$e_{h_{k,l}} = \left\| \begin{bmatrix} 1 & 0 & 0 \\ 0 & 1 & 0 \end{bmatrix} (\mathbf{r}^n_{ea} - \hat{\mathbf{r}}^n_{ea_{k,l}}) \right\|, \tag{16}$$

$$e_{t_{k,l}} = \left\| \begin{bmatrix} 1 & 0 & 0 \\ 0 & 1 & 0 \\ 0 & 0 & 1 \end{bmatrix} (\mathbf{r}^n_{ea} - \hat{\mathbf{r}}^n_{ea_{k,l}}) \right\|, \tag{17}$$

where $\mathbf{r}^n_{ea}$ is the ground-truth position of MGLA base provided by RBMC's technical report, and $\hat{\mathbf{r}}^n_{ea_{k,l}}$ is the MGLA estimated position for epoch k, and latency l. All position vectors are represented in the NED navigation frame.

C. RGNSS Performance Analysis: Sensitivity to Latency

The MGLA station was chosen as the main base to play the role of a stationary rover, whose position was to be estimated using the RGNSS algorithm. The MGV1 station, in turn, was selected to be the reference station, which provided raw pseudorange measurements so that the rover could use them for common-mode error cancellation during its own position estimation. The baseline separation between rover and reference station was known to be 59.099243 km. For each fixed value of l, the mean and standard deviation of $e_{ic_{k,l},N,E,D}$; $e_{h_{k,l}}$ and $e_{t_{k,l}}$ were computed from experimental data by averaging the last $(N_d - l_{max})$ epochs, where l_{max} is the maximum value for latency.

Figure 1 shows the Root Mean Square Error (RMSE) of each individual channel position $e_{ic_{k,l},N,E,D}$ (North, East and Down), defined in (15), as function of latency, where the time delay varies from $d = 0, ..., 1500$ seconds. Analyzing Fig. 1(A,C), one can see that the RMSE for North and Down position get larger as latency increases. For a value of latency of $d = 1500$ seconds, for instance, the RMSE for North and Down channels become 32.67% and 212.18% larger, respectively. The degradation of position accuracy with respect to latency is an expected behavior due to the common-mode errors time correlation, i.e., although they may be considered constant during a specific time frame, these errors change according to the time delay that two receivers get their GPS observable measurements, and the main goal of this paper is to analyze what is the maximum communication latency between rover and reference station that allows a correct cancellation of the common-mode errors, enabling a meter-level accuracy in RGNSS position estimation.

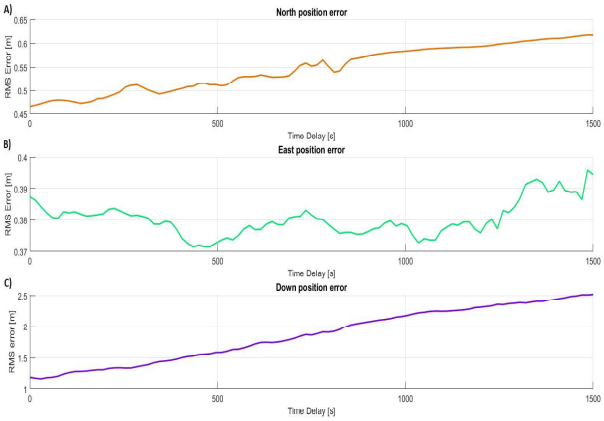

Fig. 1. Root mean square error for individual channel position as function of latency.

In contrast, as can be seen in Fig. 1(B) the RMSE for East channel increases in a small proportion if compared to North and Down ones. For latency $d = 0$ seconds, i.e, rover position estimations computed using reference station's pseudorange measurements received at the same epoch as the rover ($\nabla\rho^s_{ra,R}(k; k)$), the RMSE for East channel is 0.3873 m, and for latency $d = 1500$ seconds, when rover position estimation is computed using reference station's pseudorange measurements received 100 epochs earlier ($\nabla\rho^s_{ra,R}(k; k-100)$), the RMSE is only 0.3945 m. This small increase in the East position error, when compared to North and Down channels, can be explained by the low value of the East Dilution Of the East Precision (EDOP) [25], particularly assumed in this experiment, which indicates a greater confidence in the position solution for this channel. As can be seen in Fig. 2, the EDOP value (in brown) is significantly smaller than for other channels, specially at the end of the time frame (approx. 3.164×10^5 s), where its value is almost twice smaller than North DOP (NDOP) (in gray).

Figure 3 displays the mean error (represented by the red squares) of horizontal and total position, $e_{h_{k,l}}$ and $e_{t_{k,l}}$, respectively, for each fixed value of latency l, which varies up to 100 epochs (1500 seconds). Figure 3 also shows the plus and minus one-standard-deviation error bar (indicated by the blue bars) of position estimation for each increment of l. As can be seen, although the mean error for horizontal

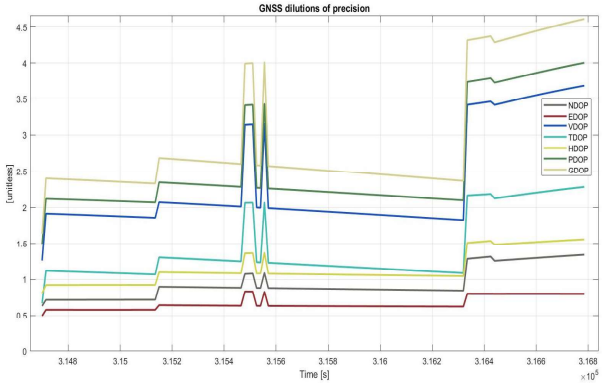

Fig. 2. GNSS Dilution Of Precision.

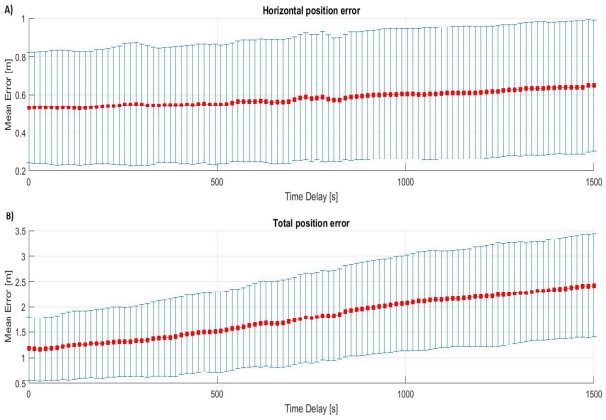

Fig. 3. Mean error of horizontal (A) and total (B) position as function of latency.

and total position grows as latency increases, the former accuracy remains less than one meter for latency up to 1500 seconds using the RGNSS approach. A recent work has investigated the effects of communication latency on position estimation accuracy using the DGNSS approach [15], where the mean horizontal position error for latency $l = 0$ was 0.97 m, and the maximum latency for horizontal position estimation accuracy to remain at one-meter level, for 1 σ, was found to be 600 seconds. Analyzing Fig. 3, one can see that horizontal position estimation accuracy has improved when using RGNSS approach, where the position accuracy remains submetric at 1 σ for a longer period of latency, namely 1500 seconds, which is 2.5 times longer than the value found for DGNSS in [15]. This indicates that the RGNSS approach is more robust to communication latency when compared to DGNSS approach.

Another outcome from Fig. 3 is that the standard deviation gets larger as l increments, specially for total error position. For $l = 0$ s, for instance, the standard deviation is $\sigma = 0.6252$ m, and when $l = 1500$ s, the standard deviation becomes $\sigma = 1.0126$ m. This indicates that as latency values get higher, there is a wider dispersion in position uncertainties, which are due to the increasingly incorrect common-mode error cancellation.

Tables I and II summarize some measures of position accuracy for horizontal and total position errors, respectively, with latency $l = 0, 40$ and 100 epochs. Column 1 shows the latency in terms of epochs. Column 2 shows the mean error, defined in (16) and (17). Column 3 displays the standard deviation. Column 4 reports the maximum value for horizontal and total position error. Columns 5 and 6 reports the percent of samples that have position error less than 1 m and 2 m (for horizontal error), 2 and 3 m (for total error). As can be seen in Table I, the horizontal mean error of 0.648 m obtained using the RGNSS approach for latency of 100 epochs (1500 seconds) is smaller than the horizontal error of 0.97 m obtained in [15] using the DGPS approach when latency is zero. In addition, 82.48% of the estimated position samples in this experiment for latency of 100 epochs remained under the submeter level, against 65% reported in [15], at no effect of latency. These outcomes reassure the robustness of RGNSS over DGNSS when we are dealing with the effects of communication latency on position estimation accuracy.

TABLE I
HORIZONTAL POSITION PERFORMANCE

Latency (epochs)	Mean (m)	Std. Dev. (m)	Max. (m)	Probability ($e_{h_{k,l}}$)	
				err < 1 m (%)	err < 2 m (%)
0	0.531	0.291	1.511	93.43%	100%
40	0.567	0.322	1.500	89.05%	100%
100	0.648	0.345	1.773	82.48%	100%

TABLE II
TOTAL POSITION PERFORMANCE

Latency (epochs)	Mean (m)	Std. Dev. (m)	Max. (m)	Probability ($e_{t_{k,l}}$)	
				err < 2 m (%)	err < 3 m (%)
0	1.178	0.625	3.466	89.05%	99.27%
40	1.647	0.819	3.641	64.96%	95.62%
100	2.422	1.013	4.630	36.50%	70.07%

IV. CONCLUSIONS AND FUTURE WORK

Accuracy in position estimation is of great interest in many commercial applications. The purpose of the investigations presented herein was to evaluate how communication latency between rover and reference station affect position estimation accuracy with stationary receivers. Relative GNSS (RGNSS) using Single-Differenced (SD) observables were discussed, and the results demonstrated that horizontal position estimation accuracy is achievable at 1 meter level (1 σ) with latency up to 1500 s. This shows that RGNSS is effective to correct common-mode errors and it has shown more robustness than Differential GNSS (DGNSS) in terms of latency sensitivity.

It is important to emphasize that the experiment herein conducted used high performance receivers in stationary conditions. As suggestions for future works, the authors intend to extend the same investigation herein presented, and also the effects of baseline distances between rover and reference station, for moving platforms equipped with low-cost, multi-constellations GNSS receivers. Another topic of interest is the use of corrections provided by specialized agencies for Precise Point Positioning (PPP), in order to obtain high level of position accuracy from a single receiver.

ACKNOWLEDGMENT

The authors thanks the Graduate Program in Automation and Systems Engineering (PPGESISA) at Federal University of Lavras (UFLA), EMBRAPA, FAPEMIG, and CNPq for supporting this study.

REFERENCES

[1] A. El-Rabbany, *Introduction to GPS: the Global Positioning System*. Artech house, 2002.

[2] A. Noureldin, T. B. Karamat, and J. Georgy, *Fundamentals of inertial navigation, satellite-based positioning and their integration*. Springer Science & Business Media, 2012.

[3] P. Teunissen and O. Montenbruck, *Springer handbook of Global Navigation Satellite Systems*. Springer, 2017.

[4] P. D. Groves, *Principles of GNSS, inertial, and multisensor integrated navigation systems*, 2nd. Artech house, 2013.

[5] J. Farrell, *Aided navigation: GPS with high rate sensors*. McGraw-Hill, Inc., 2008.

[6] B. A. Renfro, M. Stein, N. Boeker, and A. Terry, "An analysis of Global Positioning System (GPS) Standard Positioning Service (SPS) performance for 2019", *See https://www.gps.gov/systems/gps/performance/2019-GPS-SPS-performance-analysis.pdf*, 2020.

[7] G. Lachapelle, "GPS observables and error sources for kinematic positioning", in *Kinematic Systems in Geodesy, Surveying, and Remote Sensing*, Springer, 1991, pp. 17–26.

[8] P. Teunissen, "Differential GPS: Concepts and quality control", *Netherlands Institution of Navigation, Amsterdam*, vol. 10, pp. 48–60, 1991.

[9] J. Farrell, M. Grewal, M. Djodot, and M. Barth, "Differential GPS with latency compensation for autonomous navigation", in *Proceedings of the 1996 IEEE International Symposium on Intelligent Control*, IEEE, 1996, pp. 20–24.

[10] J. Farrell, M. Djodat, M. Barth, and M. Grewal, "Latency compensation for Differential GPS", *Navigation*, vol. 44, no. 1, pp. 99–107, 1997.

[11] T. B. Karamat, M. M. Atia, and A. Noureldin, "Performance analysis of code-phase-based relative GPS positioning and its integration with land vehicle's motion sensors", *IEEE Sensors Journal*, vol. 14, no. 9, pp. 3084–3100, 2014.

[12] W. Yang, Y. Liu, and F. Liu, "An improved Relative GNSS tracking method utilizing single frequency receivers", *Sensors*, vol. 20, no. 15, p. 4073, 2020.

[13] L. S. Monteiro, T. Moore, and C. Hill, "What is the accuracy of DGPS?", *The Journal of Navigation*, vol. 58, no. 2, p. 207, 2005.

[14] G. S. Carvalho, F. O. Silva, R. P. Menezes Filho, and V. H. L. Pereira, "Performance analysis of code-based Relative GPS positioning as function of baseline separation", in *2020 Latin American Robotics Symposium (LARS)*, IEEE, 2020, pp. 1–6.

[15] F. Rahman, E. Aghapour, and J. A. Farrell, "ECEF position accuracy and reliability in the presence of differential correction latency", in *2018 IEEE/ION Position, Location and Navigation Symposium (PLANS)*, IEEE, 2018, pp. 583–588.

[16] ——, "Vehicle ECEF position accuracy and reliability in the presence of DGNSS communication latency", *IEEE Intelligent Transportation Systems Magazine*, 2020.

[17] F. Rahman and J. A. Farrell, "Earth-Centered Earth-Fixed (ECEF) vehicle state estimation performance", in *2019 IEEE Conference on Control Technology and Applications (CCTA)*, IEEE, 2019, pp. 27–32.

[18] Y. He, R. Martin, and A. M. Bilgic, "Approximate iterative Least Squares algorithms for GPS positioning", in *The 10th IEEE International Symposium on Signal Processing and Information Technology*, IEEE, 2010, pp. 231–236.

[19] A. Amiri-Simkooei, P. Teunissen, and C. Tiberius, "Application of least-squares variance component estimation to GPS observables", *Journal of Surveying Engineering*, vol. 135, no. 4, pp. 149–160, 2009.

[20] M. Adjrad and P. D. Groves, "Enhancing least squares GNSS positioning with 3D mapping without accurate prior knowledge", *NAVIGATION, Journal of the Institute of Navigation*, vol. 64, no. 1, pp. 75–91, 2017.

[21] Y. Ohta, T. Kobayashi, H. Tsushima, S. Miura, R. Hino, T. Takasu, H. Fujimoto, T. Iinuma, K. Tachibana, T. Demachi, *et al.*, "Quasi real-time fault model estimation for near-field tsunami forecasting based on RTK-GPS analysis", *Journal of Geophysical Research: Solid Earth*, vol. 117, no. B2, 2012.

[22] W. Gurtner and L. Estey, "Rinex-the receiver independent exchange format-version 3.00", *Astronomical Institute, University of Bern and UNAVCO, Bolulder, Colorado.*, 2007.

[23] IBGE, *Rede brasileira de monitoramento contínuo dos sistemas GNSS - RBMC*, `https://bit.ly/2YsldI3`, Accessed: 2021-06-01, 2020.

[24] T. Hada and T. Tanaka, "Study on ionospheric delay in GPS standard positioning service", in *SICE 2004 Annual Conference*, IEEE, vol. 1, 2004, pp. 226–229.

[25] J. L. Leva, "Performance of standalone GPS", *Understanding GPS: principles and applications*, pp. 261–268, 1996.

PAPER IV - Performance Analysis of Relative GPS Positioning for Low-Cost Receiver-Equipped Dynamic Rovers

Paper to be submitted for consideration of publication in the Journal of Field Robotics - Special Issue in Agricultural Robots for Ag 4.0, in July 15^{th}, 2022. (Preliminary Version)

Performance Analysis of Relative GPS Positioning for Low-Cost Receiver-Equipped Agriculture Rovers

Gustavo S. Carvalho[1†], Felipe O. Silva[2†], Marcus Vinicius O. Pacheco [3] and Gleydson A. O. Campos [4]

[1,2,3]Department of Automatics, Federal University of Lavras, Caixa Postal 3037, Lavras, 37200-900, MG, Brazil.
[4]Department of Agricultural Engineering, Federal University of Lavras, Caixa Postal 3037, Lavras, 37200-900, MG, Brazil.

*Corresponding author(s). E-mail(s): guhcarv93@gmail.com; felipe.oliveira@ufla.br;
Contributing authors: marcuspachecomvp@gmail.com; gleydson.campos@ufla.br;
†These authors contributed equally to this work.

Abstract

Global Navigation Satellite Systems (GNSS) are now an integral part of all aspects of our lives. GNSS positioning, navigation, and timing services are central to a range of applications including road, aviation, maritime, location based services, agriculture, and surveying. The Global Positioning System (GPS) Standard Position Service (SPS) provides position accuracy up to 10 m. However, some modern-day applications, specially in Precision Agriculture, have demanded navigation technologies able to provide more accurate position at low-cost, specially for vehicle guidance and variable rate technology purpose. To improve the accuracy of GPS position estimates, the common-mode errors, presented on its observables, need to be addressed, and Relative GNSS (RGNSS) is a well-known technique to overcome this matter. This paper investigates the sensitivity of position estimation accuracy as function of two degradation factors that RGNSS is susceptible to: communication latency and baseline distances between GPS receivers. The Estimated Kalman Filter (EKF) approach was used for position estimation, considering Double-Differenced (DD) pseudorange observables. As main contribution, we show that it is possible to achieve 1.5 m horizontal accuracy at 68% of probability ($\mathbf{1\sigma}$) with latency up to 3000 s and baseline separation around 1500 km. Experimental data collected from the Brazilian Network for Continuous Monitoring of GNSS (RBMC) and moving rover equipped with low-cost GPS receiver are used to validate the analysis.

Keywords: RGNSS, COMMUNICATION LATENCY, BASELINE SEPARATION, POSITIONING ACCURACY, PRECISION AGRICULTURE

1 Introduction

Over the last several dacades, Global Navigation Satellite Systems (GNSSs) [1, 2] have become the dominant system for personal and vehicular (terrestrial or aerial) navigation [3–7]. GNSSs are "position-fixing" systems that allow a **P**osition a**N**d **T**iming (PNT) solution to be computed from synchronized ranging signals broadcast by

satellites [8, 9]. They provide three types of measurements, known as observables [8, 10–12]: pseudoranges (coarse distances between satellites and receiver during the transmission and reception of the GNSS signals), Doppler shifts (associated with the relative speed of the pairs satellites-receiver), and carrier phases (fine distances between satellites and receiver expressed in unit of cycles of the carrier wave). GNSSs' navigation solution can meet many application specifications using low-cost receivers, and the resulting position errors are bounded. However, standalone GNSS does not meet the necessary performance requirements of position accuracy and reliability in the new generation of applications (e.g., autonomous vehicles, connected vehicles, driver's assistance, and Precision Agriculture (PA)) [13–16], since their signals have low power and, consequently, they are vulnerable to numerous types of errors.

In the field of PA, it is of paramount importance the acquisition of precise position data for the effective control and analysis of a huge amount of geospatial information. This is an approach to farm management that uses information technology to deal with the spatial variability present in the farmland, ensuring that crops and soil receive exactly what they need for optimum health and productivity [17]. GNSS-based applications in precision farming are being largely used for farm planning, field mapping, soil sampling, tractor guidance, crop scouting, variable rate applications, and yield mapping [18–24].

Currently, the GNSSs comprise four constellations [8, 11]: The Global Positioning System (GPS), the oldest and most popular system, operating with Full Operational Capability (FOC) since 1995 by the United States of America government [25]; GLONASS, the Russian system with FOC dated from late 90's [26]; BeiDou, the Chinese constellation, that reached its FOC in 2020 [27]; and Galileo, the European constellation and unique system that is under civilian control [28].

Pseudorange measurements (the main GNSS observables), are primarily corrupted by seven types of errors [25, 29], which can be classified into two categories [30]:

the sum of environmental and temporal systematic errors that are present in a network of GNSS daily position time series that spans hundreds of kilometres

- *Common-mode errors* (CME): they are spatiotemporally correlated errors, i.e., the sum of environmental and temporal systematic errors that are experienced by all receivers in the same vicinity and time series. They comprise the ephemeris error, satellite clock bias, ionospheric and tropospheric delays.
- *Noncommon-mode errors* (NCME): unlike the CME, the NCME are different for each receiver, comprising the receiver clock bias, multipath error and receiver tracking noise.

The GPS Standard Position Service (SPS) provides horizontal and vertical accuracy of 9 m and 15 m, respectively [31]. Specifications such as the J2945 standard [32], determined by Society of Automotive Engineers (SAE) require horizontal and vertical accuracy of 1.5 m and 3 m with 68% probability, though. The common-mode errors are the mains responsible for the deterioration of the standalone GNSS position accuracy, therefore advanced GNSS techniques are required for achieving the level of accuracy. A number of solutions focused on mitigating the effect of common-mode errors on GNSS position estimation are available in the literature [33–37]. The Differential GNSS (DGNSS) approach is a well know technique which has been largely employed and researched by the civilian community since the beginning of the GNSS era (while Selective Availability (SA) was still activated) [38–41]. Put simply, the technique involves accurately measuring the errors in the pseudoranges observed by a receiver at a known time and location, namely a reference station, and broadcasting these corrections to a rover receiver at an unknown and possibly changing position in the reference base's vicinity. These 'differential corrections' are then applied to the pseudoranges measured by the second receiver, so that any errors which are common to the two receivers are eliminated.

As another option for GNSS common-mode error mitigation, the Relative GNSS (RGNSS) positioning has also been employed in the last few years boosted by cutting-edge communication technologies supporting high-speed and low-latency data dissemination between GNSS receivers networks [42–46]. The RGNSS technique is based on the sharing of GNSS pseudorange measurements observed in a reference station (i.e. raw observables) with a rover in the vicinity, in such

a way that these raw data are differenced from the moving GNSS receiver's own measurements. The differenced observations are used in position estimation algorithms, so that the rover position relative to the reference station is obtained. Once the reference station location is precisely known, the absolute rover position can be computed.

In reference stations-based GNSSs (like DGNSS and RGNSS), two main degradation factors are responsible for the position accuracy deterioration [47]: the baseline separation, which is the physical distance between the receivers, and the communication latency between the computed correction and actual time of use (for DGNSS) or the time difference between the reference station's raw observables availability and the current time of use during rover position estimation (for RGNSS). In [45], the effects of baseline separation on RGNSS position accuracy for a static rover equipped scenario with a high-performance GNSS receiver were investigated, showing that horizontal position errors remain submetric (1 σ) for baseline distances up to 2100 km. Communication latency on RGNSS position estimation accuracy has also been investigated in [46], again for a static rover equipped scenario with high-performance GNSS receiver, demonstrating that RGNSS positioning performance is insensitive (i.e., position accuracy remains submetric) to latency up to 1500 s. Similar investigations, devoted to dynamic rovers equipped with low-cost GNSS apparatus, however, are still rare in the literature.

Given these open issues, this paper aims at analyzing the aforementioned degrading factors, i.e., the effect of communication latency and baseline separation on Relative GPS (RGPS)[1] position estimation accuracy for dynamic rovers equipped with a low-cost GNSS receiver. The main contribution of this work is a comprehensive analysis concerning the maximum latency time and maximum distance between rover and reference station that allows RGNSS horizontal position accuracy based on low-cost receiver to achieve the J2945 standard specifications.

[1]This work focuses on results from GPS constellation only. Hence, the terms GPS and GNSS are used interchangeably hereinafter.

The remainder of this paper is organized as follows: Section 2 reviews GNSS Standalone approach, defining notation and presenting the corresponding algorithm for position solution; Section 3 presents notation and background on RGNSS position estimation with Single-Differenced (SD) and Double-Differenced (DD) pseudorange measurements. Section 4 describes the experimental data acquisition setup and presents the results on latency and baseline separation effects on position accuracy. Section 5, lastly, summarizes the paper and presents final thoughts and conclusions.

2 Standalone GNSS Position Estimation

The pseudorange measurement between a rover a and a satellite s, taking into account the errors cited in Section 1, can be modeled as

$$\rho^s_{a,R} = r_{as} + \delta\rho^a_c - \delta\rho^s_c + \delta\rho^s_{I,a} + \delta\rho^s_{T,a} + \delta\rho^s_E + \delta\rho^s_{M,a} + w^s_{p,a}, \tag{1}$$

where the time index t has been omitted for simplicity, the subscript R denotes raw measurement, and the range (Euclidean distance) from the true Earth-Centered-Earth-Fixed [2] (ECEF) position ($\mathbf{r}^e_{es}$) of satellite s to the true ECEF position ($\mathbf{r}^e_{ea}$) of rover a is defined as:

$$r_{as} = \left\| \mathbf{C}^I_e \mathbf{r}^e_{ea} - \mathbf{r}^e_{es} \right\|, \tag{2}$$

where $\mathbf{C}^I_e$ is the Direct Cosine Matrix (DCM) compensating for ECEF rotation during signal propagation [12].

The term $\delta\rho^a_c$ represents the receiver clock bias, $\delta\rho^s_c$ is the satellite clock bias, $\delta\rho^s_{I,a}$ is the ionospheric delay, $\delta\rho^s_{T,a}$ is the tropospheric delay, $\delta\rho^s_E$ is the ephemeris error, $\delta\rho^s_{M,a}$ is the multipath error, and $w^s_{\rho,a}$ is a white Gaussian-like measurement noise representing the lumped effects of tracking noise and unmodeled residual errors.

The Least Squares (LS) estimator is a well-known approach commonly used for receiver position computation based on pseudoranges [48–50].

[2]In this paper, the ECEF frame is represented by the superscript e, and is defined with its z_e axis pointing along the Earth's axis of rotation, x_e axis pointing from the center of Earth to the intersection of the equator with the Convention Zero Meridian (CZM), and y_e axis completing the right-hand orthogonal set.

Alternatively, Kalman-filter-based estimation algorithm presents itself as a more robust method for position solution estimation, since it makes use of information derived from previous measurements. The Extended Kalman Filter (EKF) is one of the most used filters for this kind of application [8, 11, 12, 45, 51, 52] because of its reliability and relatively low computational cost. For standalone GNSS positioning estimation using an Extended Kalman Filter (EKF) algorithm, the following state vector is usually defined:

$$\mathbf{x}_G^e = [(\mathbf{r}_{ea}^e)^T, (\mathbf{v}_{ea}^e)^T, \delta\rho_c^a, \delta\dot{\rho}_c^a]^T \in \mathbb{R}^n, \tag{3}$$

where the subscript G denotes standalone GNSS, $n = 8$, $\mathbf{v}_{ea}^e$ is the rover velocity, and $\delta\dot{\rho}_c^a$ is the receiver clock drift.

The dynamic model that describes how the states in (3) are propagated forward in time is given by:

$$\begin{aligned} \dot{\mathbf{r}}_{ea}^e &= \mathbf{v}_{ea}^e, \quad \frac{\partial}{\partial t}\delta\rho_c^a = \delta\dot{\rho}_c^a \\ \dot{\mathbf{v}}_{ea}^e &= 0 \quad \frac{\partial}{\partial t}\delta\dot{\rho}_c^a = 0 \end{aligned} \tag{4}$$

The main sources of increased uncertainty on the states estimates are due to user motion, random walk on the receiver clock drift, and phase noise on the clock bias. The acceleration Power Spectral Density (PSD) matrix driving the rover velocity random walk is

$$\mathbf{S}_a^e = (C_e^n)^T \begin{pmatrix} S_{aH} & 0 & 0 \\ 0 & S_{aH} & 0 \\ 0 & 0 & S_{aV} \end{pmatrix} C_e^n, \tag{5}$$

where C_e^n is the ECEF to North-East-Down (NED) DCM and S_{aH} and S_{aV} are the horizontal and vertical acceleration PSDs, respectively. The system noise is inherently context-dependent.

For a scenario encompassing a moving rover (dynamic applications), S_{aH} and S_{aV} can be tuned as 1 $m^2 s^{-3}$. The receiver clock frequency-drift PSD and clock phase-drift PSD, in turn, can be tuned as $S_{cf}^a \approx 0.04\ m^2 s^{-3}$ and $S_{c\phi}^a \approx 0.01\ m^2 s^{-1}$, respectively [8].

Equations (4) and (5) represent the dynamic model of the EKF that governs the prediction step of the standalone GNSS navigation filter. For the update step, the following measurement vector (for m satellites tracked) can be defined:

$$\mathbf{z}_G = [\rho_{a,C}^1, \rho_{a,C}^2, ...\rho_{a,C}^m]^T, \tag{6}$$

where the subscript C indicates that the pseudoranges have been partially corrected for common-mode errors, using for instance: Klobuchar model [53] to mitigate ionosphere delay, UNB3 model [9] for tropospheric delay, and satellite clock corrections transmitted in the GPS navigation message [54]. It should be noted, however, that these pseudorange measurements still contain residual components of common-mode errors that have not been totally compensated for by the aforementioned models.

The measurement innovations vector that is effectively processed by the EKF is:

$$\delta\mathbf{z}_{G,k}^- = \mathbf{z}_{G,k} - h_g(\hat{\mathbf{x}}_{G,k}^-), \tag{7}$$

where k is the iteration index and h_g is the non-linear pseudorange estimate (hat symbol) based on the predicted (superscript -) state vector $\hat{\mathbf{x}}_{G,k}^-$, given by:

$$h_g(\hat{\mathbf{x}}_k^-) = [\hat{\rho}_{a,C}^{1-}, \hat{\rho}_{a,C}^{2-}, ...\hat{\rho}_{a,C}^{m-}]^T, \tag{8}$$

The pseudorange estimate between rover a and satellite s is computed as follows

$$\hat{\rho}_{a,C,k}^{s-} = \sqrt{[\mathbf{C}_e^I\hat{\mathbf{r}}_{es}^e - \hat{\mathbf{r}}_{ea,k}^{e-}]^T[\mathbf{C}_e^I\hat{\mathbf{r}}_{es}^e - \hat{\mathbf{r}}_{ea,k}^{e-}]} + \delta\hat{\rho}_{c,k}^{a-}, \tag{9}$$

where $\hat{\mathbf{r}}_{es}^e$ is the estimated satellite position, $\hat{\mathbf{r}}_{ea,k}^{e-}$ is the estimated rover position, and $\delta\hat{\rho}_{c,k}^{a-}$ is the estimated receiver clock bias.

The measurement matrix is defined as:

$$\mathbf{H}_G^e = \begin{bmatrix} -u_{a1,x}^e & -u_{a1,y}^e & -u_{a1,z}^e & 0 & 0 & 0 & 1 & 0 \\ -u_{a2,x}^e & -u_{a2,y}^e & -u_{a2,z}^e & 0 & 0 & 0 & 1 & 0 \\ \vdots & \vdots & \vdots & \vdots & \vdots & \vdots & \vdots & \vdots \\ -u_{am,x}^e & -u_{am,y}^e & -u_{am,z}^e & 0 & 0 & 0 & 1 & 0 \end{bmatrix}, \tag{10}$$

where $\boldsymbol{u}_{as}^e = \frac{\boldsymbol{r}_{es}^e - \mathbf{r}_{ea}^e}{\|\boldsymbol{r}_{es}^e - \mathbf{r}_{ea}^e\|}$, $s \in \{1, ..., m\}$ is the unit line-of-sight vector from satellite s to rover a.

The EKF measurement noise covariance matrix, which is used to weight the uncertainties of the pseudorange observables, can be defined as:

$$\mathbf{R}_G = \begin{bmatrix} \sigma^2_{\rho 1} & 0 & \cdots & 0 \\ 0 & \sigma^2_{\rho 2} & \cdots & 0 \\ \vdots & \vdots & \ddots & \vdots \\ 0 & 0 & \cdots & \sigma^2_{\rho m} \end{bmatrix}, \tag{11}$$

where $\sigma^2_{\rho s}$ should take into account the satellite s elevation angle, since pseudorange uncertainty is expected to be larger for satellites with low elevation angle, namely:

$$\sigma^2_{\rho s} = \frac{\sigma^2_{\rho Z}}{\sin^2(\theta^{as}_{nu})}, \tag{12}$$

where $\sigma^2_{\rho Z}$ is a constant empirical value for the pseudorange uncertainty when satellite is at zenith, and θ^{as}_{nu} is the satellite s elevation angle.

Given the system and measurement models described above, standalone GNSS EKF can be implemented using the traditional discrete equations presented in standard literature. For more information, see [8, 11, 12, 55].

3 Relative GNSS Position Estimation

As mentioned in Section 1, to compute position using RGNSS approach, the rover needs to access raw observables timely provided from an available nearby reference station. Similar to (1), the pseudorange taken at the reference station r can be modeled as:

$$\rho^s_{r,R} = r_{rs} + \delta\rho^r_c - \delta\rho^s_c + \delta\rho^s_{I,r} + \delta\rho^s_{T,r} + \delta\rho^s_E + \delta\rho^s_{M,r} + w^s_{\rho,r}, \tag{13}$$

where r_{rs} is the true range from the ECEF position of satellite s, $(\mathbf{r}^e_{es})$, to the ECEF position of reference station, $(\mathbf{r}^e_{re})$.

Be the generic case where at least $m \geq 4$ satellites are in view of reference station and rover antennae, and are tracked by single-frequency GNSS receivers to which each is connected. The same number m of pseudoranges is expected to be tracked. Single-Differenced (SD) pseudoranges may be obtained by subtracting the observables of reference station r from those received by the rover a. In equation,

$$\nabla\rho^s_{ra,R} = \rho^s_{a,R} - \rho^s_{r,R}, \tag{14}$$

Applying (1) and (13) into (14) yields the following SD pseudorange model for m satellites in view [8]

$$\begin{cases} \nabla\rho^1_{ra,R} = \rho^1_{a,R} - \rho^1_{r,R} \\ = [-\boldsymbol{u}^e_{a1}]^T\mathbf{r}^e_{ra} + \Delta\rho^{ra}_c + \Delta\rho^1_{M,ra} + \Delta w^1_{\rho,ra} \\ \vdots \\ \nabla\rho^m_{ra,R} = \rho^m_{a,R} - \rho^m_{r,R} \\ = [-\boldsymbol{u}^e_{am}]^T\mathbf{r}^e_{ra} + \Delta\rho^{ra}_c + \Delta\rho^m_{M,ra} + \Delta w^m_{\rho,ra} \end{cases} \tag{15}$$

where $\boldsymbol{u}^e_{as}$, $s \in \{1, ..., m\}$ is the unit line-of-sight vector from satellite s to the antennae [3], $\Delta\rho^{ra}_c = \delta\rho^a_c - \delta\rho^r_c$, $\Delta\rho^s_{M,ra} = \delta\rho^s_{M,a} - \delta\rho^s_{M,r}$, and $\Delta w^s_{\rho,ra} = \delta w^s_{\rho,a} - \delta w^s_{\rho,r}$ are the SD receiver clock delay, multipath and white Gaussian-like measurement noise for satellite s, respectively.

A quick inspection at (15) indicates that the SD pseudorange measurements are direct function of the baseline vector ($\mathbf{r}^e_{ra} = \mathbf{r}^e_{ea} - \mathbf{r}^e_{er}$) in the ECEF frame, and are no longer corrupted by the common-mode errors $(\delta\rho^s_c, \delta\rho^s_{I,i}, \delta\rho^s_{T,i}, \delta\rho^s_E)$, $i \in \{a, r\}$, since they were canceled out during the differencing process. However, this cancellation is valid solely when the time it takes to the rover to access the reference station measurements is in a delimited time frame (latency), and when the physical separation (baseline) between both antennae is within a certain range. The investigation of both effects on moving rovers equipped with low-cost GNSS receivers is the main focus of this work.

For RGNSS positioning estimation using an EKF algorithm, the following state vector comprising $n = 8$ states can be defined:

$$\mathbf{x}^e_S = [(\mathbf{r}^e_{ra})^T, (\mathbf{v}^e_{ra})^T, \Delta\rho^{ra}_c, \Delta\dot{\rho}^{ra}_c]^T \in \mathbb{R}^n, \tag{16}$$

where the subscript S denotes SD-RGNSS, $\mathbf{v}^e_{ra}$ is the rover velocity relative to the reference station, and $\delta\dot{\rho}^{ra}_c$ is the rover clock drift relative to the reference station.

The dynamic model that describes how the states in (16) are propagated forward in time and the associated process noise PSDs are the same as in (4) and (5). Concerning the EKF update step,

[3] The GNSS antennae r and a are considered to be close enough so that their line-of-sight vectors to each satellite are parallel

in turn, the measurement vector (for m satellites tracked) comprises the SD pseudoranges and can be described as,

$$\mathbf{z}_S = [\nabla\rho^1_{ra,R}, \nabla\rho^2_{ra,R}, ...\nabla\rho^m_{ra,R}]^T, \tag{17}$$

The measurement innovations vector that is effectively processed by the EKF is:

$$\delta\mathbf{z}^-_{S,k} = \mathbf{z}_{S,k} - h_s(\hat{\mathbf{x}}^-_{S,k}), \tag{18}$$

where h_s are the nonlinear SD pseudorange estimates based on the predicted state vector $\hat{\mathbf{x}}^-_{S,k}$, given by

$$h_s(\hat{\mathbf{x}}^-_{S,k}) = [\nabla\hat{\rho}^{1-}_{ra,R}, \nabla\hat{\rho}^{2-}_{ra,R}, ..., \nabla\hat{\rho}^{m-}_{ra,R}]^T, \tag{19}$$

The SD pseudorange estimates can be computed as:

$$\nabla\hat{\rho}^{s-}_{ra,R} = \left\|\mathbf{C}^I_e\hat{\mathbf{r}}^{e-}_{es} - \hat{\mathbf{r}}^{e-}_{ea}\right\| - \left\|\mathbf{C}^I_e\hat{\mathbf{r}}^{e-}_{es} - \hat{\mathbf{r}}^{e-}_{er}\right\| + \Delta\hat{\rho}^{ra-}_c. \tag{20}$$

The measurement matrix, $\mathbf{H}^e_S$, which is the geometric matrix that characterizes the user-satellite geometry, is defined as in (10). The measurement noise covariance matrix, lastly, which is used to weight the uncertainties of the SD pseudorange observables, is:

$$\mathbf{R}_S = 2\mathbf{R}_G, \tag{21}$$

where the factor 2 arises from the SD process.

3.1 Double-Differenced RGNSS

As demonstrated in Section 3, SD pseudoranges are free from common-mode errors, however they are still corrupted by the residual SD receiver clock delay, which does not bias the position solution but still has to be estimated by the EKF (see (16)). An alternative to overcome this inconvenience is differencing the SD pseudorange measurements across satellites, i.e, forming Double-Differenced (DD) pseudorange measurements as follows

$$\begin{cases} \Delta\nabla\rho^{p1}_{ra,R} = \nabla\rho^1_{ra} - \nabla\rho^p_{ra} = [\boldsymbol{u}^e_{p1}]^T\mathbf{r}^e_{ra} \\ \qquad\qquad +\rho^{p1}_{M,ra} + w^{p1}_{p,ra} \\ \qquad\qquad \vdots \\ \Delta\nabla\rho^{pm}_{ra,R} = \nabla\rho^m_{ra} - \nabla\rho^p_{ra} = [\boldsymbol{u}^e_{pm}]^T\mathbf{r}^e_{ra} \\ \qquad\qquad +\rho^{pm}_{M,ra} + w^{pm}_{p,ra} \end{cases} \tag{22}$$

with $\boldsymbol{u}^e_{ps} = \boldsymbol{u}^e_{as} - \boldsymbol{u}^e_{ap}$, $s \in \{1, ..., m\}$, where p represents the pivot satellite (usually the satellite with highest elevation angle); $\rho^{ps}_{M,ra} = \rho^s_{M,ra} - \rho^p_{M,ra}$ is the DD multipath error; $w^{ps}_{p,ra} = w^s_{p,ra} - w^p_{p,ra}$ is the DD measurement noise.

A quick inspection at (22) indicates that all common-mode errors and also the receiver clock errors have been removed from the DD pseudorange measurements. Equation (22) can be solved using an EKF, as in Section 3, whose state vector now comprises 6 sates to be estimated,

$$\mathbf{x}^e_D = [(\mathbf{r}^e_{ra})^T, (\mathbf{v}^e_{ra})^T]^T \in \mathbb{R}^n, \tag{23}$$

where the subscript D denotes DD-RGNSS, and $n = 6$.

The EFK measurement vector now comprises DD pseudoranges, as follows:

$$\mathbf{z}_D = [\Delta\nabla\rho^{p1}_{ra,R}, \Delta\nabla\rho^{p2}_{ra,R}, ..., \Delta\nabla\rho^{pm}_{ra,R}]^T, \tag{24}$$

The measurement innovation vector is defined as:

$$\delta\mathbf{z}^-_{D,k} = \mathbf{z}_{D,k} - h_d(\hat{\mathbf{x}}^-_{D,k}), \tag{25}$$

where h_d are the nonlinear DD pseudorange estimates based on the predicted state vector $\hat{\mathbf{x}}^-_{D,k}$, given by

$$h_d(\hat{\mathbf{x}}^-_{D,k}) = [\nabla\hat{\rho}^{1-}_{ra,R}, \nabla\hat{\rho}^{2-}_{ra,R}, ..., \nabla\hat{\rho}^{m-}_{ra,R}]^T, \tag{26}$$

The DD pseudorange estimates can be computed as:

$$\begin{aligned}\Delta\nabla\hat{\rho}^{s-}_{ra,R} = &\left\|\mathbf{C}^I_e\hat{\mathbf{r}}^{e-}_{es} - \hat{\mathbf{r}}^{e-}_{ea}\right\| - \left\|\mathbf{C}^I_e\hat{\mathbf{r}}^{e-}_{ep} - \hat{\mathbf{r}}^{e-}_{ea}\right\| \\ &- \left\|\mathbf{C}^I_e\hat{\mathbf{r}}^{e-}_{es} - \hat{\mathbf{r}}^{e-}_{er}\right\| + \left\|\mathbf{C}^I_e\hat{\mathbf{r}}^{e-}_{ep} - \hat{\mathbf{r}}^{e-}_{er}\right\|.\end{aligned} \tag{27}$$

The geometric matrix, $\mathbf{H}^e_D$, now contains rows defined by $\boldsymbol{u}^e_{ps}$. In contrast to SD-RGNSS solution,

$\mathbf{H}_D^e$ does not include a column for the receiver clock bias, since this state has been canceled out in the double-differencing. Then,

$$\mathbf{H}_D^e = \begin{bmatrix} -u_{p1,x}^e & -u_{p1,y}^e & -u_{p1,z}^e \\ -u_{p2,x}^e & -u_{p2,y}^e & -u_{p2,z}^e \\ \vdots & \vdots & \vdots \\ -u_{pm,x}^e & -u_{pm,y}^e & -u_{pm,z}^e \end{bmatrix} \tag{28}$$

Finally, since the satellite p is used as pivot (by subtracting its SD observables from all satellites in view), this results in the DD pseudoranges correlated among themselves. Therefore,

$$\mathbf{R_D} = \mathbf{D}_G \mathbf{R}_S \mathbf{D}_G^T, \tag{29}$$

where

$$\mathbf{D_G} = \begin{pmatrix} 1 & 0 & \cdots & 0 & -1 \\ 0 & 1 & \cdots & 0 & -1 \\ \vdots & \vdots & \ddots & \vdots & \vdots \\ 0 & 0 & \cdots & 1 & -1 \end{pmatrix} \tag{30}$$

4 Experimental Results

In order to analyze the influence on RGNSS position accuracy caused by both degradation effects, namely, communication latency and baseline separation between rover and reference station, an experimental test was performed. The test consisted of equipping a radio-controlled rover with a low-cost u-blox C102-F9R application board connected to a u-blox multi-band/multi-constellation antenna, model ANN-MB-01. The antenna was attached to the roof of the rover as illustrated in Fig. 1.

4.1 Experimental Data Acquisition

The test was conducted in an experimental coffee plantation composed of young coffee trees with a height of about 1.5 m, located at the Federal University of Lavras (UFLA). The rover (Fig. 1) was guided through the corridors of the coffee plantation, which are approximately 130 m long (the planned path is illustrated in Fig. 2), collecting and saving, in a personal computer, GPS raw data with interval tracking of 1 second, so that the data could be post-processed (aiming at the rover's position computation) using the following two algorithms, developed in MATLAB® environment:

1. EKF-based standalone GNSS approach using pseudorange measurements. For brevity, this approach will be referred to as SA-GNSS on the ensuing text.
2. EKF-based RGNSS using double-differenced pseudorange measurements. This approach will be designated DD-RGNSS hereinafter.

For DD-RGNSS position estimation, the corresponding reference station was chosen among

Figure 1 Rover equipped with u-blox C102-F9R application board and antenna ANN-MB-01 (black box in the gray area over the robot's roof) used in the experimental test.

Figure 2 Planned path for data acquisition at coffee plantation located at Federal University of Lavras.

those belonging to the Brazilian Network for Continuous Monitoring of GNSS (RBMC), which is the most precise geodetic reference structure in Brazil, operated and maintained by the Brazilian Institute of Geography and Statistics (IBGE). It consists of 147 geodetic stations spread around the country, placed in well surveyed locations with coordinates established at high precision level. Each station is equipped with a high performance receiver that collects and stores, continuously, GNSS observables and navigation data. RBMC provides GNSS data in three different ways: real-time through the Networked Transport of RTCM via Internet Protocol (NTRIP) "caster" server [56]; at 15-seconds tracking interval in Receiver Independent Exchange Format (RINEX) 2 and RINEX 3 formats; and at 1-second tracking interval files in RINEX 3 format [57]. These data can be freely accessed by all users in [58]. Some selected RBMC stations additionally provide GNSS data in RINEX 2 format at the tracking interval of 1 second through the National Institute for Colonization and Agrarian Reform (INCRA) Network of GNSS Community Bases (RIBaC), which can be accessed in [59]. Although some of these bases are equipped with multi-frequency, multi-constellation receivers, only single-frequency (L1), Coarse-Acquisiton (C/A) pseudorange measurements for the GPS constellation were used for state estimation during the experimental tests.

In order to determine reliable ground-truth values for the rover position (so that the corresponding estimates could be compared against), precise dual-frequency positioning using wide-lane carrier-phase observables were applied, whose integer ambiguities were solved and fixed using the Least squares AMBiguity Decorrelation Adjustment (LAMBDA) method proposed in [60, 61].

To assess the estimation performance of the RGNSS, three criteria were considered: individual channel position error (e_{ic_k}), defined in (31); horizontal position error (e_{h_k}), defined in (32); and total position error (e_{t_k}), defined in (33).

$$e_{ic_k,N,E,D} = \mathbf{r}^n_{ea,N,E,D} - \hat{\mathbf{r}}^n_{ea_k,N,E,D}, \tag{31}$$

$$e_{h_{k,l}} = \left\| \begin{bmatrix} 1 & 0 & 0 \\ 0 & 1 & 0 \end{bmatrix} (\mathbf{r}^n_{ea} - \hat{\mathbf{r}}^n_{ea_k}) \right\|, \tag{32}$$

$$e_{t_{k,l}} = \left\| \begin{bmatrix} 1 & 0 & 0 \\ 0 & 1 & 0 \\ 0 & 0 & 1 \end{bmatrix} (\mathbf{r}^n_{ea} - \hat{\mathbf{r}}^n_{ea_k}) \right\|, \tag{33}$$

where $\mathbf{r}^n_{ea}$ is the ground-truth rover position resolved along the axes of the North-East-Down (NED) navigation frame, and $\hat{\mathbf{r}}^n_{ea_k}$ is the corresponding estimate.

4.2 RGNSS Performance Analysis: Sensitivity to Communication Latency

This Section presents results and discusses the experimental position estimation performance for a low-cost GNSS receiver-equipped dynamic rover considering the degradation effect of communication latency between rover and reference station. The goal is to verify the extent to which the RGNSS estimation algorithm is able to achieve the horizontal accuracy level of 1.5 meters at 1σ, as required by the SAE J2945 standard [32]. The EKF algorithm was used to process the entire batch of GNSS measurements collected during the test ($k = 1, ..., N_d$; $N_d = 800$ epochs, where 1 epoch corresponds to 1 second) as if they were occurring in real-time, i.e., incrementally, to estimate the state vector at each time index k, for a given value of latency l, using the DD pseudorange $\Delta\nabla\rho^{ps}_{ra,R}(k;\ k-l)$. The experiment was repeated for values of $l = 0, ..., 6000$ epochs, which correspond to a latency up to 100 minutes. In this extreme situation, the rover used data from reference station collected 100 minutes earlier in order to compute its own position at the current epoch.

For comparative purposes, the rover position estimated using the SA-GNSS approach was also included in the analysis. The MGLA base station (located at UFLAS's campus) belonging to RBMC was selected to be the reference station, which provided raw pseudorange measurements for the rover to use aiming at common-mode error cancellation during its own position estimation. The baseline separation between rover and reference station, i.e, the distance between the base and the coffee plantation where the test was conducted, was known to be around 1 km. For each fixed value of latency l, the mean and standard deviation of $e_{ic_{k,l},N,E,D}$; $e_{h_{k,l}}$ and $e_{t_{k,l}}$ were computed from experimental data by averaging the

last $(N_d - l_{max})$ epochs, where l_{max} is the maximum value for latency (6000). Table 1 summarizes the mean and standard deviation of the position error criteria defined in (31), (32) and (33) for latency $l = 0$ s, i.e, DD-RGNSS rover position estimation computed using reference station's pseudorange measurements received at the same epoch as the rover ($\Delta\nabla\rho^{ps}_{ra,R}(k;\ k)$). For comparison purposes, the position error statistics for the SA-GNSS approach are also included in Table 1.

Table 1 Position Error Statistics for SA-GNSS and DD-RGNSS approaches.

	SA-GNSS		DD-RGNSS	
	Mean [m]	Std. dev [m]	Mean [m]	Std. dev [m]
North	1.0501	0.498	0.528	0.351
East	0.459	0.371	0.395	0.308
Down	1.293	1.014	1.121	0.866
Horizontal	1.202	0.505	0.713	0.381
Total	1.883	0.925	1.432	0.779

As one can see in Table 1, in the absence of communication latency, the DD-RGNSS approach presented an improved performance in all error criteria if compared to SA-GNSS technique, since the mean errors of the former are closer to zero besides presenting smaller standard deviations. One can notice, as well, that SA-GNSS approach is not able to comply with SAE J2945 standard position accuracy requirements, while DD-RGNSS is. This is an indication that the common-mode errors were effectively mitigated.

The analysis that follows investigates the detrimental effect of communication latency between the rover and reference station data, where incremented latency values were purposely added in the position estimation process. Figure 3 shows the mean error along with the plus and minus one-standard-deviations (indicated by the vertical bars in each point) as function of latency. The first point (in purple) is the rover position estimation error performed by SA-GNSS algorithm, whereas the remaining points (in red) are the position estimation error performed by DD-RGNSS algorithm.

As can be noticed in Figure 3, the DD-RGNSS performance is better than SA-GNSS, which is in agreement with [46, 62, 63]. Another outcome from Figure 3 is that the DD-RGNSS horizontal position accuracy remains under 1.5 m at 1σ for latency up to 3000 s, which is sufficient to attend the SAE J2945 standard specifications. After this value of latency, the DD-RGNSS performance becomes similar to SA-GNSS and gets even worse as latency increases, indicating that the common-mode errors cancellation is no longer valid. For $l =$ 6000 s, for instance, i.e., when the rover position estimation is computed using reference station's pseudorange measurements received 6000 epochs earlier ($\Delta\nabla\rho^{ps}_{ra,R}(k;\ k-6000)$), the mean horizontal and total position errors are 1.726 m and 4.996 m, respectively, becoming 242% and 349% larger than the corresponding errors when there is no latency. The standard deviation also gets larger as l is incremented. When $l = 0$ s, the standard deviation for the mean position error in the horizontal channel is $\sigma = 0.381$ m, whereas for $l = 6000$ s the standard deviation becomes $\sigma = 0.713$ m, almost 2 times larger. This shows that the dispersion in the position uncertainties gets wider as latency values increase, which are due to the increasingly incorrect common-mode error cancellation (due to the time correlation of the common-mode errors).

Tables 2 summarizes some selected measures of position accuracy for horizontal position error, with latency $l = 0, 1500$ and 3000 epochs. Column 1 shows the latency in terms of epochs. Column 2 shows the mean error, defined in (32). Column 3 displays the standard deviation. Column 4 reports the maximum value for the horizontal position error. Columns 5 and 6, lastly, reports the percent of samples that have position error less than 1 m and 1.5 m, respectively.

A recent work by the authors investigated the effects of communication latency on position estimation accuracy for a static rover [46], whose results showed that position accuracy of 1 m at 1σ is achievable for latency up to 1500 s. Compared to the results herein presented (Fig. 3), one sees that such accuracy cannot not be achieved, at $1sigma$, not even for the DD-RGNSS approach under no latency. It is important to highlight, however, the fact that, in [46], the position estimation was made using a high performance GNSS receiver mounted on a static rover, while here a low-cost receiver was employed (mounted on a dynamic rover). Those factors have a significant impact on the position accuracy since they affect the quality of the data collected, as suggested in [64].

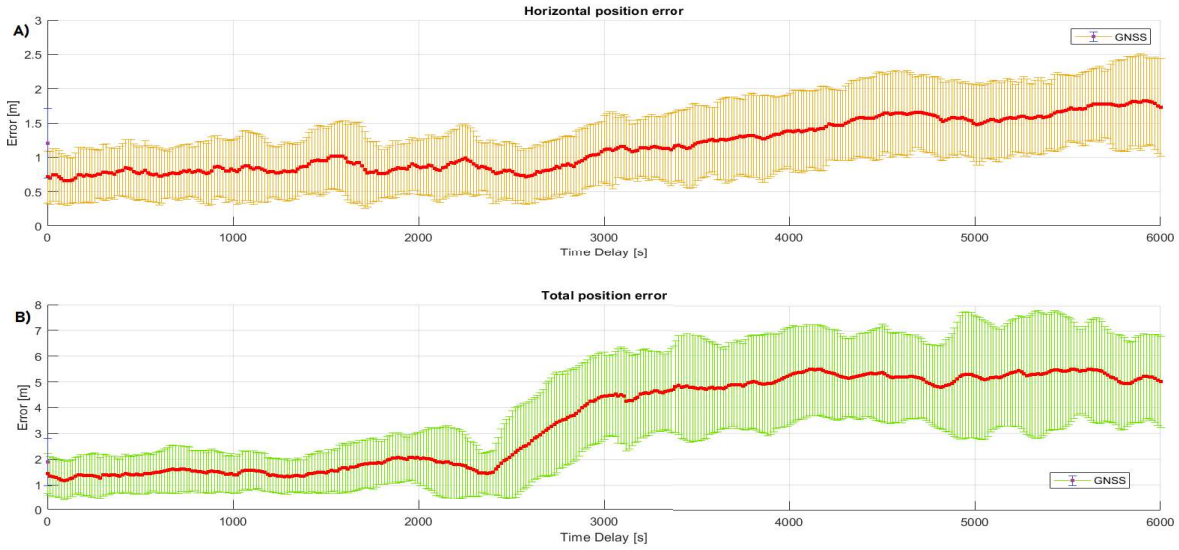

Figure 3 Mean error of horizontal (A) and total (B) position as function of latency. The first plotted data refers to the position estimation performed by SA-GNSS algorithm (highlighted in purple) and the remaining data (red squares) refer to DD-RGNSS algorithm.

4.3 RGNSS Performance Analysis: Sensitivity to Baseline Separation

The second purpose of the experimental test was to analyze the degradation effect of baseline separation in RGNSS positioning accuracy. As in Section 4.2, the main goal was to identify the maximum baseline separation between rover and reference station that still allows the horizontal position accuracy to remain at 1.5 meters (1σ).

The same GNSS data set collected in the coffee plantation test was used, and the rover position was again estimated by using the SA-GNSS and DD-RGNSS approaches. For the latter, 23 RBMC bases were selected to be the reference stations, which provided raw pseudorange measurements for the rover so that the common-mode errors could be canceled out during its position estimation process. The reference stations were selected according to their baseline separations from the coffee plantation located at UFLA, so that the distances gradually increased in the range of 1 km to 3355 km. Since this is a dynamic test with moving rover, the distance between the rover and the reference station was defined using the home point of the experiment (highlighted by the red circle in Fig. 2). The chosen bases were MGLA, MGV1, CHPI, MGIN, SPBP, POLI, SPS1, MGUB, SJRP, NEIA, SPFE, UFPR, GOJA, SCCH, RSPE, RSAL, PIFL, MTLA, MTJI, ROJI, POVE, AMCR, SAGA, which are displayed in Figure 4. During the experiment, the rover's trajectory was defined towards the MGLA station, where the greatest distance between rover and reference for this specific situation is 1 km, when the rover is at the home point.

Table 2 Horizontal Position Performance for DD-RGNSS given different values of latency.

Latency (epochs)	Mean (m)	Std. Dev. (m)	Max. (m)	Probability (e_{h_k}) err <1 m (%)	err <1.5 m (%)
0	0.713	0.381	2.039	77.32	96.43
1500	0.952	0.471	2.295	56.18	86.24
3000	1.115	0.494	2.961	42.80	79.36

To analyze the sensitivity of position estimation accuracy w.r.t. baseline separation, the rover position was estimated using the SA-GNSS and DD-RGNSS algorithms. Each algorithm processed the same set of the rover's GNSS measurements ($k = 1, ..., N_d$; $N_d = 800$) as if they were occurring in real-time (i.e., incrementally) to estimate the state vector at each time index k. For DD-RGNSS approach, the rover's position was estimated by considering the selected different reference stations. The error criteria defined in (31), (32) and (33) were used to asses the performance of both algorithms.

Figure 5 depicts the mean horizontal and total position error (red squares) as function of baseline distances between receivers. It also displays the standard deviation (vertical bars) of the mean estimated position errors. The first point in the graph (in purple) is the error obtained by using the SD-GNSS algorithm, whereas the remaining points are the mean error obtained by using the DD-RGNSS algorithm with different reference stations. As expected, Figure 5 indicates an improvement in horizontal and total position estimation of DD-RGNSS over the SA-GNSS. The former presented a horizontal position accuracy slightly over 1 meter at 1σ when using the first 2 reference stations (baseline separation of 1.184 km and 60.038 km, respectively), whereas the later presented position accuracy of about 1.7 m.

Another interesting outcome from Figure 5 is that DD-RGNSS approach presented improved performance over SA-GNSS for reference stations with baseline distances up to 1441 km. For the remaining reference stations (located further away) the position error increased, making the DD-RGNSS performance to be worse than SA-GNSS. Moreover, the very same reference station with baseline distance of 1441 km proved to be the limit to which the DD-RGNSS technique is able to comply with the J2945 standard specifications for horizontal position accuracy. An unexpected behavior can be noticed in the mean error trend when using reference stations with baseline distances greater than 2000 km, since the mean error value starts to decrease fro this point. This behavior is attributed to a circumstantial fact of the experiment since the position error is supposed to increase as the distance between rover and reference station gets greater due to its spatial correlation, in which the premise of the common-mode error cancellation is not valid anymore.

Table 3, finally, shows the individual distances between rover and the different reference stations, and also summarizes the mean and standard deviations of the horizontal error criteria. A quantitative analysis shows that the mean error increases 50% (from $0,921$ m to 1.377 m) when the reference station is changed from base RSAL to PIFL, both located 1441.826 km and 1619.417 km away from the coffee plantation, respectively. This indicates that from this point on, the common-mode errors cancellation is no longer valid, which significantly impacts the position estimation accuracy (a proof of the common-mode errors spatial correlation).

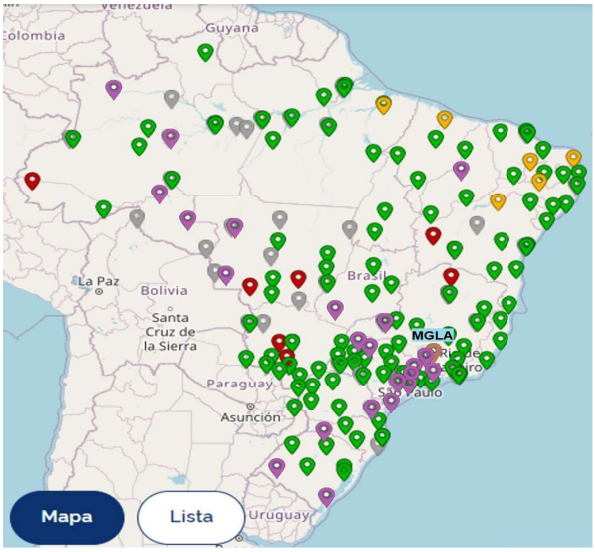

Figure 4 RBMC stations used in the experiment with different baseline distances (highlighted in purple) and MGLA base, located where the test was conducted (highlighted in brown). The points highlighted in gray, yellow and red refer to RBMC stations deactivated, in maintenance and without communication, respectively.

5 Conclusion

This paper addressed the effect of two common degradation factors of Relative Global Navigation System (RGNSS) position accuracy: the baseline separation and communication latency between the rover and reference station receivers. A radio controlled robot was equipped with a low-cost GNSS receiver to evaluate the performance of RGNSS technique in a dynamic scenario. A comprehensive review of the main common-mode errors that corrupt the GNSS signals was given, as well as an in-depth analytical description of how RGNSS approach mitigate them.

As most important verifications from the comprehensive analyses of the effect of communication latency and baseline separation between rover and reference station, the accuracy of position estimation with RGNSS was shown to improve in comparison to standalone (SA)-GNSS, especially in the horizontal channel. The timely and spatially correlation of the GNSS common-mode errors were demonstrated, and the maximum communication latency and baseline separation required

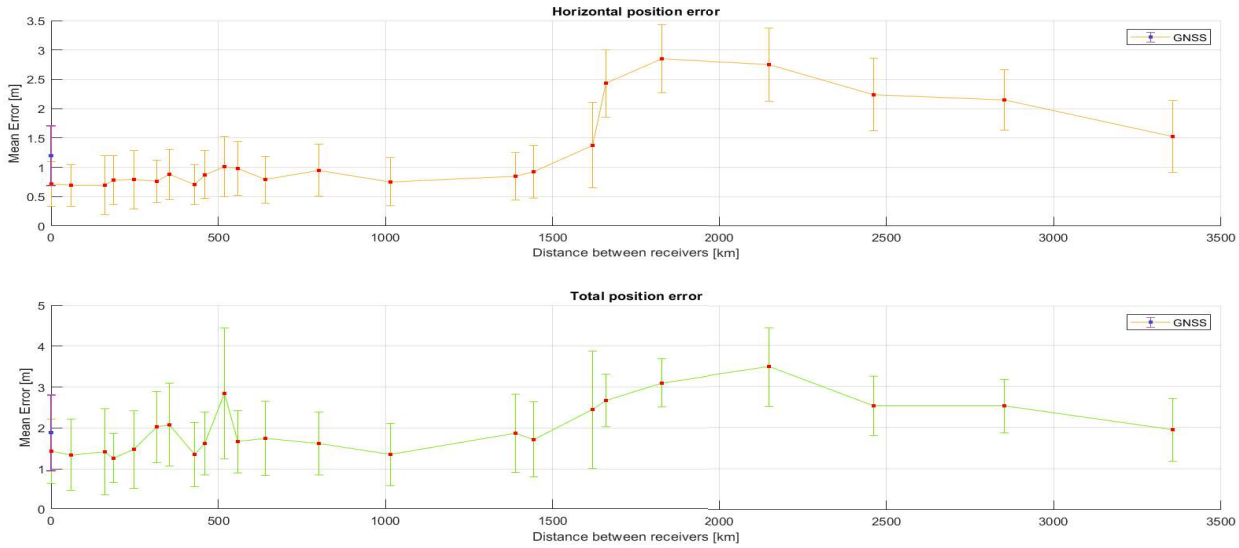

Figure 5 Horizontal position error as function of baseline separation for the DD-RGNSS approach. For distance 0 km, the plotted data refers to the position estimation performed by SA-GNSS algorithm (highlighted in purple) for a visual comparison between both approaches.

to attend SAE J2945 standard specifications were found to be up to 3000 s and 1441.826 km for a dynamic rover equipped with a low-cost receiver.

As suggestions for future works, the authors plan to investigate Real-Time Precise Point Positioning (RT-PPP), which consists of using precise corrections of common-mode errors produced by specialized institutions, such as International GNSS Service (IGS). Another topic of interest is the integration between Inertial Navigation Systems (INSs) and GNSSs as they are complementary in terms of advantages/drawbacks.

Acknowledgments The authors thanks the Graduate Program in Systems Engineering and Automation (PPGESISA) at the Federal University of Lavras (UFLA) for supporting the research.

Declarations

Funding This work was supported by the Research Development Foundation (FUNDEP - ROTA 2030), under grant 27192.02.02/2021.01.00, the Brazilian National Council for Scientific and Technological Development (CNPq), under grant 313160/2019-8, the Brazilian Agricultural Research Corporation (EMBRAPA), under grant 212-20/2018, and the Minas Gerais Research Foundation (FAPEMIG), under grant CAG-APQ-01449-17.

Conflict of interest/Competing interests The authors declare that they have no known competing financial interests or personal relationships that could have appeared to influence the work reported in this paper.

Ethics Approval Not Applicable.

Consent to Participate Not Applicable.

Consent for Publication Not Applicable

Availability of Data The data set generated during and/or analyzed during the current study are available in the FIGSHARE repository, https://doi.org/10.6084/m9.figshare.19946063.v1

Code Availability Not Applicable

Author Contributions Gustavo de Souza Carvalho is the corresponding author of the article, who along with Felipe Oliveira e Silva contributed to the study conception, design and data analysis. Material preparation and data collection were performed by Gustavo de Souza Carvalho, Felipe Oliveira e Silva, Marcus Vinicius Oliveira Pacheco and Gleydson Antônio de Oliveira Campos. The

Table 3 Horizontal Position Error Statistics for each reference station used by DD-RGNSS approach. The first column is the position estimation metrics obtained with SA-GNSS algorithm.

	Baseline separation [km]	Mean Error [m]	Std. dev [m]
SA-GNSS	Does not apply	1.202	0.505
MGLA	1.184	0.713	0.381
MGV1	60.038	0.692	0.357
CHPI	162.245	0.696	0.503
MGIN	185.908	0.782	0.416
SPBP	248.682	0.789	0.501
POLI	316.228	0.763	0.362
SPS1	355.443	0.881	0.426
MGUB	429.269	0.703	0.341
SJRP	459.137	0.875	0.412
NEIA	519.199	1.012	0.517
SPFE	558.059	0.976	0.457
UFPR	640.374	0.790	0.400
GOJA	800.357	0.95	0.442
SCCH	1015.505	0.754	0.406
RSPE	1389.495	0.851	0.405
RSAL	1441.826	0.921	0.448
PIFL	1619.417	1.377	0.729
MTLA	1658.773	2.43	0.572
MTJI	1825.606	2.849	0.576
ROJI	2148.614	2.752	0.627
POVE	2460.694	2.241	0.615
AMCR	2853.128	2.15	0.518
SAGA	3354.927	1.525	0.615

first draft of the manuscript was written by Gustavo de Souza Carvalho and all authors commented on previous versions of the manuscript. All authors read and approved the final manuscript.

References

[1] G. Blewitt, Basics of the GPS technique: observation equations. Geodetic applications of GPS **10**, 54 (1997)

[2] P. Misra, P. Enge, *Global Positioning System: signals, measurements and performance*, vol. 206, 2nd edn. (Ganga-Jamuna Press, 2006)

[3] A. Gardi, R. Sabatini, S. Ramasamy, T. Kistan, Real-time uas guidance for continuous curved GNSS approaches. Journal of Intelligent & Robotic Systems **93**(1), 151–162 (2019)

[4] G. Zhang, L.T. Hsu, A new path planning algorithm using a GNSS localization error map for UAVs in an urban area. Journal of Intelligent & Robotic Systems **94**(1), 219–235 (2019)

[5] S. Bijjahalli, S. Ramasamy, R. Sabatini, A novel vehicle-based GNSS integrity augmentation system for autonomous airport surface operations. Journal of Intelligent & Robotic Systems **87**(2), 379–403 (2017)

[6] L.R. Sahawneh, M.A. Al-Jarrah, K. Assaleh, M.F. Abdel-Hafez, Real-time implementation of GPS aided low-cost strapdown inertial navigation system. Journal of Intelligent & Robotic Systems **61**(1), 527–544 (2011)

[7] A.R. Vetrella, F. Causa, A. Renga, G. Fasano, D. Accardo, M. Grassi, Multi-uav carrier phase differential GPS and vision-based sensing for high accuracy attitude estimation. Journal of intelligent & robotic systems **93**(1), 245–260 (2019)

[8] P.D. Groves, *Principles of GNSS, inertial, and multisensor integrated navigation systems*, 2nd edn. (Artech house, 2013)

[9] D. Kaplan Elliott, J. Hegarty Christopher, *Understanding GPS: principles and applications* (Artech House, 2006)

[10] A. Noureldin, T.B. Karamat, J. Georgy, *Fundamentals of inertial navigation, satellite-based positioning and their integration* (Springer Science & Business Media, 2012)

[11] P. Teunissen, O. Montenbruck, *Springer handbook of Global Navigation Satellite Systems* (Springer, 2017)

[12] J. Farrell, *Aided navigation: GPS with high rate sensors* (McGraw-Hill, Inc., 2008)

[13] F. Kitchener, T. English, D. Gopalakrishna, V. Garcia, A. Ragan, R. Young, M. Ahmed, D. Stephens, N.U. Serulle, et al., Connected vehicle pilot deployment program phase 2, data management plan: Wyoming. Tech. rep., United States. Department of Transportation. Intelligent Transportation (2017)

[14] F. Kitchener, R. Young, M. Ahmed, G. Yang, S. Gaweesh, T. English, V. Garcia, A. Ragan, N.U. Serulle, D. Gopalakrishna, et al., Connected vehicle pilot deployment program: Phase 2 final system performance report, baseline conditions–WYDOT CV Pilot. Tech. rep., United States. Dept. of Transportation (2018)

[15] S. Li, M. Zhang, Y. Ji, Z. Zhang, R. Cao, B. Chen, H. Li, Y. Yin, Agricultural machinery GNSS/IMU-integrated navigation based on fuzzy adaptive finite impulse response kalman filtering algorithm. Computers and Electronics in Agriculture **191**, 106,524 (2021)

[16] F. Rovira-Más, I. Chatterjee, V. Sáiz-Rubio, The role of GNSS in the navigation strategies of cost-effective agricultural robots. Computers and electronics in Agriculture **112**, 172–183 (2015)

[17] J.F.G. Monico, *Posicionamento pelo Navstar-GPS* (Unesp, 2000)

[18] J. Poteko, D. Eder, P.O. Noack, Identifying operation modes of agricultural vehicles based on GNSS measurements. Computers and Electronics in Agriculture **185**, 106,105 (2021). https://doi.org/https://doi.org/10.1016/j.compag.2021.106105. URL https://www.sciencedirect.com/science/article/pii/S016816992100123X

[19] S. Li, M. Zhang, Y. Ji, Z. Zhang, R. Cao, B. Chen, H. Li, Y. Yin, Agricultural machinery GNSS/IMU-integrated navigation based on fuzzy adaptive finite impulse response kalman filtering algorithm. Computers and Electronics in Agriculture **191**, 106,524 (2021). https://doi.org/https://doi.org/10.1016/j.compag.2021.106524. URL https://www.sciencedirect.com/science/article/pii/S016816992100541X

[20] Y. Liang, K. Zhou, C. Wu, Environment scenario identification based on GNSS recordings for agricultural tractors. Computers and Electronics in Agriculture **195**, 106,829 (2022). https://doi.org/https://doi.org/10.1016/j.compag.2022.106829. URL https://www.sciencedirect.com/science/article/pii/S0168169922001466

[21] Y. Chen, G. Li, X. Zhang, J. Jia, K. Zhou, C. Wu, Identifying field and road modes of agricultural machinery based on GNSS recordings: A graph convolutional neural network approach. Computers and Electronics in Agriculture **198**, 107,082 (2022). https://doi.org/https://doi.org/10.1016/j.compag.2022.107082. URL https://www.sciencedirect.com/science/article/pii/S0168169922003994

[22] X. He, D. Zhang, L. Yang, T. Cui, Y. Ding, X. Zhong, Design and experiment of a GPS-based turn compensation system for improving the seeding uniformity of maize planter. Computers and Electronics in Agriculture **187**, 106,250 (2021). https://doi.org/https://doi.org/10.1016/j.compag.2021.106250. URL https://www.sciencedirect.com/science/article/pii/S0168169921002672

[23] M. Pérez-Ruiz, D. Slaughter, C. Gliever, S. Upadhyaya, Automatic GPS-based intra-row weed knife control system for transplanted row crops. Computers and Electronics in Agriculture **80**, 41–49 (2012). https://doi.org/https://doi.org/10.1016/j.compag.2011.10.006. URL https://www.sciencedirect.com/science/article/pii/S0168169911002341

[24] M.G. Wing, J. Frank, Vertical measurement accuracy and reliability of mapping-grade GPS receivers. Computers and Electronics in Agriculture **78**(2), 188–194 (2011). https://doi.org/https://doi.org/10.1016/j.compag.2011.07.006. URL https://www.sciencedirect.com/science/article/pii/S0168169911001530

[25] P. Teunissen, Differential GPS: Concepts and quality control. Netherlands Institution of Navigation, Amsterdam **10**, 48–60 (1991)

[26] P. Daly, GLONASS approaches full operational capablllty (FOC). Proceedings of the 8th International Technical Meeting of the

Satellite Division of The Institute of Navigation (ION GPS 1995) pp. 1021–1030 (1995)

[27] P.R. of China. Development of the BeiDou navigation satellite system. http://en.beidou.gov.cn/SYSTEMS/Officialdocument/ (2019). BeiDou is operated and maintained by the China Satellite Navigation Office. Accessed: 2022-02-25

[28] E. Commission. Galileo. https://www.esa.int/Applications/Navigation/Galileo (2022). Galileo is operated by European GNSS Agency and maintained by European Space Agency. Accessed: 2022-02-15

[29] G. Lachapelle, GPS observables and error sources for kinematic positioning. Kinematic Systems in Geodesy, Surveying, and Remote Sensing pp. 17–26 (1991)

[30] J. Farrell, M. Grewal, M. Djodot, M. Barth, Differential GPS with latency compensation for autonomous navigation. Proceedings of the 1996 IEEE International Symposium on Intelligent Control pp. 20–24 (1996)

[31] B.A. Renfro, M. Stein, N. Boeker, A. Terry. An analysis of Global Positioning System (GPS) Standard Positioning Service (SPS) performance for 2019. https://www.gps.gov/systems/gps/performance/2019-GPS-SPS-performance-analysis.pdf (2020). Accessed: 2022-01-11

[32] S. J2945/1. On-board system requirements for V2V safety communications. https://saemobilus.sae.org/content/j2945/1_201603 (2016). Accessed: 2022-03-15

[33] S. Mahato, G. Shaw, A. Santra, S. Dan, S. Kundu, A. Bose, Low cost GNSS receiver RTK performance in forest environment. URSI Regional Conference on Radio Science (URSI-RCRS) pp. 1–4 (2020)

[34] X. Yang, J. Yang, Discussion on the practice of data processing of GNSS Precision Point Positioning. 28th International Conference on Geoinformatics pp. 1–6 (2021)

[35] P. Schwarzbach, P. Tauscher, A. Michler, O. Michler, V2X based probabilistic cooperative position estimation applying GNSS double differences. 2019 International Conference on Localization and GNSS (ICL-GNSS) pp. 1–6 (2019)

[36] T. Suzuki, Time-relative RTK-GNSS: GNSS loop closure in pose graph optimization. IEEE Robotics and Automation Letters **5**(3), 4735–4742 (2020)

[37] W. Jiang, Y. Liu, B. Cai, C. Rizos, J. Wang, Y. Jiang, A new train integrity resolution method based on online carrier phase relative positioning. IEEE Transactions on Vehicular Technology **69**(10), 10,519–10,530 (2020)

[38] M. Shao, X. Sui, Study on differential GPS positioning methods. 2015 International Conference on Computer Science and Mechanical Automation (CSMA) pp. 223–225 (2015)

[39] C. Shuxin, W. Yongsheng, C. Fei, A study of differential GPS positioning accuracy. 2002 3rd International Conference on Microwave and Millimeter Wave Technology, 2002. Proceedings. ICMMT 2002. pp. 361–364 (2002)

[40] D. Walsh, S. Capaccio, D. Lowe, P. Daly, P. Shardlow, G. Johnston, Real time differential GPs and GLONASS vehicle positioning in urban areas. Space communications **14**(4), 203–217 (1997)

[41] C. Cai, J. Hu, Design and implementation of dual-mode pseudorange differential positioning. 2019 IEEE International Conference on Power, Intelligent Computing and Systems (ICPICS) pp. 283–286 (2019)

[42] P. Zeller, B. Siebler, A. Lehner, S. Sand, Relative train localization for cooperative maneuvers using GNSS pseudoranges and geometric track information. 2015 International Conference on Localization and GNSS (ICL-GNSS) pp. 1–7 (2015)

[43] N. Alam, A.T. Balaei, A.G. Dempster, Relative positioning enhancement in VANETs: A tight integration approach. IEEE Transactions on Intelligent Transportation Systems

14(1), 47–55 (2012)

[44] K. Liu, H.B. Lim, E. Frazzoli, H. Ji, V.C. Lee, Improving positioning accuracy using GPS pseudorange measurements for cooperative vehicular localization. IEEE Transactions on Vehicular Technology **63**(6), 2544–2556 (2013)

[45] G.S. Carvalho, F.O. Silva, R.P. Menezes Filho, V.H.L. Pereira, Performance analysis of code-based Relative GPS positioning as function of baseline separation. 2020 Latin American Robotics Symposium (LARS) pp. 1–6 (2020)

[46] G.S. Carvalho, F.O. Silva, Performance analysis of relative GPS positioning as function of communication latency. 2021 Latin American Robotics Symposium (LARS), 2021 Brazilian Symposium on Robotics (SBR), and 2021 Workshop on Robotics in Education (WRE) pp. 252–257 (2021)

[47] L.S. Monteiro, T. Moore, C. Hill, What is the accuracy of DGPS? The Journal of Navigation **58**(2), 207 (2005)

[48] Y. He, R. Martin, A.M. Bilgic, Approximate iterative Least Squares algorithms for GPS positioning. The 10th IEEE International Symposium on Signal Processing and Information Technology pp. 231–236 (2010)

[49] A. Amiri-Simkooei, P. Teunissen, C. Tiberius, Application of least-squares variance component estimation to GPS observables. Journal of Surveying Engineering **135**(4), 149–160 (2009)

[50] M. Adjrad, P.D. Groves, Enhancing least squares GNSS positioning with 3D mapping without accurate prior knowledge. NAVIGATION, Journal of the Institute of Navigation **64**(1), 75–91 (2017)

[51] F. Rahman, E. Aghapour, J.A. Farrell, Vehicle ECEF position accuracy and reliability in the presence of DGNSS communication latency. IEEE Intelligent Transportation Systems Magazine (2020)

[52] F. Rahman, J.A. Farrell, Earth-Centered Earth-Fixed (ECEF) vehicle state estimation performance. 2019 IEEE Conference on Control Technology and Applications (CCTA) pp. 27–32 (2019)

[53] J. Klobuchar, Global Positioning System: theory and applications. Vol. I, Cap **12**, 485–515 (1996)

[54] G. Navstar, Space segment/navigation user interfaces, interface control document GPS (200), no. ICD GPS **200** (2019)

[55] B. Hofmann-Wellenhof, H. Lichtenegger, E. Wasle, *GNSS–global navigation satellite systems: GPS, GLONASS, Galileo, and more* (Springer Science & Business Media, 2008)

[56] Y. Ohta, T. Kobayashi, H. Tsushima, S. Miura, R. Hino, T. Takasu, H. Fujimoto, T. Iinuma, K. Tachibana, T. Demachi, et al., Quasi real-time fault model estimation for near-field tsunami forecasting based on RTK-GPS analysis. Journal of Geophysical Research: Solid Earth **117**(B2) (2012)

[57] W. Gurtner, L. Estey, Rinex-the receiver independent exchange format-version 3.00. Astronomical Institute, University of Bern and UNAVCO, Bolulder, Colorado. (2007)

[58] IBGE. Rede brasileira de monitoramento contínuo dos sistemas GNSS - RBMC. https://bit.ly/2YsldI3 (2021). Accessed: 2021-12-15

[59] INCRA. Rede Incra de Bases Comunitárias do GNSS - RIBaC. https://bityli.com/KQMBU (2021). Accessed: 2021-12-15

[60] B. Li, S. Verhagen, P.J. Teunissen, Gnss integer ambiguity estimation and evaluation: Lambda and ps-lambda. China satellite navigation conference (CSNC) 2013 Proceedings pp. 291–301 (2013)

[61] S. Verhagen, B. Li, P.J. Teunissen, Ps-lambda: ambiguity success rate evaluation software for interferometric applications. Computers & geosciences **54**, 361–376 (2013)

[62] D. Yoon, C. Kee, J. Seo, B. Park, Position accuracy improvement by implementing the DGNSS-CP algorithm in smartphones. Sensors **16**(6) (2016). URL https://www.mdpi.com/1424-8220/16/6/910

[63] D. Weng, X. Gan, W. Chen, S. Ji, Y. Lu, A new DGNSS positioning infrastructure for android smartphones. Sensors **20**(2) (2020). URL https://www.mdpi.com/1424-8220/20/2/487

[64] M.E. Hodgson, On the accuracy of low-cost dual-frequency GNSS network receivers and reference data. GIScience & Remote Sensing **57**(7), 907–923 (2020). URL https://doi.org/10.1080/15481603.2020.1822588